Research Paper

GEOSPHERE

GEOSPHERE; v. 13, no. 2

doi:10.1130/GES01356.1

25 figures; 4 tables; 2 supplemental files

CORRESPONDENCE: atwater@usgs.gov; atwater@u.washington.edu

CITATION: Atwater, B.F., ten Brink, U.S., Cescon, A.L., Feuillet, N., Fuentes, Z., Halley, R.B., Nuñez, C., Reinhardt, E.G., Roger, J.H., Sawai, Y., Spiske, M., Tuttle, M.P., Wei, Y., and Weil-Accardo, J., 2017, Extreme waves in the British Virgin Islands during the last centuries before 1500 CE: Geosphere, v. 13, no. 2, p. 301–368, doi:10.1130/GES01356.1.

Received 3 May 2016
Revision received 9 November 2016
Accepted 4 January 2017
Published online 17 March 2017

Extreme waves in the British Virgin Islands during the last centuries before 1500 CE

Brian F. Atwater[1], Uri S. ten Brink[2], Anna Lisa Cescon[3], Nathalie Feuillet[4], Zamara Fuentes[5], Robert B. Halley[6,*], Carlos Nuñez[7], Eduard G. Reinhardt[8], Jean H. Roger[9], Yuki Sawai[10], Michaela Spiske[11,12], Martitia P. Tuttle[13], Yong Wei[14,15], and Jennifer Weil-Accardo[4]

[1]U.S. Geological Survey at Department of Earth and Space Sciences, University of Washington, Seattle, Washington 98195-1310, USA
[2]U.S. Geological Survey, Quissett Campus, 384 Woods Hole Road, Woods Hole, Massachusetts 02543-1598, USA
[3]Department of Geography and Environmental Sciences, University of Ulster, Cromore Road, Coleraine, Northern Ireland BT52 1SA, UK
[4]Institut de Physique du Globe de Paris, Sorbonne Paris Cité, Université Paris Diderot UMR (Unité Mixte de Recherche) 7154, CNRS (Centre National de la Recherche Scientifique), F-75005, Paris, France
[5]Department of Marine Sciences, University of Puerto Rico, Mayagüez 00682, Puerto Rico
[6]I-Guana Farm, 13765 2600 Road, Cedaredge, Colorado 81413, USA
[7]School of Earth, Environmental, and Marine Sciences, University of Texas Rio Grande Valley, One West University Boulevard, Brownsville, Texas 78520, USA
[8]School of Geography & Earth Sciences, McMaster University, Hamilton, Ontario L8S 4L8, Canada
[9]3 Rue de l'Artimon, 35400 Saint-Malo, France
[10]National Institute of Advanced Industrial Science and Technology, AIST Tsukuba Central 7, 1-1-1 Higashi, Tsukuba, Ibaraki, 305-8567, Japan
[11]Institut für Geologie und Paläontologie, Westfälische Wilhelms-Universität, Corrensstrassê 24, 48149 Münster, Germany
[12]Universität Trier, Geozentrum, Behringstrassê 21, 54296 Trier, Germany
[13]M. Tuttle & Associates, P.O. Box 345, Georgetown, Maine 04548, USA
[14]National Oceanic and Atmospheric Administration, 7600 Sand Point Way NE, Seattle, Washington 98115, USA
[15]JISAO (Joint Institute for the Study of the Atmosphere and Ocean), University of Washington, 3737 Brooklyn Ave NE, Seattle, Washington 98195-5672, USA

ABSTRACT

Extraordinary marine inundation scattered clasts southward on the island of Anegada, 120 km south of the Puerto Rico Trench, sometime between 1200 and 1480 calibrated years (cal yr) CE. Many of these clasts were likely derived from a fringing reef and from the sandy flat that separates the reef from the island's north shore. The scattered clasts include no fewer than 200 coral boulders, mapped herein for the first time and mainly found hundreds of meters inland. Many of these are complete colonies of the brain coral *Diploria strigosa*. Other coral species represented include *Orbicella* (formerly *Montastraea*) *annularis*, *Porites astreoides*, and *Acropora palmata*. Associated bioclastic carbonate sand locally contains articulated cobble-size valves of the lucine *Codakia orbicularis* and entire conch shells of *Strombus gigas*, mollusks that still inhabit the sandy shallows between the island's north shore and a fringing reef beyond. Imbricated limestone slabs are clustered near some of the coral boulders. In addition, fields of scattered limestone boulders and cobbles near sea level extend mainly southward from limestone sources as much as 1 km inland. Radiocarbon ages have been obtained from 27 coral clasts, 8 lucine valves, and 3 conch shells. All these additional ages predate 1500 cal yr CE, all but 2 are in the range 1000–1500 cal yr CE, and 16 of 22 brain coral ages cluster in the range 1200–1480 cal yr CE. The event marked by these coral and mollusk clasts likely occurred in the last centuries before Columbus (before 1492 CE).

The pre-Columbian deposits surpass Anegada's previously reported evidence for extreme waves in post-Columbian time. The coarsest of the modern storm deposits consist of coral rubble that lines the north shore and sandy fans on the south shore; neither of these storm deposits extends more than 50 m inland. More extensive overwash, perhaps by the 1755 Lisbon tsunami, is marked primarily by a sheet of sand and shells found mainly below sea level beneath the floors of modern salt ponds. This sheet extends more than 1 km southward from the north shore and dates to the interval 1650–1800 cal yr CE. Unlike the pre-Columbian deposits, it lacks coarse clasts from the reef or reef flat; its shell assemblage is instead dominated by cerithid gastropods that were merely stirred up from a marine pond in the island's interior.

In their inland extent and clustered pre-Columbian ages, the coral clasts and associated deposits suggest extreme waves unrivaled in recent millennia at Anegada. Bioclastic sand coats limestone 4 m above sea level in areas 0.7 and 1.3 km from the north shore. A coral boulder of nearly 1 m³ is 3 km from the north shore by way of an unvegetated path near sea level. As currently understood, the extreme flooding evidenced by these and other clasts represents either an extraordinary storm or a tsunami of nearby origin. The storm would need to have produced tsunami-like bores similar to those of 2013 Typhoon Haiyan in the Philippines. Normal faults and a thrust fault provide nearby tsunami sources along the eastern Puerto Rico Trench.

INTRODUCTION

This paper wrestles with problems in earthquake and coastal geology. The seismological issue is whether tsunamis are generated along a plate-bounding trench in the northeast Caribbean. The coastal challenge is how to distinguish, in hurricane alley, between the bouldery traces of a tsunami and those of a storm.

*Retired from U.S. Geological Survey

Hypothetical Hazards from the Puerto Rico Trench

Tsunamis in Caribbean written history were generated remotely in a few cases and locally in most (Lander et al., 2002). The Lisbon tsunami in the year 1755, of the common era (CE), produced the largest of the far-traveled waves. All but one of the local tsunamis arose from sources within the Caribbean plate. No documented tsunami is known to have arisen along the Puerto Rico Trench (Fig. 1A), although the trench coincides with several conjectural sources of Caribbean and North Atlantic tsunamis (ten Brink et al., 2014).

The largest of these conjectural sources is the subduction thrust that dips southward from the trench as a predominantly strike-slip boundary between the Caribbean plate and the North American plate (Fig. 1B). A tsunami in Hispaniola was generated during a 1946 earthquake on a western continuation of this fault (Lynch and Bodle, 1948; Dolan and Wald, 1998). All historical tsunamis generated elsewhere in the northeast Caribbean, however, can be associated with faults within the Caribbean plate (ten Brink et al., 2011). Interplate coupling inferred from satellite geodesy is negligible along the Puerto Rico Trench (ten Brink and López-Venegas, 2012). To the southeast, where plate convergence is more nearly orthogonal to the trench axis, the Lesser Antilles subduction thrust is thought to be partly coupled (Hayes et al., 2014; Symithe et al., 2015). The fault in this area is the inferred source of a large earthquake in 1946 that may have been accompanied by a few tens of centimeters of tectonic subsidence (Weil-Accardo et al., 2016). It is also the inferred source of a larger earthquake in 1843 (Feuillet et al., 2011; Roger et al., 2013), but accounts of the 1843 earthquake provide few hints of an attending tsunami and no evidence for tsunami damage (Bernard and Lambert, 1988; Shepherd, 1992; Bernard and Lambert, 1992).

Tsunami sources along the Puerto Rico Trench may also include normal faults of the outer rise. Their distinct but undated scarps furrow the incoming North America plate on the outer trench wall (ten Brink, 2005; Andrews et al., 2013) (Fig. 1C). Normal faulting in this tectonic setting can generate tsunamis efficiently by displacing tall water columns with high-angle dip slip (Craig et al., 2014). Along the Japan Trench, for example, normal faulting produced strong shaking and a disastrous tsunami in 1933 (Kanamori, 1971; Usami, 2003). In the northeast Caribbean, the outer rise was neglected as a regional earthquake source (Mueller et al., 2003) but modeled as a potential source of Puerto Rican tsunamis (Mercado Irizarry and Justiniano Sepulveda, 2003). However, like the subduction thrust along the Lesser Antilles, the outer rise along the Puerto Rico Trench is not known to have generated a regional tsunami in written history that begins with Columbus in 1492.

Other potential sources of tsunamis are marked by scarps of youthful reverse faults and submarine landslides south of the trench (Fig. 1C). A reverse fault that displaces the ocean floor has been mapped for a distance of 20 km in deep water northwest of Anegada, south of Main Ridge (Grindlay et al., 2005). Large submarine slides, farther west, have estimated recurrence intervals of ~100,000 yr (ten Brink et al., 2006). A large example is directly north of San Juan, Puerto Rico.

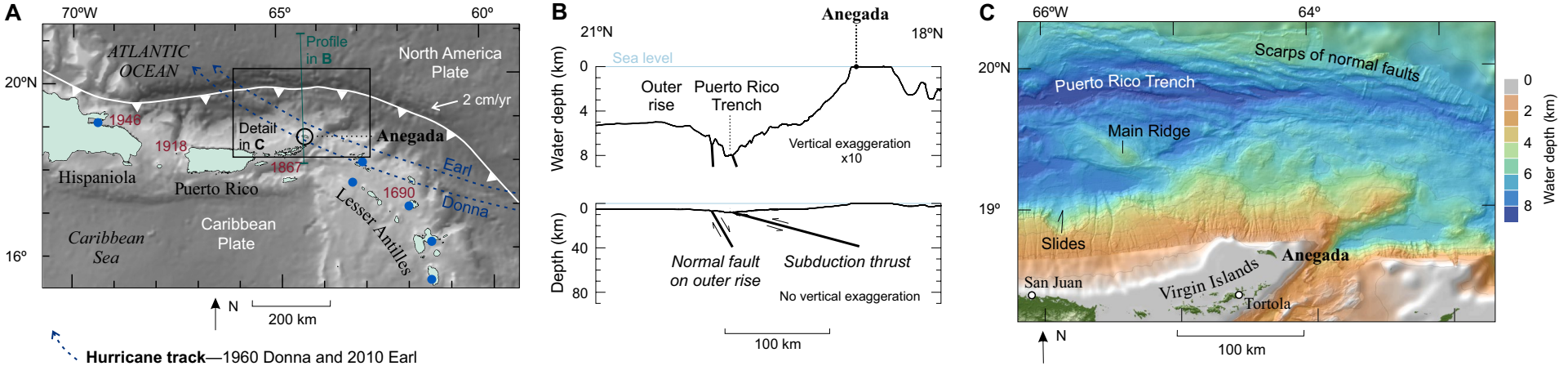

Figure 1. Setting. (A) Plate boundary (barbed line), source areas of near-field tsunamis, tracks of 1960 Hurricane Donna and 2010 Hurricane Earl, and sites where the 1755 Lisbon tsunami was noted (Lander et al., 2002; Roger et al., 2010). (B) Generalized physiographic profile. Location shown in green in A. (C) Swath bathymetry (Andrews et al., 2013).

This paper presents evidence for extreme waves of pre-Columbian age at Anegada, a low-lying island 120 km south of the Puerto Rico Trench (Figs. 1 and 2). We put this evidence in context by reviewing previous work on Anegada's deposits from recent hurricanes, and on the island's assorted evidence for southward inundation earlier in post-Columbian time. We differentiate some of this evidence from signs of southward flooding during the last centuries before Columbus. The main goals of the paper are to describe several kinds of pre-Columbian deposits, constrain their time of emplacement, and provide constraints for modeling that might eventually show whether these deposits represent a Puerto Rican Trench tsunami or an unusual storm.

Coastal Boulders as Ambiguous Clues to Tsunami Hazards

It is rare that a prehistoric tsunami can be shown to be responsible for boulders on storm-prone shores. The case for a tsunami commonly hinges on evidence that storm waves are incapable of having emplaced clasts that are exceptionally large and/or inland (Frohlich et al., 2009; Ramalho et al., 2015). Site-specific effects of physiographic setting and clast provenance have confounded attempts to identify, in boulder deposits, a field signature of tsunami deposition that is both unique and global (Switzer and Burston, 2010; Terry et al., 2013, p. 65–66).

Anegada is exposed to several kinds of extreme waves, known or plausible. As reviewed herein (in the section headed "Exposure to Extreme Waves") recent hurricanes have flooded parts of the island with storm surge, and exceptional storms might produce tsunami-like bores by analogy with 2013 Typhoon Haiyan in the Philippines (details in "Tsunami-Like Bores Analogous to Those from Typhoon Haiyan"). The island is subject to far-field tsunami waves like those associated with the Lisbon earthquake of 1755, as well as hypothetical tsunamis from historically latent sources along the Puerto Rico Trench.

This paper focuses less on comparisons with modern storm and tsunami deposits of distant shores, than on field-based comparison among extreme-wave effects on Anegada. Combining previous findings with new observations, we assign Anegada's evidence for extreme waves to three generalized groups, listed here by increasing rank and age.

1. Deposits of modern storms (Fig. 3) consist mainly of microbial debris deposited around interior salt ponds and fans, along with localized fans of sand and mud deposited along the island's south shore. Boulders moved onshore by these storms are probably limited to a coral rubble ridge within a few tens of meters of the island's north shore.

2. An inland sheet of sand and shell is found mainly beneath low-lying salt ponds (Fig. 3). This deposit, encountered almost entirely below mean sea level, extends more than 1 km southward from the island's north shore. This sheet was deposited quickly, sometime between 1650 and 1800 calibrated years in the common era. This event age, expressed herein as the range 1650–1800 cal yr CE, or simply 1650–1800, is consistent with deposition by far-traveled waves of the 1755 Lisbon tsunami. We will infer that the sheet of 1650–1800 sets an upper bound for extensive Anegadan deposits of a large tsunami of remote origin. That is, the sheet either represents the 1755 tsunami, or it was laid down by a tsunami or storm between 1650 and 1800 that exceeded the 1755 tsunami in its depositional effects at Anegada.

3. The deposits of highest rank include fields of scattered coral boulders and cobbles (Fig. 4). Evidence of this rank includes, in addition to the coral clasts, the shells of large marine mollusks, an extensive sheet of bioclastic sand, and fields and clusters of limestone boulders and cobbles. Some of this evidence was previously lumped with the sand and shell sheet of 1650–1800 cal yr CE. To explain the deposits of highest rank, we will invoke offshore erosion and onshore flooding during an extreme-wave event sometime between 1200 and 1480 cal yr CE (herein, 1200–1480 cal yr CE, or simply 1200–1480). We will infer that this event exceeded any other extreme waves at Anegada in the past few thousand years, and we attribute it to either a Puerto Rico Trench tsunami or to tsunami-like bores from a Haiyan-like storm.

For convenience, we use the term "extreme wave" across these three degrees of extremeness, and without regard for wave period. Modern storm overwash that deposited sand and gravel on the island's shores fell short of floods from the sea that produced the inland deposits dated to 1650–1800 and 1200–1480. As interpreted herein, those prior floods may have been tsunamis, or they might represent storm-generated bores intermediate in period between storm and tsunami waves.

We stop short of comparing the field evidence with storm and tsunami models. A previous comparison of field evidence with storm and tsunami modeling included estimation of forces involved in transporting the largest clasts in two low-lying fields of limestone boulders at Anegada. The emplacement of these clasts was found to be better explained by tsunamis generated along the Puerto Rico Trench than by a category 5 hurricane or the Lisbon tsunami (Buckley et al., 2012; Watt et al., 2012). This initial finding needs reappraisal in light of the additional field observations presented herein, the accompanying bathymetry and topography from lidar (light detection and ranging) surveys, and the tsunami-like bores from 2013 Typhoon Haiyan.

Guide to Figures, Tables, and Supporting Data

The paper contains three sets of illustrations[1]. One set provides overviews of regional setting (Fig. 1), local geography and physiography (Fig. 2), previous field evidence (Fig. 3), new field evidence (Fig. 4), dating (Fig. 5), and estimates of inundation distance and height along nine cross-island profiles (Fig. 6). The other two sets provide supporting details, grouped by theme and location. Figures A1–A12 summarize field evidence by clast type, plotted island-wide. Figures B1–B7 provide closer views of field evidence, using large-scale maps of parts of the island (index map, Fig. 2A) and including photographs of most of the dated clasts.

[1]For the full-sized version of each figure, please visit http://doi.org/10.1130/GES01356.S1 or the full-text article on www.gsapubs.org.

[2]Supplemental Material. Tables giving locations and elevations of most of the points that are plotted on the figures, along with measurements of size and orientation of some of the clasts. Please visit http://doi.org/10.1130/GES01356.S2 or the full-text article on www.gsapubs.org to view the Supplemental Material.

TABLE 1. SOURCES OF TOPOGRAPHIC AND BATHYMETRIC DATA, ANEGADA ISLAND AREA, CARIBBEAN SEA

Area	Source
Anegada, including interior salt ponds	Bare-earth terrain model derived from lidar (light detection and ranging) survey 21 January 2014 by Quantum Spatial for the Puget Sound Lidar Consortium. Optech Orion M300 sensor system. Cessna 210 Caravan aircraft.
Fringing reef and reef flat north of Anegada	Lidar survey 19–20 March 2014, led by C. Wayne Wright, U.S. Geological Survey. Experimental Advanced Airborne Research Lidar, version B, emitting 3 simultaneous 532 nm laser pulses at 700 ps intervals. Cessna 310 aircraft.
Deeper water north of Anegada	Atlantic depths below 40 m depth from Andrews et al. (2013).
Waters south of island in the area depicted in text Figure 2 and on index maps in the Supplemental Material (see footnote 2).	These Caribbean depths are everywhere <10 m on the nautical chart compiled by the Defense Mapping Agency (1996). The more nearly primary source of this bathymetry is the 1964 edition of British Admiralty Chart 2008. The original soundings predate 1930.

Note: Lidar data available from the U.S. Geological Survey (Fredericks et al., 2016).

Also presented are lists of physiographic data sources (Table 1), radiocarbon ages (Table 2), details about the control points in Figure 6 (Table 3), and author contributions (Table 4). Further lists, containing most of the points plotted on the various maps, can be found in the Supplemental Material[2]. Included are the locations and elevations of all plotted points of coral clasts, reef rock, beach rock, and a widespread unit termed the main sand sheet. Clast size and sand thickness are reported there, although these measurements were not made routinely in reconnaissance mapping. The Supplemental Material also contains details of ~27 sets of limestone slabs that were systematically measured for clast size and orientation.

The lidar data in this report are available from the U.S. Geological Survey (Fredericks et al., 2016). The data are from two surveys, one terrestrial and the other shallow water, made in 2014 (Table 1). The resulting base maps are presented with a Universal Transverse Mercator grid, with northings and eastings in zone 20N.

SETTING

Offshore Features North of the Island

Bathymetry

Anegada is situated on the north edge of a shelf that is perched south of the Puerto Rico Trench. Along a bathymetric profile proceeding southward from an Atlantic abyssal plain 5–6 km below sea level, the outer rise descends across fault scarps on the outer trench wall, reaches the trench floor at water depths of 8 km, rises from there to the vicinity of the island's north shore, and continues south of the island on a shelf a few tens of meters deep (Fig. 1B).

Fringing Reef and Reef Flat

The north side of Anegada, facing the Atlantic Ocean, is fringed by a coral reef. The reef extends along most of the 17 km length of the island and continues another 15 km farther southeast. The seaward edge of the reef, at 10–20 m water depth, forms a smooth west to southeast arc. Breaking waves mark a discontinuous reef crest (Fig. 2A), as further delineated by shallow-water lidar data from 2014 (Table 1; Fig. 2B). The reef is separated from the island's north shore by a reef flat, a few meters deep at most, that extends 100–1500 m perpendicular to shore. The fringing reef has probably existed throughout the past few thousand years, as judged from the greatest of the 27 radiocarbon ages obtained on coral clasts found inland (Table 2, sample 32). This age, 1960 ± 60 radiocarbon years before 1950 CE (^{14}C yr B.P.), corresponds to the range 216–550 cal yr CE.

Coral taxa of the fringing reef and the reef flat, when surveyed in the 1970s by Dunne and Brown (1979), included the brain coral *Diploria strigosa* (Fig. A5), the boulder star coral *Montastraea* (now *Orbicella*) *annularis* (Fig. A6), the mustard hill coral *Porites astreoides* (Fig. A7), and the elkhorn coral *Acropora palmata* (Fig. A8). Despite losses of coral cover on Caribbean reefs since the 1970s (Gardner et al., 2003), we found living colonies of all these species near Anegada's shore in the past few years. All these taxa are represented in the pre-Columbian deposits described in this paper.

Those pre-Columbian deposits also include two edible mollusks that today inhabit the reef flat. The conch *Strombus gigas*, still harvested today, was noted on the reef flat north of the island in the 1970s (Dunne and Brown, 1979), and is represented in pre-Columbian shell mounds at the East End (Schomburgk, 1832; Davis and Oldfield, 2003), remains a local food source. We found juveniles of the tiger lucine *Codakia orbicularis* living in sand of the reef flat of Windlass Bight in 2016 (Fig. A9). Near the Florida Keys, this bivalve is most abundant in shallows of the passages between islands, in similarly open marine conditions (Perkins and Turney, 1972). In the southern Caribbean, *C. orbicularis* was part of the diet of pre-Columbian peoples in Grenada (Giovas, 2013).

Synonyms at the genus level have been widely used for two of these species. *Orbicella annularis* was known as *Montastraea annularis* before molecular and morphological revision of reef-coral taxonomy (Budd et al., 2012). The alternatives to *Strombus* in *S. gigas* include *Lobatus* and *Eustrombus* (National Marine Fisheries Service, 2014; National Marine Fisheries Service, undated). The paper uses *Orbicella annularis* and *S. gigas*.

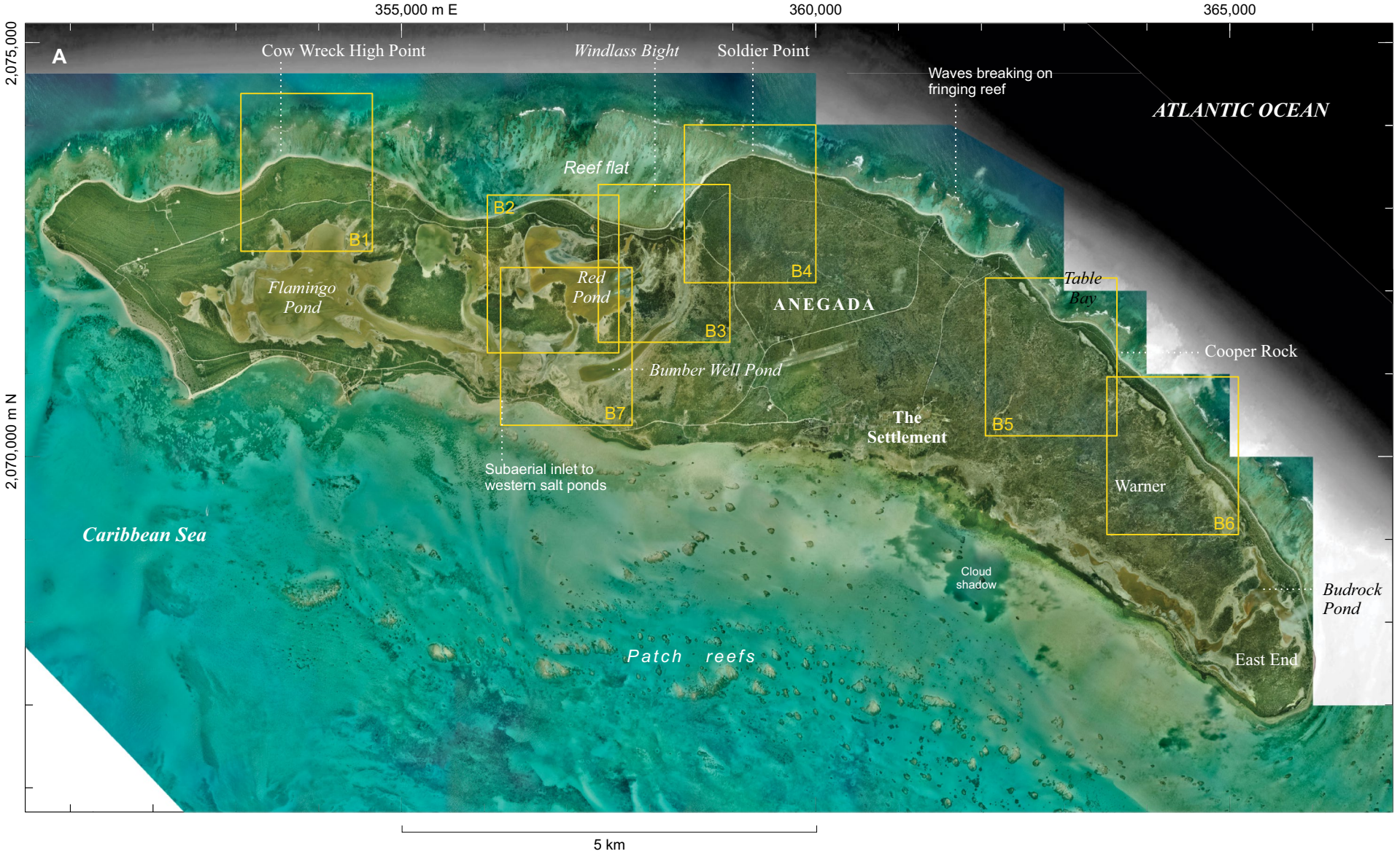

Figure 2 (*on this and following page*). Overviews of Anegada. (A) Mosaic of air photos taken 2002. Locations of Figures B1–B7 are indicated.

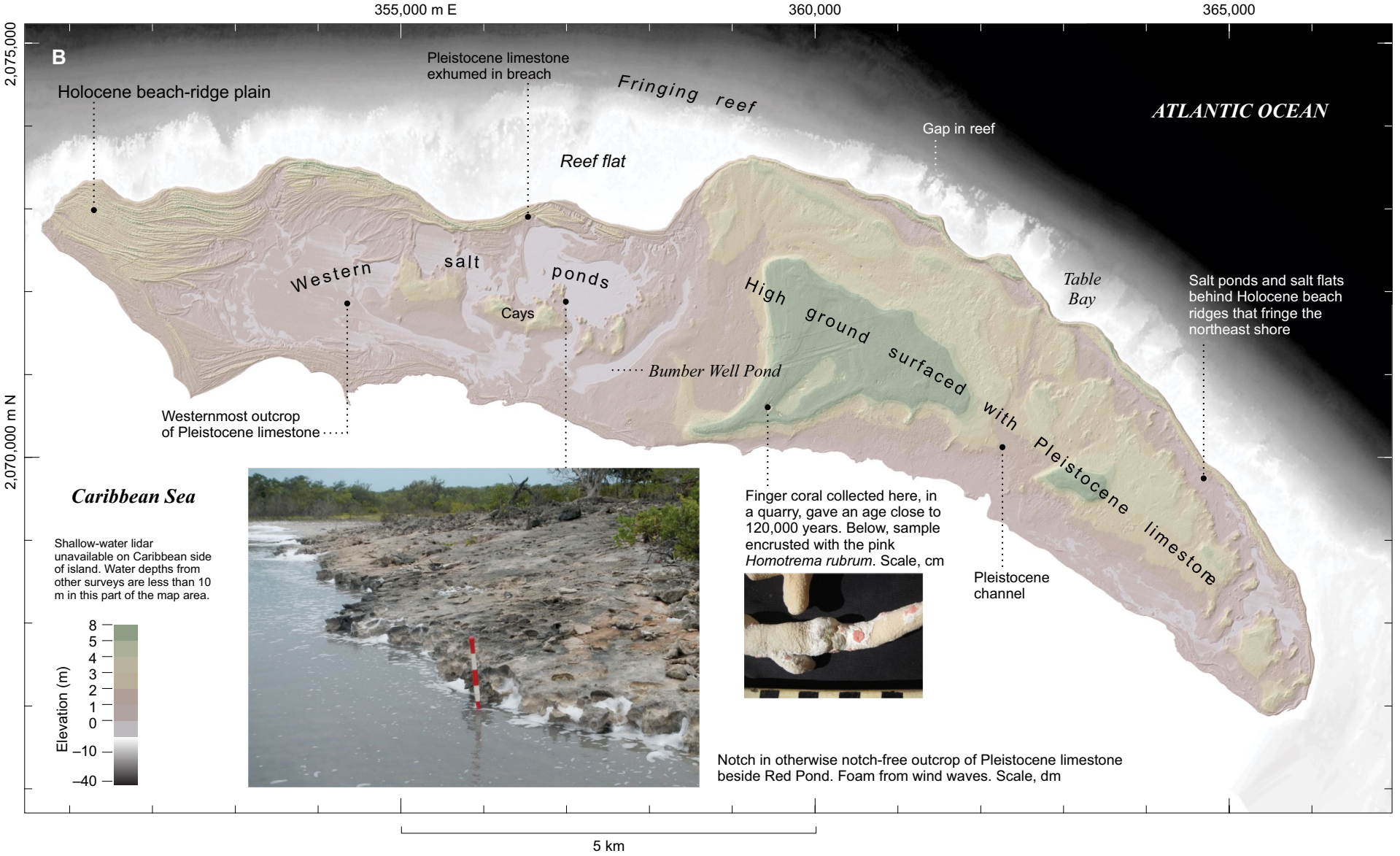

Figure 2 (*continued*). (B) Physiography and generalized geology on base map of bare-earth lidar (light detection and ranging) topography and shallow-water lidar bathymetry (Table 1).

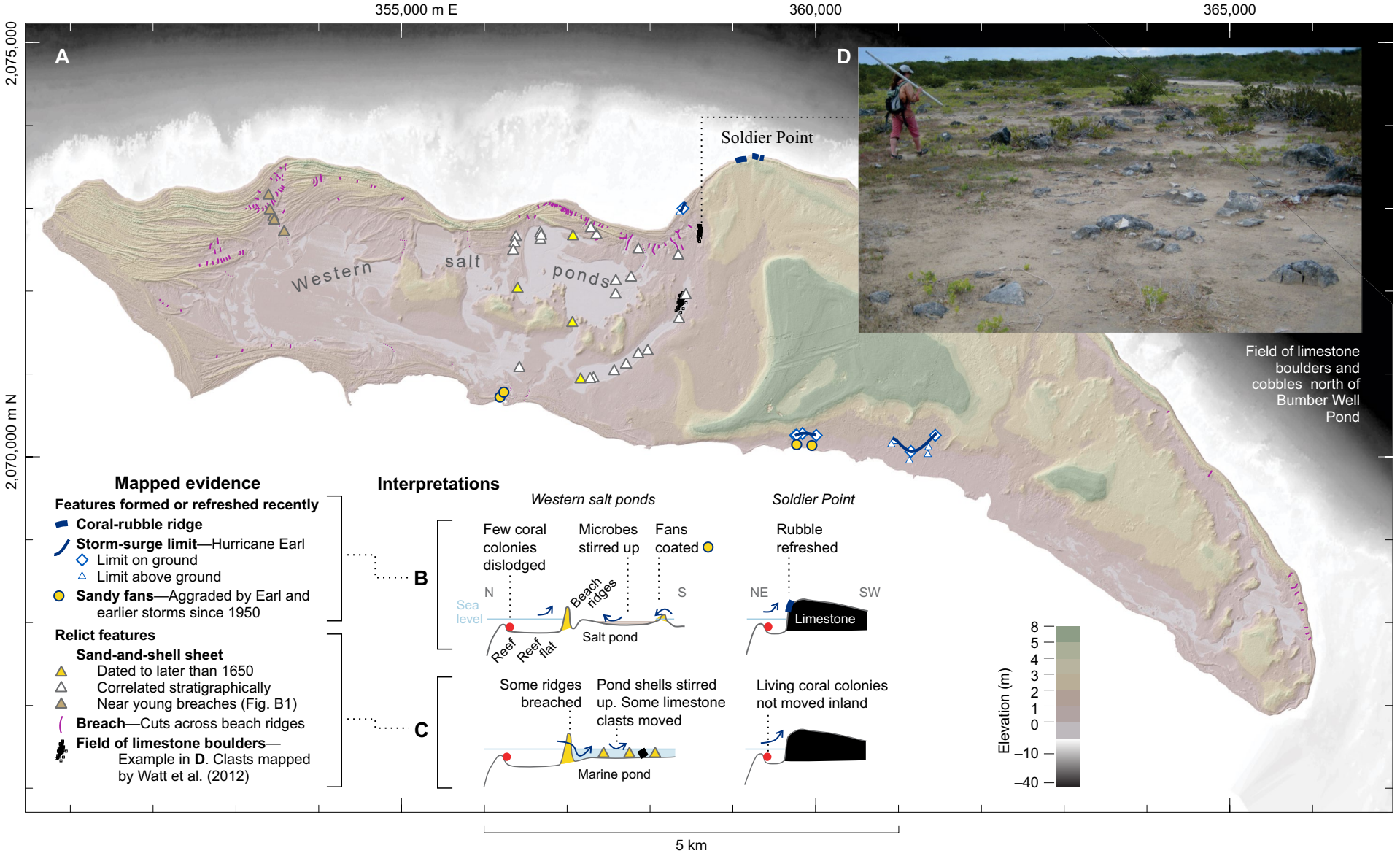

Figure 3. Evidence for extreme waves dated mostly to the centuries since 1492 CE (post-Columbian time). Observed mainly in 2008 and 2009, and during later surveys of the effects of a 2010 storm. (A) Mapped distribution. (B) Schematic interpretation of evidence assigned to recent storms. (C) Schematic interpretation of evidence assigned to an unusual storm or a tsunami in 1650–1800 cal yr CE. (D) Example of a boulder field in C.

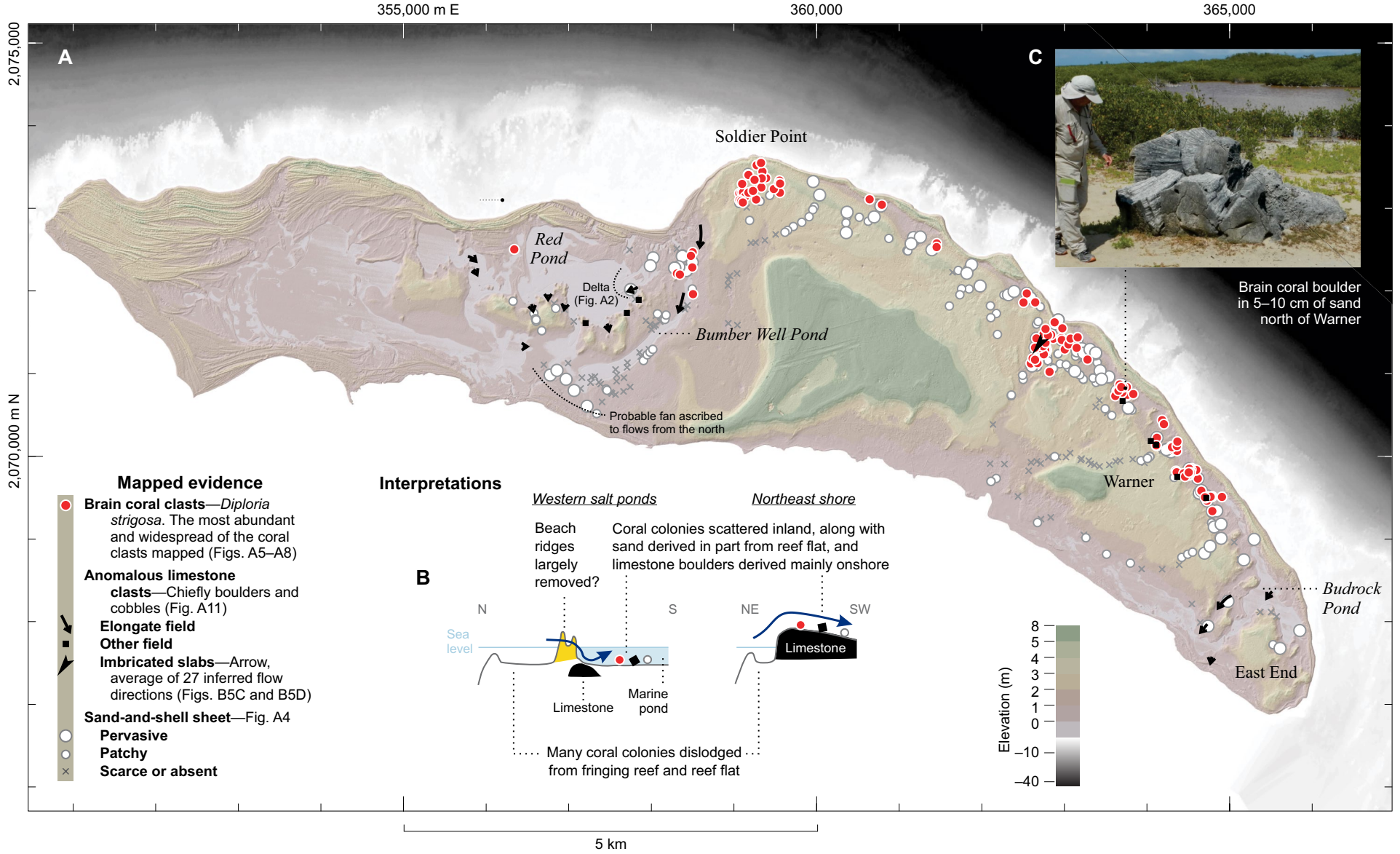

Figure 4. Evidence for extreme waves of pre-Columbian age, from findings in 2011–2016. (A) Mapped distribution, with coral clasts limited to brain coral for legibility. (B) Schematic interpretation of evidence assigned to an extraordinary storm or a tsunami of nearby origin. (C) Largest coral clast mapped.

The tide range at Anegada is <0.5 m. The range at Tortola, 50 km to the southwest (Fig. 1C), is similarly small in official predictions discontinued after 2013 (http://www.ntslf.org/sites/ntslf/files/pdf/predictions/Tortola_2013_+0400.pdf). Tide ranges were measured at Anegada during a day in 2008 and across one week in 2009, in support of geological studies (Atwater et al., 2012; Watt et al., 2012).

Landforms, Surficial Geology, and Human Settlement

Many of the landforms of Anegada, although partly obscured by trees and shrubs, are apparent in bare-earth topography computed from the terrestrial lidar survey in 2014 (Figs. 2B and 6). The entire island is <9 m above sea level. Pleistocene deposits in the east underlie benches above the 5 m contour. Salt ponds in the east are hemmed in between a narrow line of Holocene beach ridges and high ground underlain by Pleistocene deposits. Larger salt ponds occupy much of the island's western interior at elevations at or slightly below mean sea level. The western ponds adjoin knolls of Pleistocene deposits and are mostly enclosed by Holocene beach ridges. Additional beach ridges extend westward beyond the western ponds.

Pleistocene Deposits

The island's Pleistocene deposits consist of shallow-water carbonate deposits of reefs, beaches, and channels. Reefs are abundantly evidenced by coral skeletons preserved in surficial limestone (Dunne and Brown, 1979). A beach is marked by imbricated slabs of beach rock in the quarry plotted in Figure 2B. Relict channels trending across Anegada, between its Atlantic and Caribbean sides, are evidenced by the topographic trough holding Bumber Well Pond and, most distinctly, by a meandering, branching topographic low south of Table Bay (Fig. 2B and profile F-F′ of Fig. 6). Landforms of the Pleistocene deposits also include the limestone knolls that form high ground and localized coarse-clast sources within and among the western salt ponds. Many such knolls can be seen in shaded relief in Figures B2B and B3B.

A finger coral specimen from the Pleistocene deposits has been dated to marine oxygen isotope stage 5e by uranium series methods. Well-preserved specimens of *Porites furcata* were collected from unconsolidated Pleistocene deposits in the wall of a quarry ~3 m below the natural ground surface of the largest area of high ground southeast of Bumber Well Pond (Fig. 2B). The specimens evidently formed near their former sea level; they are conformably overlain by a unit containing imbricated slabs of beach rock. Some of these coral clasts retain pink encrustations of the reef-dwelling protozoan *Homotrema rubrum*. The age of one of the specimens was measured by William G. Thompson of Woods Hole Oceanographic Institution. Thompson's reported age of 121,110 ± 166 yr (2 standard deviations) includes corrections for measured evidence of exchange of U and Th with the environment. Details can be found in Atwater et al. (2014, Fig. S2 therein).

Subaerial weathering since the last interglaciation has cemented the uppermost 1–2 m of the Pleistocene deposits. The resulting limestone pavement armors most of eastern Anegada and forms a hard substrate, at depths rarely more than 2 m below present sea level, that underlies Holocene beach ridges, salt flats, and salt ponds as far west as Red Pond (example beneath a salt flat, Fig. B3C). The limestone is pitted from dissolution and is widely pocked with sinkholes (Fig. B4B). The pavement is typically broken into slabs and blocks, and the breaks commonly coincide with roots of trees and shrubs.

Holocene Beach Ridges and Ponds

Bioclastic sand forms numerous beach ridges at Anegada (Fig. 2B). The ridges are fewer in the east, where they line the shore, than in the west, where they have accreted outward from the interior and have built the island 3 km beyond the westernmost limestone knolls. The highest of the ridges in the west are between 5 and 8 m above sea level (Figs. B1B, B1D). The ridges are founded on gently dipping, locally pebbly layers deposited by waves. A cross-bedded, probably eolian cap is exposed on eroding parts of the north shore and in sand pits (including the pit labeled in Fig. B3B). Many of the sand grains are pink from *Homotrema rubrum* derived from the fringing reef and the reef flat (Pilarczyk and Reinhardt, 2012). Longshore drift, driven by prevailing easterly winds, probably accounts for the island's westward accretion (Schomburgk, 1832).

Salt ponds and their microbial mats occupy low areas, near sea level, that make up much of the island's western half. The hydrology and microbial biology of these western ponds were examined by Jarecki and Walkey (2006); they found that the most saline of the large western ponds attain dry-season salinities of 250 parts per thousand; that the large western ponds merge when engorged by rain; that the areas flooded intermittently form seasonal salt flats with patchy mangroves; and that at least one of the ponds is connected to the sea more by percolation than by a tiny inlet on the south shore (location noted in Fig. 2A).

We doubt that the western ponds had an additional inlet, on the north shore, in the early 1800s. Such an inlet was reported by Schomburgk (1832, p. 158), who surveyed Anegada in 1831; writing of the western salt ponds, he stated that "a junction with the sea" had existed on the island's northern side until "the hurricane of 1819 stopped its passage." The island map in Schomburgk (1832) suggests that this inlet was north of Flamingo Pond. The mapped inlet, however, is not apparent in lidar topography of this area, which instead shows a complex of breaches and beach ridges between Flamingo Pond and the sea (Figs. B1A, B1B). Perhaps rain from the 1819 hurricane ponded in this area.

The main western salt ponds are vestiges of a single, merged pond, with an inlet probably large enough for salinities to remain close to that of ocean water, that occupied much of the area of western Anegada for thousands of years. This bygone marine pond is evidenced by muddy deposits that contain cerithid gastropods and other mollusks (Reinhardt et al., 2012). It was replaced by salt ponds, to the complete exclusion of this molluscan assemblage, at a time indistinguishable from an overwash event in 1650–1800 cal yr CE (Atwater

et al., 2012, p. 74, 78). This timing is evidenced by stratigraphic superposition: the sand and shell sheet of 1650–1800 separates marine pond deposits below from salt-pond deposits above (Bumber Well photos in Fig. A3).

The island was first called *anegada*, Spanish for flooded, in 1493, during Columbus's second voyage (Morison, 1942, v. 2, p. 78, 98). The name does not necessarily refer to the bygone marine pond, which might have been difficult to see from ships that remained outside the fringing reef on the north or beyond patch reefs to the island's south. However, stratigraphy and paleoecology suggest that a marine pond covered much of western Anegada in 1493 and that such a pond persisted until the overwash event of 1650–1800 (Atwater et al., 2012).

The bygone marine pond likely accounts for a shoreline notch cut into Pleistocene limestone at an elevation close to present mean sea level. The notch, probably cut in part by endolithic bacteria, is conspicuous on some of the margins of the western salt ponds (Fig. 2B). No higher shoreline notch is evident at Anegada (Atwater et al., 2012, p. 62). Accordingly, we infer that the catastrophic inundation of Anegada in 1200–1480 cal yr CE took place when the island's relative sea level was ordinarily no higher than it is today.

Early Historical Records

Anegada's documented history of post-Columbian settlement begins in 1776 or 1784 (Dookhan, 1975; Pickering, 1983; Faulkner, 2005; Atwater et al., 2012; supplementary text ESMT-1 therein). A Methodist church counted 82 Anegadian members in 1796 (Pickering, 1983). A nautical survey in 1811 tabulated the island's human population as 197 and noted production of livestock and cotton (Blachford, 1813).

Schomburgk (1832) reported that some of the island's trees had been logged, and that some areas were devoted to crops or grazing. Areas he mapped as farmed correspond today to areas laced with stone walls, many of them overgrown (Figs. B4F, B5C, and B5D). Most of the island's permanent population, then as now, resided in the place known as The Settlement (location, Fig. 2A).

Exposure to Extreme Waves

Physiographic setting predisposes Anegada's north shore (its Atlantic side, facing the Puerto Rico Trench) more to flooding by a tsunami than to flooding by an ordinary hurricane. Frequency of occurrence of course exposes the island overwhelmingly to storms. But in case of either a tsunami or a storm, how would inundation from each be affected by the deep water and the fringing reef north of the island? In the possibilities considered herein, the focus is on the north shore because the most dramatic of the island's extreme-wave evidence extends inland from there (Fig. 4). The potential causes of flooding from the north include tsunami-like bores comparable to those generated in the Philippines during 2013 Typhoon Haiyan.

Tsunamis of Remote Origin

The written history of human settlement at Anegada begins a few decades after the Caribbean's most widely documented tsunami, the transatlantic waves of the 1755 Lisbon tsunami. As summarized in Figure 1A, these far-traveled waves were noted in the Lesser Antilles, Hispaniola, and Cuba, and its effects exceeded those of the Lisbon tsunami of 1761 (Lander et al., 2002; Barkan et al., 2009; Roger et al., 2010, 2011).

In the concluding section, "Inferred History of Extreme Waves," we speculate that the 1755 tsunami accounts for geological evidence summarized in Figures 3 and A3. This evidence, as reported previously (Atwater et al., 2012; Pilarczyk and Reinhardt, 2012; Reinhardt et al., 2012), suggests that Atlantic waters poured southward into the interior of western Anegada in 1650–1800 cal yr CE.

Hypothetical Tsunamis from the Puerto Rico Trench

The deep water north of Anegada should facilitate tsunami inundation across the island's north shore. A hypothetical tsunami advancing southward from a source in the Puerto Rico Trench remains in deep water until it closely approaches the island (Fig. 1B). Traversing this deep water extracts less energy than would shoaling on the shelf to the island's south. Simulated tsunamis generated by faulting in the Puerto Rico Trench produce extensive flooding of northern Anegada (Buckley et al., 2012).

The fringing reef to the island's north fails to prevent this extensive flooding in the simulations of Buckley et al. (2012). In simulations for other places, onshore inundation was found to be reduced by generic reefs (Kunkel et al., 2006) or to vary with reef parameters (Roger et al., 2014), or to increase in onshore height and inundation distance after crossing a fringing reef in American Samoa (Gelfenbaum et al., 2011).

Storm Surge from Atmospheric Pressure and Wind

In contrast with its effect on an incident tsunami, the deep water north of Anegada should limit storm surge from set-up by wind. When setting up a storm surge, surface wind stress is resisted by the entire water column, a resistance greater in deep water than in shallow water. Computed storm surge is accordingly smaller in the deep water to Anegada's north than on the shelf to the south (Caribbean Disaster Mitigation Project, 2002).

Storm surges observed at Anegada are consistent with these expectations. The main example documented is from 2010 Hurricane Earl (Atwater et al., 2014). This storm was at category 4 when it passed 30 km north of the island (Fig. 1A). Its surge reached elevations of 1 m along the south shore, as judged from wrack lines and eyewitness accounts in The Settlement and from wrack surveyed beside nearby spillover fans (Figs. 3 and A1; profiles D-D′ and E-E′,

Fig. 6). In the north, wrack beside Windlass Bight marked a high-water line that was surveyed as approaching 2 m above sea level, but this line represents the combined effects of surge and swash (Fig. B3B; profile C-C′ of Fig. 6).

In the absence of tsunami-like bores, storm effects on Anegada's north shore may be further limited by the presence of a fringing reef and the reef flat. In a simulated hurricane of category 5 at Anegada, the storm surge from atmospheric pressure and wind set-up is 1 m off the island's north shore, and the storm waves break on the fringing reef and dissipate further across the reef flat (Buckley et al., 2012).

Eyewitness observations of the storm surge from 1960 Hurricane Donna are available for the south shore only. Donna was at category 3 or 4 when its eye passed over Anegada. Its reported winds blew counterclockwise, from the north as the storm approached, and from the southwest after the eye had passed. Smooth water of a storm surge entered The Settlement only after the eye had passed, according to eyewitnesses interviewed in 2008 and 2009. This surge reached 2.5 m above sea level at reference points later surveyed by differential global positioning system (Atwater et al., 2012), and it extended several hundred meters farther inland than did the surge from Hurricane Earl (Fig. A1). A Donna limit in The Settlement is 1.5 m above the sea-level datum of the terrestrial lidar survey (Fig. 6, profile E-E′).

Tsunami-Like Bores Analogous to Those from Typhoon Haiyan

Parts of the Pacific coast of Eastern Samar, in the Philippines, resemble the north shore of Anegada in that they are protected from wind-driven storm surge by the deep water of a nearby trench, and from ordinary storm waves by a fringing reef. This coast was abundantly flooded, however, during 2013 Typhoon Haiyan (Shimozono et al., 2015; Kennedy et al., 2016; Soria et al., 2016). The Eastern Samar town of Hernani was entered by three or four bores recorded on video (Roeber and Bricker, 2015). The flooding during each bore was on the order of minutes; the bores were intermediate in period between a storm wave (tens of seconds) and a tsunami wave (tens of minutes).

These tsunami-like effects of an unusually large tropical cyclone have been explored with numerical models (Shimozono et al., 2015; Roeber and Bricker, 2015; Kennedy et al., 2016). In simulations for Hernani, sets of large waves alternate with sets of smaller waves that produce tsunami-like bores by interacting with the fringing reef and the reef flat. More generically the phenomenon is known as surf beat, infragravity waves, or wave group run-up. In model runs with Philippine storms of various sizes, the fringing reef protects the shore from incident waves of lesser storms as much as half the intensity (central pressure and maximum wind speed) of Typhoon Haiyan. In additional model runs with various reef widths, wave effects greater than Haiyan's were obtained for reef widths that produce resonance with surf beat (Roeber and Bricker, 2015). Such Haiyan-like effects have not yet been modeled for Anegada.

PREVIOUS WORK

Previous studies at Anegada have documented geological evidence of recent storms and assorted geological evidence for greater overwash in 1650–1800 cal yr CE (Fig. 3). The following review, updated with new findings about this post-Columbian overwash, highlights discrepancies that are resolved in subsequent parts of the report by inference of greater overwash in pre-Columbian time (Fig. 4).

Traces of Recent Storms

Geological effects of 2010 Hurricane Earl were examined at Anegada in February 2011, six months post-storm, with surveys of high-water lines and of predominantly fine-grained deposits (Atwater et al., 2014). The storm's effects were considered further in 2013 and 2015 with studies of a coral rubble ridge (Spiske and Halley, 2014; Spiske, 2016).

Microbial Debris, Sand, and Mud

The fine-grained deposits noted in 2011 consisted of widespread microbial debris and localized sand and mud. The microbial debris formed a desiccating layer, a few centimeters thick at most, on salt flats beside salt ponds from which the debris was likely derived. The layer probably consisted of microbial cells and their extracellular polymeric substances that storm waves had stirred up. The layer was drying as chips in 2011 (Figs. A1 and B2C), and these became progressively less evident in subsequent years.

The microbial debris affords comparisons, at the same place, between modern storm deposits and the island's pre-Columbian fields of scattered coarse clasts. The microbial debris, derived from the island's interior, contrasts starkly with boulders that the debris surrounded (Atwater et al., 2014, Fig. S6 therein). For example, microbial debris from Hurricane Earl coated salt flats from where stray coral boulders protrude (Figs. B2C and B6D).

The localized sand and mud accumulated on spillover fans that extend a few tens of meters inland from the island's south shore west of The Settlement (Figs. 3 and A1). A new fan deposit, consisting of sand and lime mud 10 cm thick at most, was found on top of a black microbial mat. Pit walls revealed underlying sand sheets intercalated with earlier microbial layers. Leaves in the earlier mat layers were found to contain post-bomb levels of ^{14}C; the leaves gave ages mostly younger than 1950 cal yr CE (Atwater et al., 2014, Figs. S4 and S5 therein).

Coral Rubble

The coral rubble ridge on Anegada's north shore differs from the fields of scattered coral clasts in landscape position, internal structure, clast size, clast composition, and age. Here we summarize published descriptions (Spiske and Halley, 2014; Spiske, 2016), cite ridge clast ages obtained by Xu et al. (2015), and briefly compare the ridge with storm deposits on rocky coasts elsewhere.

Ridge at Soldier Point. A coral rubble ridge extends discontinuously along ~1.5 km of Anegada's north shore, at and near Soldier Point (map views, Figs. 3 and B4B; field photos, Figs. A1 and B4E). In fair weather it is separated from the water's edge by a mostly bare platform of Pleistocene limestone as much as 10 m wide. The ridge has a maximum measured width of 15 m and a crest elevation as high as 3.5 m. The seaward side of the ridge slopes more steeply than its landward side; local slumps probably contribute to steepness on the seaward side. The ridge is outboard (north) of a higher limestone surface that crests nearly 4 m above sea level to the south (Fig. 6; Table 3, profile D-D′).

The internal deposits and structure of the ridge were examined in a trench (location in Fig. B4B). The deposits are as thick as 0.8 m, and consist mainly of coral rubble that is rounded, encrusted, and bored (brain coral examples photographed nearby; Fig. A3F). The dominant coral genus was *Acropora*. Also noted were minor conch shells, serpulid rock, beach rock, and karstified Pleistocene limestone. The clast diameters, in centimeters, averaged 16 cm by 11 cm by 4 cm, and the largest measured was 75 cm by 40 cm by 5 cm. Coarse clasts support the ridge, without interstitial sand, and show seaward-dipping imbrication.

The coral rubble locally continues a few tens of meters inland from the ridge as scattered clasts. The landward margin of the ridge usually coincides with ground-covering plants (Fig. 3) that obscure the rubble limit and probably impede rubble transport (Spiske and Halley, 2014). However, 180 m west of the trench site, coral rubble of cobble size extends as much as 50 m inland through a gap in vegetation. Here the remains of a stone wall approach the north shore (Fig. B4F), and the most inland of the rubble extends to these remains.

Storms routinely refresh the ridge. The ridge accretion was at first thought infrequent because the subaerially exposed rubble surfaces are gray (Spiske and Halley, 2014). This patina, ascribed to endolithic bacteria, was assumed to represent tens of years of subaerial exposure. Ridge-altering storms were therefore supposed greater than 2010 Hurricane Earl. However, the trench dug in 2013, and left open at that time, was found in 2015 to have been partly filled (Spiske, 2016). In addition, clasts at the trench-fill surface had already turned gray. These findings showed that the coral rubble ridge had been both refreshed and newly weathered between 2013 and 2015.

Recent deposition is further evidenced by boulder ages. Xu et al. (2015) sampled the coral rubble ridge at Soldier Point to assess Sr/Ca ratios in skeletons of the brain coral *D. strigosa* as indicators of sea-surface temperatures. Xu et al. (2015) cored three of the freshest-looking coral boulders, and dated the cores by means of uranium-series dating (two boulders), pattern matching of growth-band density (among all three boulders), and further matching with patterns of sea-surface temperatures observed elsewhere (three boulders). The outermost growth band of one of the boulders was found to represent 1976. In each of the other two boulders the outermost growth band was assigned to 2008.

Comparison with storm deposits on other coasts. The coral rubble ridge at Soldier Point has the internal structure and external form of storm deposits on other rocky shores (Spiske and Halley, 2014). The hundreds of waves in a storm commonly organize coarse clasts as the imbricated framework of a shore-parallel ridge, an effect neither known nor expected from tsunamis (Weiss, 2012; Terry et al., 2013, p. 64–65). Modern storms have refreshed bouldery coastal ridges in Ireland (Hall et al., 2006; Knight and Burningham, 2011; Cox et al., 2012), Iceland (Etienne and Paris, 2010), France (Fichaut and Suanez, 2011), Hawaii (Richmond et al., 2011), and the southeast Caribbean (Morton et al., 2008).

These coastal, shore-parallel ridges contrast with the inland fields of scattered or clustered boulders and cobbles that the comparatively few waves in a tsunami have produced (Paris et al., 2009; Etienne et al., 2011; Goto et al., 2011; Richmond et al., 2011; Yamada et al., 2014). However, inland fields of scattered coarse clasts have also resulted from storms in settings similar to Anegada's north shore. In the Philippines, flooding from the sea during Typhoon Haiyan shifted isolated boulders a few tens of meters on a shore behind a fringing reef (May et al., 2015) and deposited limestone boulders 1 m in diameter as much as 150 m from the shore (Kennedy et al., 2016). Near Okinawa, storms and tsunamis have both moved boulders from a fringing reef onto a reef flat; the main difference is distance of transport, thought greater for a 1771 tsunami than for subsequent typhoons (Araoka et al., 2010; Goto et al., 2010a, 2010b). Inland fields of scattered coarse clasts have been documented, in addition, in northwestern France, where boulders quarried and scattered by giant historical waves extend a few hundred meters downslope in the lee of a coastal cliff top (Fichaut and Suanez, 2011).

Evidence for Unusual Overwash

Evidence for unusual flooding from the north was previously reported from Anegada's western salt ponds and their margins. The findings were based on field work in 2008 and 2009, and on related laboratory work and modeling, and they were reported in a set of papers dated 2012. The field observations focused on breaches in the northern beach ridges and on two kinds of deposits to their south that were mapped chiefly at and below sea level: a sand and shell sheet, and inland fields of scattered limestone boulders and cobbles. The various lines of evidence, summarized in Figure 3, were presented in an introductory paper (Atwater et al., 2012), in paleontological reports on the sand and shell sheet (Reinhardt et al., 2012; Pilarczyk and Reinhardt, 2012), and in papers that describe the scattered limestone clasts (Watt et al., 2012) and model their emplacement (Buckley et al., 2012).

Nearly all this initial evidence was ascribed, by Occam's razor, to a single storm or tsunami in 1650–1800 cal yr CE. This simplification leads to contradictions that are highlighted in this section, and that are resolved thereafter by evidence, found chiefly since 2009 and summarized in Figure 4, for truly catastrophic overwash in 1200–1480 cal yr CE.

Breaches in Beach Ridges

Breaches transect beach ridges and overwash fans of Anegada's north shore (Figs. 3, A2, B1A–B1D, B2A, B2B, B3A, and B3B). The deepest breaches hold salt ponds that likely began as plunge pools. Shallower breaches are

marked by seasonally flooded salt flats, and still shallower breaches contain mangroves.

Evidence for multiple times of breaching. Two sets of breaches at Anegada are evident in bare-earth lidar topography south of Cow Wreck High Point (Fig. B1B). Their seaward limits are distinctly separated by geomorphic superposition of ridges on this accretionary part of the island. The inner, earlier set of breaches coincides with a muted beach-ridge topography that may represent decapitation of ridges by sheet-like overflow (seen also northwest of Red Pond; Fig. B2B). An inner set of breaches was previously mapped southeast of Cow Wreck High Point on the basis of air-photo interpretation (Atwater et al., 2012, Fig. 2B therein), but those inferred breaches are disallowed by intact ridges now seen in lidar (Figs. B1A, B1B).

Two times of breaching are less evident geomorphically in the narrower beach-ridge plain farther east beside Red Pond and Bumber Well Pond (Figs. B2B and B3B). In this area, breaches cut in pre-Columbian time might have been reused in post-Columbian time. Stratigraphic evidence for such multiple use, noticed in reconnaissance (Atwater et al., 2012, p. 75 therein), is beyond the scope of this paper.

Post-Columbian age of a younger time of breaching. The younger set of breaches south of Cow Wreck High Point probably dates to post-Columbian time, according to limiting radiocarbon ages obtained in the past few years.

Pieces of the staghorn coral *A. cervicornis* were mapped in an area south of the point, and ages were measured on four pieces that retained branches (Fig. B1). Most of the mapped pieces track the tall beach ridges in the northeast and their projected extension to the southwest. The pieces stand in beach-ridge sand as if exhumed from it, rather than deposited on top of it. We therefore infer that storms deposited the staghorn pieces during construction of the ridges.

Two of the dated pieces were collected from a beach ridge that is conspicuously breached to the northeast and to the southwest. The younger of these gave an age corresponding to 1479–1672 cal yr CE. The breaching likely occurred after this interval and may therefore correlate with deposition of the sand and shell sheet of 1650–1800 cal yr CE (Fig. 5). Sand deposits that may correlate with this sheet have been found along the low-altitude path inland from the dated breach (Fig. 6, profile A-A'; field photo, Fig. A3).

Examples of breaches on other shores. The various breaches at Anegada can be compared to breaches elsewhere that have been cut during storms or tsunamis. In some cases these breaches on other shores were used more than once.

During a hurricane in Texas, overtopping of a barrier island created dozens of breaches, particularly where the storm surge covered all but the highest dunes (Suter et al., 1982). The large breaches, upon emerging from constrictions, splayed landward as distributary channels of washover fans. Some of the breaches followed paths cut in prior storms. In a more recent example, 2012 Hurricane Sandy cut breaches tens of meters across a sandy barrier in New Jersey (Irish et al., 2013).

Tsunamis in 1960, 2004, and 2011 are among those known to have cut through sandy beach ridges. The 1960 Chilean tsunami poured through Chilean beach ridges (Atwater et al., 2013) and breached paddy-field berms in Japan (Kon'no et al., 1961). Some of the Chilean breaches had also been used by tsunamis in previous centuries. The 2004 Indian Ocean tsunami cut and/or widened breaches in Thailand, Sri Lanka, and Indonesia (Choowong et al., 2007; Goff et al., 2007, p. 11, 29, 31; Fagherazzi and Du, 2008; Jankaew et al., 2008, Fig. S1 therein; Liew et al., 2010; Kain et al., 2014). Along the Japan Trench, breaches in beach ridges have been correlated with a documented tsunami of 1454 (Sawai et al., 2015), and sand spits were breached by the catastrophic tsunami of 2011 (Tanaka et al., 2012).

Sand and Shell Sheet

A layer of sand and shells extends beneath and beside the western salt ponds as much as 1.5 km south from the breached ridges (Figs. 3 and A3). Its thickness is mostly in the range 1–25 cm. The sheet is preserved best beneath microbial mats of perennial parts of the salt ponds. These areas lack crab burrows that commonly homogenize deposits beneath the seasonally flooded salt flats.

Composition. The sand is chiefly bioclastic in the north and pelletal in the south. The bioclastic sand includes pink *Homotrema rubrum* grains that were ultimately derived from the reef or the reef flat, but that may have been sourced more immediately from breaching of the north-shore beach ridges (Pilarczyk and Reinhardt, 2012). The pelletal grains could have been suspended from deposits of the interior marine pond.

Also present, where the sheet extends beneath the length of Bumber Well Pond, are angular grains, granules, and pebbles of limestone (dark gray in lower close-up photo, Fig. A3). Similar limestone clasts today litter limestone pavements that flank the pond.

The shell assemblage in the sheet resembles that of the underlying marine pond deposits (Reinhardt et al., 2012). As in those deposits, the main taxa of the sheet are cerithid gastropods (*Cerithium variabile*, *Cerithidea beattyi*, *Cerithium eburneum*, *Batillaria minima*), small bivalves (*Anomalocardia brasiliana*, *Anomalocardia cunimeris*), and bubble shells (*Bulla striata*). Many of the bivalves are articulated. It is unlikely that any of these molluscan species derived from settings as exposed to the sea as the reef flat. Similar assemblages have been found, instead, on muddy flats on the landward side of the Florida Keys (Perkins and Turney, 1972).

Where overlain by microbial mat layers of salt ponds, the sand and shell sheet includes an uppermost layer of lime mud a few centimeters thick. The lime mud commonly contains mangrove leaves and crab claws, and its contact with the mats locally coincides with a white crust a few millimeters thick (Atwater et al., 2012, Fig. 8 therein).

Numerical and relative ages. Radiocarbon dating and negative historical evidence together bracket the sand and shell sheet in the range 1650–

1800 cal yr CE. Emplacement not before 1650 cal yr CE, at two standard deviations, is shown by radiocarbon ages of mangrove leaves and a twig in the mud cap (Atwater et al., 2012, Fig. 8 therein). The most definitive of these samples were obtained from margins of Red Pond and Bumber Well Pond (Figs. 5A and A3). Emplacement after 1800 is unlikely because no extensive sand or shell deposits have resulted from Anegadan storms of the past 65 years or more, and because there are ample reasons to doubt Schomburgk's (1832) secondhand report that a hurricane in 1819 closed a northern inlet to a western salt pond (details in "Traces of Recent Storms" and "Holocene Beach Ridges and Ponds," respectively).

By relative dating, deposition of the sand and shell sheet coincided with demise of the marine pond with its conversion into salt ponds (reviewed in "Holocene Beach Ridges and Ponds"). Shelly marine pond deposits are overlain by the sand and shell sheet, which in turn is overlain by microbial mats (Fig. 3). The hypersaline waters of the salt ponds excluded the marine pond mollusks, which have yet to return to the western interior of Anegada (Jarecki, 2003).

Interpretations. The sand and shell sheet might represent tsunami overwash, hurricane overwash, waves generated inside the marine pond, and the opening of tidal channels. Reinhardt et al. (2012) found that among these possibilities, tsunami overwash best explains this sheet's lateral extent and form. Citing provenance of the shells and preservation of articulated bivalves, they inferred that the overwash widely eroded and winnowed bottom sediments of the bygone marine pond.

Reinhardt et al. (2012) puzzled over this exclusively inland provenance of the shells in the sheet. They expected a tsunami that poured across Anegada from the north to have introduced shells from the reef flat, and made an analogy with a lagoon in Oman where tsunami overwash is evidenced by allochthonous shells derived from offshore (Donato et al., 2008). Many of the shells in the Omani case remain articulated, and many are sharply broken but otherwise fresh, in contrast to bored and disarticulated shells of the lagoon.

At Anegada, during the field work of 2008 and 2009, several coarse clasts derived from the reef flat, or from the reef, were found in the area of the sand and shell sheet, but were not given due weight. They include a boulder of the brain coral *D. strigosa* north of Bumber Well Pond (Figs. A5 and B3C; Atwater et al., 2012, supplementary figure ESMF-7 therein); a larger brain coral colony protruding from a salt flat west of Red Pond (Figs. B2C–B2E); and articulated and disarticulated valves of the tiger lucine *C. orbicularis* beside northeastern Red Pond (photo, Fig. A3).

Herein we show that both clasts of these kinds consistently predate the sand and shell sheet by several centuries. In contrast with Atwater et al. (2012; Figs. 5 and 6A therein), who assigned nearly all evidence to a single inferred flood from the sea in 1650–1800, we find that a previously unrecognized time of flooding dates to the last centuries before Columbus, and we infer that flooding in 1650–1800 merely overwrote its effects. Those effects likely included emplacement of limestone boulders and cobbles that were previously thought coeval with the sand and shell sheet of 1650–1800.

Fields of Limestone Boulders and Cobbles

Distribution. Several fields of coarse limestone clasts were noted in 2008 and 2009 in western Anegada (Atwater et al., 2012, Figs. 2A, 5, and 7 therein). Two of these fields were mapped in detail (Watt et al., 2012) and their largest boulders were used to test possible causes of overwash (Buckley et al., 2012). The individual clasts of these two fields, north of Bumber Well Pond, are mapped in Figures 3 and B3B, and the generalized trends plotted in Figure B3B are reproduced in Figures 4 and A11. In addition, the northern field can be seen in profile view along line C-C′ of Figure 6.

Both these boulder fields north of Bumber Well Pond extend southward from inland outcrops of Pleistocene limestone from which most of the clasts were probably derived. One field extends 200 m southward from outcrops 300 m from the north shore, and the southern half of the other field extends 100 m southward from a limestone knoll that is 800 m from the north shore. The spacing between clasts was found to increase southward in both fields.

Time of emplacement. The emplacement of these and other coarse limestone clasts was previously dated, during field work in 2009, by assessing the stratigraphic position of the lowest parts of the clasts (Atwater et al., 2012, p. 75). If resting on sand, or at least above the top of shelly marine pond mud, a clast was interpreted in 2009 as having been transported during deposition of the sand and shell of 1650–1800 cal yr CE. Conversely, if surrounded by shelly marine pond mud, a limestone boulder or cobble was interpreted in 2009 as having been emplaced before the sand and shell sheet of 1650–1800. This relative dating presupposes an isochronous change from marine pond to hypersaline ponds immediately after the deposition of that sand and shell sheet (reviewed in "Holocene Beach Ridges and Ponds").

Watt et al. (2012, Fig. 5 therein) accordingly checked the stratigraphic positions of the keels of 161 limestone clasts in the 2 fields north of Bumber Well Pond. Among these dispersed limestone boulders and cobbles, 77 were found within sand, 54 on top of sand, 31 on Pleistocene limestone, 3 at or above a contact between sand and shelly marine pond mud, and none beneath that contact.

The results of this methodical work do not necessarily show, however, when the limestone boulder fields north of Bumber Well Pond were first emplaced. In Atwater et al. (2012, p. 75), it was presupposed that all sand in contact with the coarse limestone clasts belongs to the sand and shell sheet of 1650–1800. Not considered was the possibility that coarse limestone clasts first accumulated with an earlier sand body, or that sand brought in by later overwash merely remobilized the smallest of the limestone clasts.

Inferred mechanism of emplacement. A tsunami probably emplaced both of the fields of scattered limestone boulders and cobbles north of Bumber Well Pond, according to Watt et al. (2012) and Buckley et al. (2012). Emplacement by storm was deemed unlikely on the basis of location far inland and elongation perpendicular to shore (Watt et al., 2012). A category 5 hurricane was found insufficient to produce the flows inferred by modeling transport of the largest of the boulders (Buckley et al., 2012), before 2013 Typhoon Haiyan made clear

that an unusually large storm can produce tsunami-like bores in a setting like that of Anegada's north shore.

Watt et al. (2012) made analogy with modern tsunami deposits in which coarse clasts were scattered inland. They contrasted the two fields with shore-hugging ridges elsewhere in the Caribbean that Morton et al. (2008) attributed to storms. Not considered, however, were examples of boulders that storms managed to scatter (comparisons in "Coral Rubble").

Buckley et al. (2012) estimated flow velocities for transport of the largest of the boulders and compared the results with flow velocities computed from simulations of four potential sources of extreme waves at Anegada. The simulations were plotted along a physiographic profile without the bathymetric and topographic constraints now available from lidar. The extreme waves simulated were from a category 5 hurricane, a Lisbon tsunami generated during an earthquake of M 9.0, a Puerto Rico Trench tsunami generated on the subduction thrust during an earthquake of M 8.7, and a Puerto Rico Trench tsunami generated by normal faulting on the outer rise during an earthquake of M 8.0. Only the scenarios of tsunamis from the Puerto Rico Trench were found capable of transporting the boulders. However, this conclusion preceded the widespread recognition, from 2013 Typhoon Haiyan, that storms can produce prodigious tsunami-like bores.

The preferred scenario of Buckley et al. (2012) is a tsunami from normal faulting during an earthquake of M 8.0 on the outer wall of the Puerto Rico Trench (Fig. 1B). A steep fault dip yields waves of shorter period than does slip on a subduction thrust. The relatively short-period waves break on the fringing reef. The maximum water heights exceed 5 m across the reef flat and the north shore. The maximum simulated flow velocities are nearly 10 m/s across the reef and the reef flat, and above 5 m/s as much as 500 m inland from the north shore.

Reconciling Limestone Boulders with a Sand and Shell Sheet

A sand and shell sheet that lacks large offshore clasts appears incongruent with inland fields of limestone boulders and cobbles. How did south-directed flows fail to bring in brain coral boulders and tiger lucine valves, while still dislodging and transporting limestone boulders from sources hundreds of meters inland? This puzzle was recognized by Reinhardt et al. (2012), who wondered why, if emplaced by a tsunami, the sand and shell sheet of 1650–1800 contains no molluscan taxa other than those of an interior marine pond.

These puzzling combinations of flow competence and clast provenance are reconciled herein by interpreting western Anegada as a geomorphic palimpsest, akin to a reused writing surface that retains traces of previous text. A sandy fan containing articulated reef-flat shells predates a sand and shell sheet that is inset into it. The later sheet is limited to the lowest flow paths, and its molluscan assemblage is limited to that of an interior pond. Catastrophic emplacement of inland limestone boulders and cobbles in pre-Columbian time preceded lesser flooding from the north. The lesser flooding, in 1650–1800, merely reworked the smaller limestone clasts.

METHODS

Sequential Dating, Mapping, and Digging

Evidence for a pre-Columbian catastrophe, although mapped chiefly in eastern Anegada (Fig. 4), began to be recognized in 2011 with field work on the effects of Hurricane Earl on western Anegada. Samples were collected then from the brain coral boulders west of Red Pond (Fig. B2D) and north of Bumber Well Pond (Fig. B3C), and from an additional brain coral clast found upside-down in reconnaissance of an eastern salt pond (Figs. B6A, B6B, B6D). All three were expected to date, like deposits in Figure 3, to the post-Columbian decades between 1650 and 1800. However, the ^{14}C ages instead suggested that all three coral colonies died in the last centuries before Columbus (Table 2; samples with 2011 prefix).

This confounding result spurred searches for additional coral clasts. Many were encountered during further reconnaissance in eastern Anegada in 2012. The coral rubble ridge at Soldier Point was noticed, as were inland fields of scattered coral boulders and cobbles inland from there. Inland coral clasts were sampled south of Soldier Point (Fig. B4) and to the southeast near Table Bay (Fig. B5) and Warner (Fig. B6). Nineteen ^{14}C samples were submitted, and all gave pre-Columbian ages (Table 2, samples without prefix). Also noted, but not dated, were brain coral fragments incorporated in stone walls (e.g., Fig. B4F).

Dozens of additional coarse clasts were encountered inland in 2013, 2015, and 2016. Anomalous groups of limestone boulders were noted between Bumber Well Pond and Red Pond (Fig. 3D). More coral clasts were mapped near Soldier Point, Cooper Rock, and Table Bay. Radiocarbon ages were obtained on two of the most inland of the brain coral heads near Table Bay, to check for the possibility that age would vary with distance from shore.

The mapping in 2015 and 2016 took advantage of newly acquired lidar topography and expanded in the variety of clast types that the entire field parties sought. The prior mapping focused on the easily recognized clasts of brain coral. The mapping on lidar located *D. strigosa* (Fig. A5) among other coral clast types, some of which can superficially resemble clasts of the Pleistocene limestone: the boulder star coral *Orbicella* (formerly *Montastraea*) *annularis* (Fig. A6), the mustard hill coral *P. astreoides* (Fig. A7), and the elkhorn coral *A. palmata* (Fig. A8). The recent work also increased attention to the cobble-size valves of the lucine *C. orbicularis*, encountered chiefly in pits (Fig. A9), and to clasts of reef rock and beach rock (Fig. A10). The mapping in 2015 and 2016 included attempts to keep track of bioclastic sand associated with these various marine clasts, and to identify its approximate inland limit. This work was commonly impeded in eastern Anegada by spiny shrubs and trees, and attempts to determine where the sand is absent were further confounded by difficulties in identifying, in the field, trace amounts of the sand in brown soil that commonly coats the Pleistocene limestone.

Also sought since 2011 were stratigraphic tests of repeated overwash, that is, whether the traces of a pre-Columbian event are juxtaposed with evidence

for overwash in 1650–1800. The main result presented in this paper is the stratigraphy correlated among pits along a cross section that passes through the coral boulder exposed west of Red Pond (Figs. B2F). In an additional example, a buried crust is interpreted as the subtle contact between the sand and shell sheet of 1650–1800 and underlying sand that contains articulated lucine valves (Fig. B3F).

Radiocarbon Dating

The most catastrophic flooding of Anegada in recent millennia has been dated to the last centuries before Columbus by radiocarbon analyses of 27 coral clasts from central and eastern Anegada, 11 radiocarbon ages on mollusks, and 3 ages on plant fragments. All but five of the coral clasts dated are brain coral. Eight lucine valves and three conch shells were dated from sites near Red Pond and Bumber Well Pond. The dated plant fragments were a twig west of Red Pond and wood associated with a brain coral boulder in the Warner area (Figs. 5, 6, and B2–B6).

Still other radiocarbon ages were measured on staghorn coral pieces from near Cow Wreck High Point (Figs. 5, 6, and B1). These ages (as interpreted "Breaches in Beach Ridges") provide evidence that some of the breaches in western Anegada were first cut after Columbus (after 1492) by extreme waves later than those inferred from most of the field evidence in Figure 4. This post-Columbian overwash is speculatively ascribed herein ("Inferred History of Extreme Waves") to the 1755 Lisbon tsunami.

Reservoir Correction

Radiocarbon measurements on marine shells and coral skeletons require adjustment for the ^{14}C age of the water from which the calcium carbonate was precipitated. In the northeast Caribbean, this reservoir correction is complicated by multiyear changes in the mixing of water masses of differing ^{14}C age (Kilbourne et al., 2007).

We used a local marine-reservoir adjustment, ΔR, of –50 ± 50 ^{14}C yr (one standard deviation), where ΔR is the age offset between local and modeled global reservoir ages of near-surface ocean waters (Stuiver and Brazunias, 1993). The negative sign in ΔR means water more enriched in ^{14}C than in the global model. Constraints on ΔR near Anegada were obtained by Kilbourne et al. (2007) from a coral colony offshore southwestern Puerto Rico; their results for the 1950 growth band correspond to ΔR of –27 ± 24 ^{14}C yr, according to the marine-reservoir compilation of Stuiver et al. (2016).

Data obtained by Kilbourne et al. (2007) from earlier growth bands, back to the year 1751, suggest variable mixing of two different water masses: upwelled equatorial water that is relatively depleted in ^{14}C, and subtropical surface water that is relatively enriched in ^{14}C. The results further suggest that Caribbean waters in 1950 were toward the depleted end of the range. Using ΔR = –50 ± 50 ^{14}C yr allows for a broad range of local marine-reservoir values that is centered on slight enrichment in ^{14}C relative to the global marine-reservoir model.

Contamination of Coral Skeletons

Contamination of four of the brain coral samples was checked by analysis of calcite content. Because the coral skeletons are precipitated as aragonite, the calcite is diagenetic and, at Anegada, may contain old carbon derived from Pleistocene deposits. The measured values, with respect to total calcium carbonate, are 0.66% in sample 24 and 1.23% sample 22, both east of Warner (Fig. A7); 1.53% for sample 2011–1, the solitary boulder west of Red Pond (Fig. A1); and 1.92% for sample 14, south of Soldier Point.

According to Olsson (1974), contamination of a young sample by 1% carbon of infinite age increases the sample's age by 80 ^{14}C yr, and for 2% contamination the increase is 160 ^{14}C yr. The contamination evidenced by calcite may have thus increased the age of sample 24 by as much as 50 ^{14}C yr, and sample 14 by as much as 150 ^{14}C yr.

Weathered exteriors were present on three of the four dated staghorn samples from the vicinity of Cow Wreck High Point. The weathering rinds were removed before these samples were submitted for dating (Fig. B1E).

Conversion to Calendar Ages

Adjusted for marine-reservoir age but not for contamination, radiocarbon ages of the coral and shell samples were converted to ranges in calendar years by means of the Marine13 calibration data of Reimer et al. (2013) and version 7.1 calibration software of Stuiver et al. (2015). The radiocarbon ages of a twig west of Red Pond (Fig. A1F) and of wood east of Warner (Fig. B6D) were converted with the IntCal13 calibration of Reimer et al. (2013) and the same calibration software. Details by sample are listed in Table 2.

CLAST TYPES

Allochthonous clasts ranging from sand to boulders extend inland from the north and northeast shore of Anegada (Fig. 4). Most of these deposits terminate on Pleistocene uplands within 1 km of the shore, but some approach the south shore by way of paths near sea level through Red Pond, Bumber Well Pond, and Budrock Pond. The most widespread of the deposits consists of sand that continuously coats much of low ground near the north shore but becomes difficult to identify as it yields inland to brown soil and bare limestone. This sand, termed the main sand unit because of its extent, is commonly associated with coral boulders and cobbles, and with anomalous limestone clasts.

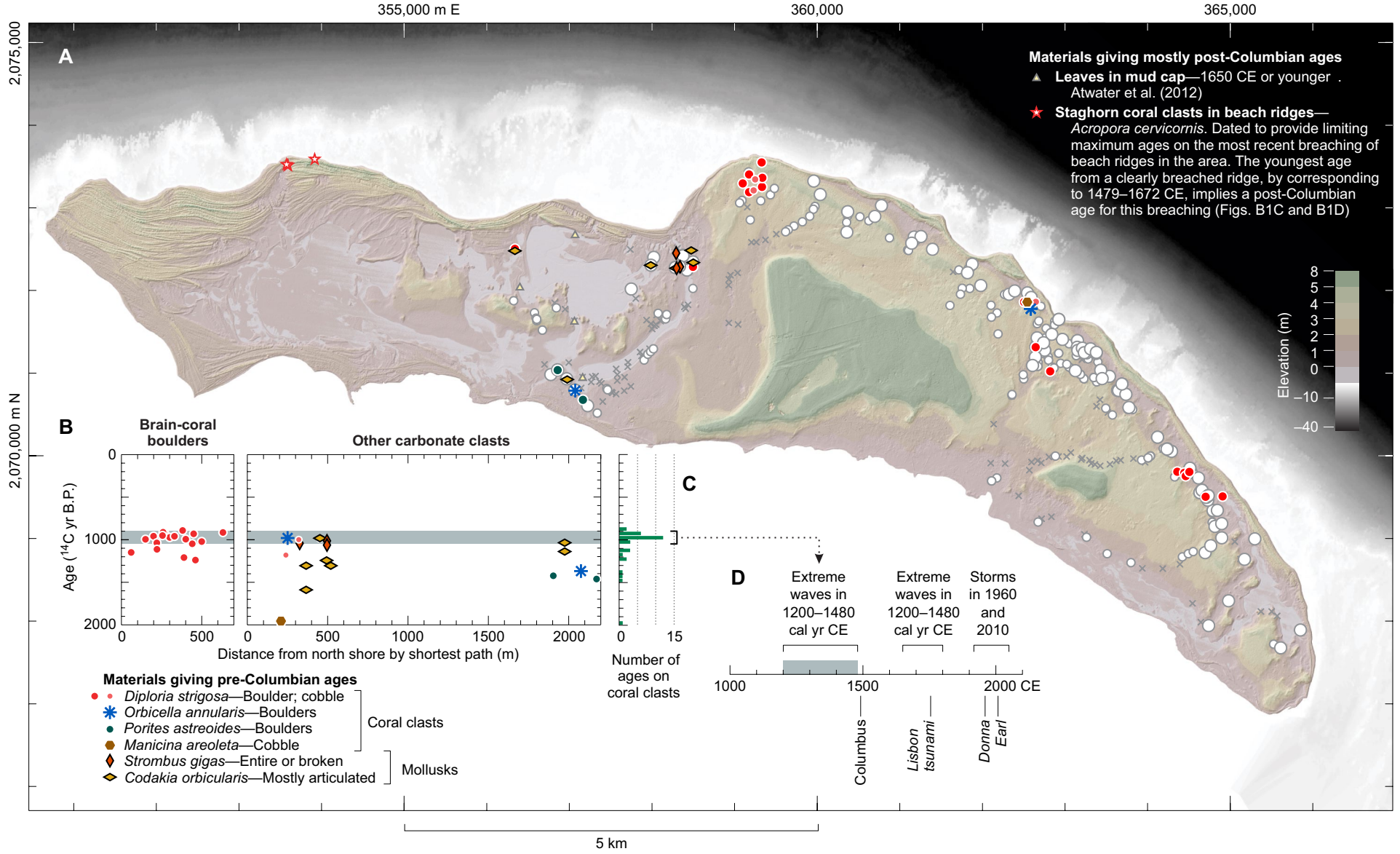

Figure 5. Chronology. (A) Distribution of dated samples (color). The coral and shell ages are listed in Table 2; the dated coral and shell samples are shown in Figures B1–B7. White circles and x symbols show the main sand sheet, as in Figure 4. (B) ^{14}C ages of coral clasts and associated mollusks, plotted by distance from nearest shore. (C) Histogram of coral ages. (D) Correlations with calendar time.

TABLE 2. RADIOCARBON AGES ON CORAL CLASTS AND ASSOCIATED FOSSILS AT ANEGADA ISLAND, CARIBBEAN SEA

Submitter's number*	Boulder of laboratory number (OS prefix)	Material dated†	Location map or photo (Fig. B)	UTM E (m)	UTM N§ (m)	Elevation# (m)	Distance from north shore# (m)	Age (^{14}C yr B.P.)	Age (cal yr CE)**
13-27	118962	A	1A-1E	353,577	2,073,532	2.5	n/a	435 ± 15	1715 – 1949
13-30	104165	A	1A-1E	353,591	2,073,520	2.5	n/a	680 ± 15	1479 – 1672
15-16	118961	A	1A-1E	353,594	2,073,521	2.5	n/a	805 ± 25	1385 – 1617
15-80	118959	A	1A-1E	353,918	2,073,595	1.3	n/a	535 ± 20	1597 – 1949
2013-11††	113832	Ca	2F, 2H	356,341	2,072,504	–0.1	450	1280 ± 20	967 – 1213
2011-1	87311	D	2A, 2B, 2D-2H	356,341	2,072,504	0.0	420	930 ± 30	1294 – 1458
2012-17B§§	104568	twig	2F	356,380	2,072,673	–0.1	280	810 ± 30	1169 – 1269
16-B135A	125948	P	7A-7D	356,859	2,071,640	0.1	1905	1430 ± 20	788 – 1031
16-B87B	125947	Ca	7A, 7B, 7F	356,967	2,070,932	0.0	1980	1040 ± 25	1202 – 1408
16-B87A	125946	Cd	7A, 7B, 7G	356,967	2,070,932	0.0	1980	1150 ± 25	1071 – 1297
16-B86	125945	O	7A, 7B, 7H–7K	357,064	2,070,797	–0.1	2080	1380 ± 20	818 – 1080
16-B137A	126005	P	7A, 7B	357,157	2,070,687	–0.1	2175	1470 ± 20	742 – 1004
16-M54	125942	Ca	3A, 3B, 3E	357,985	2,072,305	0.1	365	1310 ± 15	919 – 1172
16-M54	125943	Ca	3A, 3B, 3E	357,985	2,072,305	0.1	365	1600 ± 20	647 – 876
16-B52A	125867	Cd	3A, 3B	358,287	2,072,279	0.0	495	1250 ± 20	1001 – 1230
16-B52C	125941	S	3A, 3B, 3I	358,287	2,072,279	0.0	495	1020 ± 30	1221 – 1421
16-M63	125944	S	3A, 3B, 3G	358,287	2,072,459	0.1	325	1050 ± 30	1186 – 1405
16-M37	125787	S	3A, 3B, 3H	358,332	2,072,294	0.4	495	1070 ± 15	1174 – 1360
16-B48A	125941	Ca	3A, 3B, 3F	358,375	2,072,430	0.1	520	1310 ± 20	916 – 1174
2011-2	87330	D	3A–3C	358,495	2,072,287	0.0	575	1020 ± 25	1225 – 1418
2013-2A	113831	Ca	3A, 3B, 3D	358,499	2,072,469	0.2	450	970 ± 20	1278 – 1439
14	95856	D	4A–4C	359,099	2,073,297	2.5	295	970 ± 25	1276 – 1441
17	95858	D	4A–4C	359,175	2,073,191	2.5	415	1240 ± 20	1011 – 1239
13	98476	D	4A–4C	359,175	2,073,405	2.7	195	1110 ± 20	1111 – 1329
12	98444	D	4A–4C	359,177	2,073,408	2.6	195	1040 ± 30	1197 – 1411
20	95860	D	4A–4C	359,230	2,073,211	2.8	400	990 ± 20	1261 – 1431
19	95859	D	4A–4C	359,249	2,073,346	3.3	275	1000 ± 20	1249 – 1426
11	95855	D	4A–4C	359,327	2,073,551	3.4	75	1150 ± 35	1064 – 1301
6	95854	D	4A–4C	359,331	2,073,254	2.6	365	1210 ± 20	1038 – 1261
10	98445	D	4A–4C	359,336	2,073,364	3.0	255	925 ± 20	1301 – 1457
30	96013	D	5A, 5B, 5E	362,505	2,071,862	1.2	230	1180 ± 50	1037 – 1294
32	96014	M	5A, 5B, 5E	362,542	2,071,862	1.2	210	1960 ± 40	216 – 550
33	96015	O	5A, 5B, 5E	362,586	2,071,779	2.9	250	985 ± 35	1253 – 1441
2015-3	118957	D	5A, 5B, 5F	362,645	2,071,316	1.7	450	1050 ± 15	1197 – 1398
34	96016	D	5A, 5B, 5E	362,647	2,071,864	0.5	130	995 ± 35	1242 – 1435
2015-4	118958	D	5A, 5B, 5G	362,820	2,071,024	2.4	635	905 ± 20	1309 – 1468
23	95906	D	6A–6C	364,359	2,069,808	2.7	360	995 ± 30	1246 – 1433
24	95907	D	6A–6C	364,443	2,069,795	2.0	265	965 ± 20	1282 – 1440
26	95908	D	6A–6C	364,460	2,069,755	1.2	310	960 ± 40	1271 – 1453
28	98443	D	6A–6C	364,504	2,069,807	0.4	245	915 ± 20	1305 – 1462
27	95909	D	6A–6C	364,508	2,069,807	0.4	240	950 ± 20	1290 – 1446
22	95905	D	6A–6C	364,702	2,069,506	0.9	350	890 ± 25	1313 – 1482
2011-3	87337	D	6A–6C	364,907	2,069,510	–0.1	180	960 ± 25	1283 – 1444
ee14a	87309	wood	6A, 6B, 6D	364,907	2,069,510	–0.1	200	790 ± 30	1192 – 1278
ee14b	87310	wood	6A, 6B, 6D	364,907	2,069,510	–0.1	200	805 ± 25	1189 – 1271

Note: Entries listed from west to east. n/a—not applicable. Distances inland are not reported for coral clasts that were likely exhumed on beach ridges without having been transported further.

*If year not provided, year is 2012 (for coral clasts submitted).

†A—*Acropora cervicornis* (staghorn coral); C—*Codakia orbicularis* (tiger lucine, a robust bivalve; Ca—articulated; Cd—disarticulated); D—*Diploria strigosa* (brain coral); M—*Manicina areoleta* (rose coral); O—*Orbicella annularis* (boulder star coral; formerly in the genus *Montastraea*), S—*Strombus gigas* (conch). Material labeled wood was a single piece of wood from an organic horizon that may extend beneath the entire coral boulder of sample 2011-3. The piece of wood contained about 20 annual rings. Sample ee14a was from inner rings, and sample ee14b was from outer rings (see text Fig. B6D).

§Zone 20N, WGS 84 (World Geodetic System 1984); UTM—Universal Transverse Mercator.

#Measured by geographic information system with terrestrial lidar (light detection and ranging). Vertical datum is approximately mean sea level. Distances from north shore measured along the shortest path.

**Range at 2 standard deviations computed with the calibration data of Reimer et al. (2013) and version 7.1 calibration software of Stuiver et al. (2015). Calibration data used: twig—IntCal13; coral and shell—Marine13. The calibration for coral and shell incorporates a local marine-reservoir adjustment, ΔR, of –50 ± 50 ^{14}C yr (1 standard deviation). Details are provided in the text in the discussion of Methods.

††Articulated specimen near the projected level of the bottom of the nearby *Diploria* boulder (Fig. B1H).

§§In a north-south cross section through a series of pits, the stratigraphic position of this twig projects below the level of the bottom of the *Diploria* boulder of laboratory identification OS-87311 (boulder in Figs. B1C–B1G).

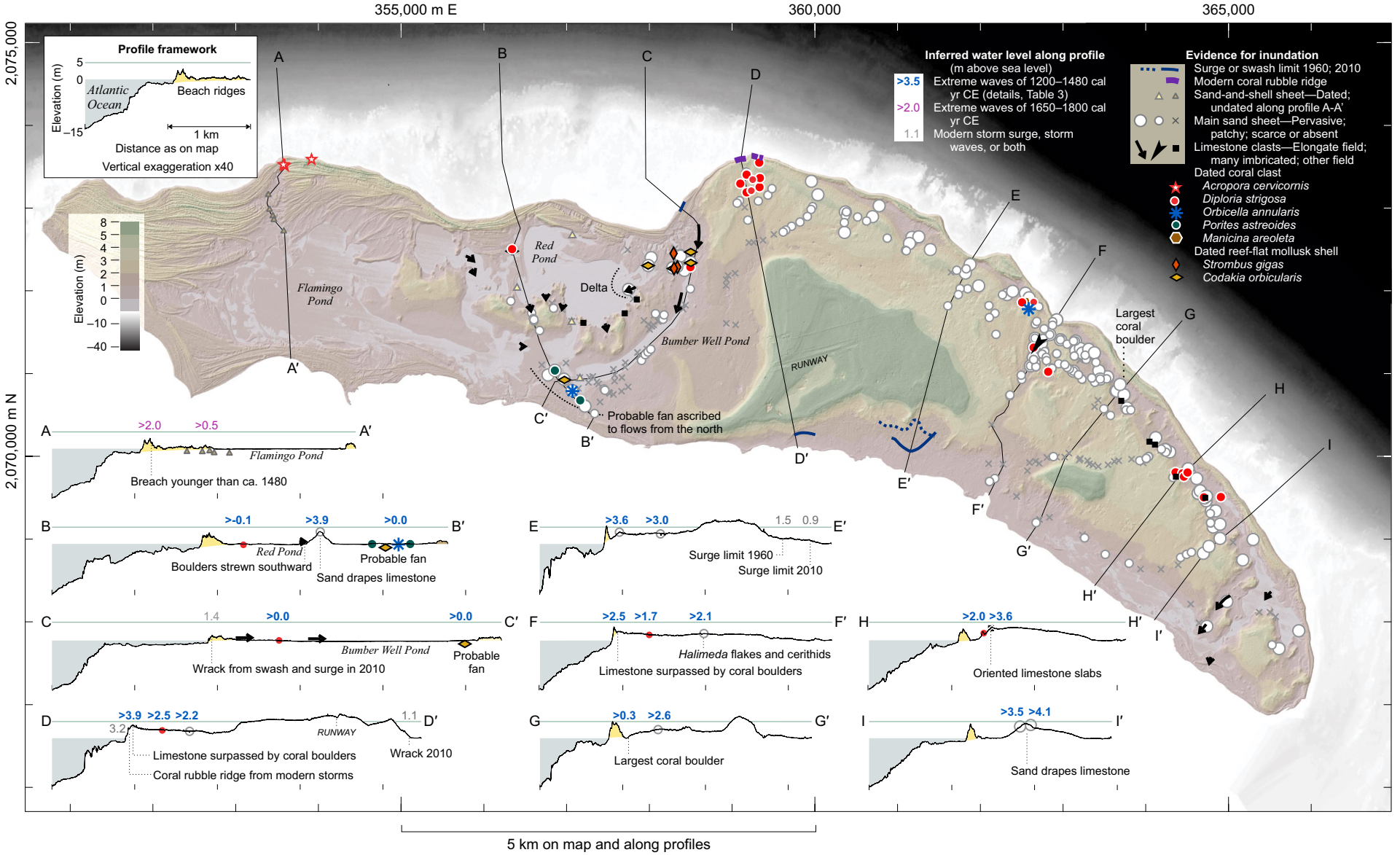

Figure 6. Inferred inundation heights and distances along nine profiles across Anegada. Control points are described and interpreted further in Table 3.

TABLE 3. CONTROL POINTS FOR ESTIMATES OF INUNDATION DISTANCES AND HEIGHTS ATTAINED BY EXTREME WAVES 1200–1480 CAL YR CE, ANEGADA ISLAND

Profile	Easting (m)	Northing (m)	Shortest distance from north shore (m)	Elevation (m)	Evidence	Interpretation
B-B′	356,341	2,072,504	420	–0.1	*Diploria strigosa* colony, nearly intact, upright, 1.5 m wide and 1.1 m tall, dating to 1294–1458 (Figs. B2D–B2H). Associated with articulated lucine dating to 967–1213, and an entire conch. Adjoins beach ridges with low relief to northwest.	Southward flooding that widely attained elevations of 4 m or more is evidenced collectively by the *Diploria strigosa* colony, field of limestone clasts, and sand coating. The coral colony was dislodged offshore, probably on the reef flat, and was transported across beach ridges, or through breaches in them, into a marine pond. The lucine and the conch were brought in with the coral colony. The lucine, given its age, died a few centuries before the coral colony; though articulated, the valves may have been recycled from reef-flat deposits scooped out by breaching of a beach ridge. Breaching of some beach ridges may have been accompanied by decapitation of many others, now muted. In an area 1.1 km from the present north shore, the water scattered the limestone cobbles and boulders from a knoll. Sandy water proceeded over a limestone cay crest, which it coated with sand nearly 4 m above present sea level at a distance 1.3 km from the north shore.
B-B′	356,561	2,071,796	1160	–0.1	Limestone cobble and boulder field 50 m long, 1150 m from the island's north shore. Clasts are mainly 10–40 cm in longest diameter, strewn southwestward to southeastward from limestone knoll (photo in Fig. A11).	
B-B′	356,605	2,071,634	1330	3.9	Patchy sand on crest of limestone cay 1350 m from the nearest part of the island's north shore. Additional patches are on either side of crest (Figs. A4 and B7B).	
C-C′	358,597	2,072,797	305	0.4	Limestone boulder field, north end. Extends 200 m southward. Mean A, B, and C axes of five largest boulders (m): 0.99, 0.68, 0.38 (Buckley et al., 2012). A second field with smaller clasts is centered 900 km farther south (Watt et al., 2012).	The trough now containing Bumber Well Pond provided a low-altitude path for southward flooding that emplaced limestone boulder fields, brought in the round *Diploria strigosa* colony, and moved the *Codakia* valves and the large *Orbicella* boulder an estimated 3 km. A fan southwest of the trough was probably built by deceleration of sandy water as it spread from the outlets of the trough and of narrows south of Red Pond. The time of fan deposition, if approximated by the 1202–1408 age of the articulated *Codakia* valves, is not statistically different from the time of death of the round *Diploria* colony, 1225–1418. The *Orbicella annularis* embedded in the fan deposits was probably dead on arrival, its skeleton having been bored offshore. The transport distance for this large boulder and the *Codakia* valves was 3 km if these clasts were entrained on the reef flat near the north shore, and if they transited the Bumber Well trough. Like the discordant *Codakia* beside the *Diploria* colony along profile B-B′, the older of the dated *Codakia* valves south of Red Pond may have been derived by breaching that entrained reef-flat deposits beneath a beach ridge.
C-C′	358,495	2,072,287	575	0.0	*Diploria strigosa* colony, upright and circular in plan view, 50 cm in diameter and 30 cm high. Embedded 15 cm in sand, with flat base of colony 15 cm above Pleistocene limestone (Figs. A5 and B3C). Dated to 1225–1418.	
C-C′	356,967	2,070,932	1980	0.0	*Codakia orbicularis* valves in sand 25–30 cm thick with *Halimeda* flakes (Fig. B7E). Disarticulated but matching pair dating to 1071–1297 (Fig. 7G), articulated pair dating to 1202–1408 (Fig. 7F). Approximately 2800 m from north shore by way of Bumber Well Pond.	
B-B′	356,857	2,071,040	2080	–0.1	*Orbicella annularis* boulder, 1.0 m by 0.8 m by 0.8 m, bored, dated to 818–1080 (Figs. B7H–B7K). Embedded in sand with *Halimeda* flakes (Fig. A4). Approximately 2800 m from north shore by way of Bumber Well Pond.	
D-D′	359,118	2,073,542	60	3.9	Crest of limestone ridge north of coral colonies, chiefly *Diploria strigosa* boulders, found as much as 475 m farther south. The 9 coral colonies dated from this area gave ages between 1011–1239 and 1301–1457 (Fig. B4B). A coral-rubble ridge (Fig. A1) plastered onto the seaward flank of the limestone ridge crests 30–40 m seaward of the limestone ridge crest and 0.5 m below it. Limestone extends beneath the rubble to the modern shore.	Extreme inundation carried coral clasts across the limestone ridge that crests 0.1 km south of Anegada's north shore near Soldier Point. The water exceeded 4 m in elevation as it crossed the ridge. The coral clasts were transported a maximum inland distance of nearly 0.5 km. Sand was deposited farther south, at maximum inland distances nearly 0.8 km. By contrast, the evident deposits of storm waves since 1500 CE are restricted to the seaward flank of the limestone ridge.
D-D′	359,251	2,072,868	755	2.2	Patchy sand 60 m west-southwest of profile. Patchy sand similarly extends 780 m inland in an area 400 m east-southeast of profile D-D′.	
E-E′	361,830	2,072,265	180	3.6	Patchy sand on crest of low limestone ridge, flanked seaward and landward by areas of pervasive sand.	Sandy water poured over this limestone ridge and continued inland no less than 0.6 km.
E-E′	361,608	2,071,819	680	3.0	Patchy sand, most inland example mapped in reconnaissance of this area.	

(*continued*)

TABLE 3. CONTROL POINTS FOR ESTIMATES OF INUNDATION DISTANCES AND HEIGHTS ATTAINED BY EXTREME WAVES 1200–1480 CAL YR CE, ANEGADA ISLAND (*continued*)

Profile	Easting (m)	Northing (m)	Shortest distance from north shore (m)	Elevation (m)	Evidence	Interpretation
F-F′	362,861	2,071,612	80	2.7	Limestone lip at northern entrance to Pleistocene channel followed by profile F-F′.	Atlantic waters pouring across this part of northern Anegada were funneled into the relict Pleistocene channel. They carried coral clasts over a lip at the northern intake, aligned and stacked limestone slabs in an area 0.4 km inland, transported *Diploria* clasts as much as 0.6 km inland, and deposited sand recognized today as much as 1.1 km inland. The sand may have been derived in large part by erasure of an ancestor of the small beach ridge that today adjoins the lip. A former marine pond, impounded between a former beach ridge and limestone, may have supplied the cerithids. It is unclear whether the overwash reached the island's south shore.
F-F′	362,645	2,071,316	450	1.7	*Diploria strigosa* colony, spherical, nearly 1 m in diameter, dating to 1197–1398 (Figs. A5 and B5F). Near landward end of field, 100 m by 150 m, of imbricated limestone slabs as large as 1.7 m by 1.0 m by 0.2 m. Also nearby are a slab of *Acropora palmata* 0.5 m by 0.5 m, an *Orbicella annularis* cobble, and areas of pervasive sand (Fig. B5B–B5D).	
F-F′	362,593	2,071,124	640	1.8	Two *Diploria strigosa* boulders with smoothly arcuate margins terminated abruptly at radial breaks. The more complete probably retains one-half to two-thirds of a former colony's circumference, and the longest ray perpendicular to the exterior extends 0.4 m. A similarly broken *Diploria* 245 m to the southeast, ~635 m inland, was dated to 1309–1468 (Fig. B5G), the second-youngest of the *Diploria* ages island wide (Table 2). These are the most inland *Diploria* clasts observed south of Table Bay (Fig. B5B), and they are among the most inland of the *Diploria* clasts noted island wide (Fig. A12).	
F-F′	362,359	2,070,742	1100	2.2	Patch of silty sand with foraminifera, cerithids, *Halimeda* flakes, and bivalve fragments. The most inland of the marine sand observed in the Pleistocene channel.	
G-G′	363,728	2,070,846	230	0.3	*Diploria strigosa* colony ~2.5 m in diameter that rests, spalled but upright, on limestone and is surrounded by sand a few tens of centimeters thick (Fig. 4C). It is the largest *Diploria* colony observed island wide (Fig. A12). Found behind a beach ridge 100 m wide and as much as 5 m above sea level; ~12 other *Diploria* clasts and a reef-rock boulder 2.1 m by 1.4 m by 0.8 m (Fig. A10) were mapped within 100 m of the outsize colony (Fig. A5).	Overwash that brought ashore this outsize *Diploria* colony continued southwestward across limestone, where it deposited sand nearly 0.6 km inland. The sand may have been derived in large part from an ancestor of the large beach ridge that today borders the coast. Additional mapping would be needed to determine whether the outsize colony correlates with an anomalous patch of sand nearly 1.5 km inland.
G-G′	363,615	2,070,731	390	1.8	The most inland of the *Diploria* clasts directly inland from the outsize one.	
G-G′	363,494	2,070,575	590	2.6	Patchy sand. An additional patch of sand was found 1430 m inland near profile G-G′, in an area where marine sand was otherwise found scarce or absent (Fig. 6). The intervening area has not been mapped.	
H-H′	364,443	2,069,795	260	2.0	*Diploria strigosa* colony 1.0 m diameter, 265 m inland (Fig. B6C, sample 24). One of seven *Diploria* boulders dated in the area, their ages clustered between 1246–1433 and 1305–1462 (Fig. B6B). The highest of these is 2.7 m above sea level and 360 m inland (Table 2, sample 23) and the largest is a microatoll 1.7 m in diameter (Fig. B6C, sample 22).	An extreme wave event dislodged large *Diploria* colonies offshore and deposited them in this area in the thirteenth, fourteenth, or fifteenth century. The colonies included a microatoll likely derived from the reef crest, which is now ~0.3 km offshore. The coral clasts came to rest as much as 0.3 km inland and at heights to 2.7 m above sea level. Also transported were limestone slabs in an area 3.6 m above present sea level at a distance nearly 0.4 m inland.
H-H′	364,372	2,069,744	390	3.6	Limestone slabs, imbricated and (or) consistently dipping seaward, as large as 0.5 m by 0.5 m by 0.2 m (Fig. B6E).	
I-I′	364,897	2,069,008	490	0.6	Pervasive sand at landward edge of sandy flat.	Sandy water overtopped a ridge crest 0.7 km inland and 4.4 m above present sea level. The water continued down the far side of the ridge at least as far as 1.0 km from the island's north shore.
I-I′	364,764	2,068,913	650	3.5	Pervasive sand on seaward side of a broad limestone ridge.	
I-I′	364,695	2,068,828	755	4.1	Pervasive sand on inland side of this limestone ridge. The intervening ridge crest is slightly higher, 4.4 m, and its distance from the modern shore is 700 m. Northwest of the profile, marine sand was found to continue inland, though patchy, to a site 1,010 m inland and 2.5 m in elevation (Fig. 6).	

Notes: Easting and northing refer to UTM (Universal Transverse Mercator), zone 20N. Elevation refers to the sea-level datum of the lidar surveys. In the Evidence and Interpretation columns, the age ranges are in cal yr CE at two standard deviations (Table 2).

Main Sand Sheet

The main sand sheet consists mainly of fine to medium carbonate sand. Most of the grains are subangular or subrounded. Some are rod-shaped and are speckled with silt-size particles (examples at right in Fig. A4), and perhaps originated as fecal pellets. Under a hand lens, pink grains of *Homotrema rubrum* are more evident where the sand is thick and well preserved than in inland soils where the grains appear bleached and chalky.

We mapped the main sand sheet as pervasive where sand more than 5 cm thick covers at least three-quarters of an area tens of meters on a side; as patchy where sand is thinner, less extensive, or both; and as scarce or absent where we were unable to identify it with confidence in the field. The patchy sand is commonly mixed with soil and confined to depressions in limestone pavement. The symbols for these three categories appear in Figures 4 and 5, A4–A12, and B2–B7, and as page names in the data tables of the Supplemental Material (footnote 2).

The thickness of the pervasive sand, at the 20 sites where it was recorded, does not exceed 50 cm and is rarely more than half that amount (Supplemental Material). Internal structure is mostly obscured or obliterated by crab burrows (Fig. B3l), aside from three successive normally graded beds at one site (Fig.

B3D), and a common overall upward fining of framework grains (Figs. B7C, B7H). Lime mud high in the sand contributes to this upward fining, but the mud may have been introduced from above by bioturbation of pond deposits (Fig. B2H).

Unlike the sand and shell sheet of 1650–1800, which was found chiefly beneath microbial mats of salt ponds at or below sea level, the main sand sheet extends as much as 4 m above sea level (Fig. 6, profiles B-B′ and I-I′). The main sand further differs from the sand and shell sheet by being associated with coral clasts and with conch and lucine shells (Figs. B3G, B3I, B7F, B7G), and in rarely containing shell assemblages dominated by cerithid gastropods. The two sand units differ distinctly in age if the main sand unit is coeval with the 24 associated coral clasts and 11 associated mollusks dated; all of these have given age ranges that extend no later than the year 1500 (Table 2; Fig. 5).

The main sand sheet notably extends onto limestone uplands southwest of Red Pond and in the Warner area (Fig. A4). Southwest of Red Pond it discontinuously coats a limestone hill, known locally as a cay, across a crest 4 m above sea level (Fig. 6; Table 3, profile B-B′). Likewise in the Warner area, pervasive sand extends across a limestone ridge 4 m above sea level (Fig. 6 and Table 3, profile I-I′). In additional Warner examples, rod-shaped grains 1–2 mm long, similar to those evident in the pervasive sand, were found by washing soil samples midway across the island, in an area where sand was judged scarce or absent in the field (photographs in Fig. A4).

Salt flats near the south shore, south of the outlets of Red Pond and Bumber Well Pond, are widely underlain by sand that likely correlates with the main sand sheet. Sand commonly 20–30 cm thick overlies muddy sand that contains abundant cerithids (Figs. A4 and B7E). Coral clasts embedded in the sand (Figs. A4 and A7) include an *Orbicella* boulder 100 cm by 85 cm by 80 cm (Fig. B7H). Also common are flakes of the microalgae *Halimeda* (Figs. A4, B7C, and B7E). The sand far exceeds, in its combination of thickness and inland extent, the deposits of storm overwash deposits west of The Settlement (reviewed in "Previous Work").

This southern sand probably represents a fan built from the north during the time when coral clasts were being scattered widely on the island (Figs. 4–6). This interpretation is supported by the ages of the associated lucine valves (Table 3, profile C-C′) and by limiting maximum ages from coral clasts (Fig. B7B; Table 3, profile B-B′). The probable fan can be explained by the same southward flow of Atlantic water that likely accounts for the numerous breaches and the washover fan northeast of Red Pond, and for a delta built from there into the site of Red Pond (Fig. A2, air photo; Fig. B3B). The water level exceeded 4 m as it deposited patchy sand on a limestone cay south of the main part of Red Pond (Table 3, profile B-B′). It built the probable fan upon emerging and spreading out from constrictions at the south end of what is now Red Pond, and at the southwest end of the trough that now holds Bumber Well Pond.

Inland limits of the main sand sheet are rarely apparent where it tapers southward on limestone east of the eastern half of the island. The patches can be difficult to identify where the grains make up small fractions of brown silty soil. Sand at low elevation along the south shore, south of Warner, may have been derived from southern ponds and beaches, and it may contain salt crystals mistaken for bioclastic sand. Sand in the Warner area and south of Red Pond has been locally reworked by wind. Eolian reworking may have extended the apparent area of the sand after inundation destroyed much of the vegetation, or after land was cleared for agriculture and livestock in the eighteenth and nineteenth centuries. However, we have not noticed widespread sand dunes associated with the main sand except on salt flats south of Red Pond, where drifting sand is being trapped, chiefly by vegetation, southwest of the dated coral clasts and lucines that are plotted in Figure B7A. An eolian cap as much as 10 cm thick may surround a dated *P. astreoides* boulder in that area (Fig. B7C).

Coral Clasts

The Supplemental Material lists 225 coral boulders and cobbles that have been found inland of Anegada's north shore. They are scattered across various kinds of terrain to elevations as great as 4 m. Their collective distribution is approximated, in large part, by their most abundant variety, *D. strigosa* (Figs. 4, A5, and A12); brain coral makes up nearly two-thirds of the coral clasts mapped. Most of the coral clasts are in fields that extend onto Pleistocene uplands of eastern Anegada. Other clasts, near Red Pond and Bumber Well Pond, are more nearly solitary and were found near sea level (Figs. A12, B2, and B3). Few of the clasts were found more than 0.5 km from the north shore, except in the fan deposits south of Red Pond and Bumber Well Pond. There, the shortest distance to the north shore is 2 km and the inferred transport distances are 3 km (Fig. 6; Table 3; profiles B-B′ and C-C′).

The coral boulders mapped in eastern Anegada extend from Soldier Point to the East End. At Soldier Point, a field of 30 mapped coral boulders and cobbles extends 470 m inland, in stark contrast to the shore-hugging form of the coral rubble ridge (Fig. B4B). This field rests on a pavement of Pleistocene limestone that crests broadly 50–100 m inland at elevations of 4–5 m, and that descends gently landward from there (Fig. 6, profile D-D′). Coral boulders found in eastern Anegada extend farthest inland south of Table Bay, to a distance of 635 m (Fig. 6, profile F-F′; Fig. B5B). The setting there is a relict Pleistocene channel that is aligned with a gap in the modern ridge crest (Fig. 2B). The southeasternmost field identified, east of Warner (Fig. 6, profile D-D′; Fig. B6B), extends 350 m inland and rises from a seasonally flooded salt flat, from which some of the clasts barely protrude (Figs. B6C, B6D).

Most of the *D. strigosa* clasts are in the range 0.5–1.0 m in diameter; a particularly large one, south of Cooper Rock, spans 2.7 m (Fig. 4). A solitary brain coral boulder 1.7 m in diameter protrudes from a salt flat west of Red Pond (Fig. B2C). Maximum clast size diminishes with distance from the north shore and with elevation, but the many small clasts were found in the north and on low ground (Fig. A12).

Many of the brain coral clasts, including the large one west of Red Pond, resemble entire living colonies in having smoothly convex outer surfaces parallel to annual growth bands (Fig. A5). Some of these surfaces are dimpled where the coral colony probably grew around a worm tube (Figs. B2D and

B5G), a skeletal response described by Patton (1976, p. 6). Some of the largest colonies have fractured into multiple pieces, perhaps as a result of centuries of subaerial exposure. The individual pieces remain adjacent to each other and may easily be mentally reassembled to estimate the original size of the colony (Figs. B2D, B5F, and B6C, sample 26).

Irregular surfaces that truncate growth bands give evidence for erosion, mechanical, biological, or both. One such brain coral boulder surface is encrusted with serpulids and *Homotrema* (Fig. B4D). Others, of cobble size, resemble clasts of the modern coral rubble ridge (samples 19 and 20; Figs. B4C, B4E).

Other Coral Species

Approximately 33 of the listed coral clasts are boulders or cobbles of the boulder star coral *Orbicella annularis* (Fig. A6). They include boulders both north and south of Bumber Well Pond, and numerous boulders east of Warner. A dated *O. annularis* northwest of Table Bay (Fig. B5E, sample 22) was found near a cobble-size piece of *Manicina areolata*, also dated (Fig. B5E, sample 32). A second dated *O. annularis* boulder, south of Red Pond and Bumber Well Pond (Figs. B7H–B7K), was found at sea level 2 km from the north shore (Fig. 6; Table 3; profile B-B′).

Of the coral clasts tabulated and mapped, 25 are of the mustard hill coral *P. astreoides* (Fig. A7). Many more were doubtless overlooked, because the corallites of this species are tiny, and the original form is bumpy. The species predominates, for unknown reasons, on the probable fan south of the outlets of Red Pond and Bumber Well Pond. Closer study of some of those southern clasts might show that they contain additional materials and are better termed reef rock, like a reef rock clast mapped north of Bumber Well Pond (Fig. 10).

Mapped clasts of the elkhorn coral *A. palmata* extend along the northeast shore and are most numerous near Table Bay (Fig. A8). As with *P. astreoides*, the clasts are easily overlooked because of superficial resemblance to Pleistocene limestone.

Mollusks

Large molluscan shells were encountered in pits near the western salt ponds. The majority of these are sand-filled valves of the tiger lucine *C. orbicularis* (Fig. A9). We found them articulated at most of the lucine sites mapped north of Red Pond and Bumber Well Pond (Figs. B2H, B3B, B3D, and B3E), in a pit south of Red Pond (Figs. A9, B7E, B7F, and B7G), and in a pit in the East End. A disarticulated valve was found in sand beneath a limestone boulder at the distal end of a limestone boulder field that forms part of an incised delta in northeast Red Pond (delta, Fig. B3A; pit, Fig. A9).

Conch shells of *S. gigas* are widespread at the ground surface as well as present in the subsurface. We did not map surficial specimens because many contain holes likely made by people when extracting the muscle. The specimens found underground were entire or broken. An example of an entire specimen was found in a pit 1 m from the coral boulder west of Red Pond, within the depth range of the nearly horizontal bottom of the boulder (Figs. B2G, B2H). This conch shell was associated with articulated *C. orbicularis*. Another entire conch shell was found in a pit north of Bumber Well Pond (Fig. B3G).

Limestone Clasts

Anomalous limestone clasts are far more extensive on Anegada than implied by the maps in this paper. The mapped examples are limited to fields of coarse clasts, most of them elongate, and to certain clusters of imbricated slabs (Fig. A11). Not plotted or listed are anomalous clasts that might possibly be explained by upturning from tree roots, or by effects of land clearing or wall building.

The elongate fields not mapped previously include several small ones that extend southward from probable sources near the south shore of Red Pond (example at upper left in Fig. A11; identified also along profile B-B′ of Fig. 6), and larger fields evident on air photos of the East End (small example at bottom of Fig. A11). Southward emplacement of the boulder fields near the south shore of Red Pond is congruent with the presence of sand across the crest of the limestone cay farther south (Fig. B2B and profile B-B′ of Fig. 6).

The imbricated clasts mapped are limited to those where numerous slabs dip in a consistent direction. The orientations were measured systematically south of Table Bay among brain coral clasts that include the large round colony shown in Figures A5 and B5F. The mean of the 27 measurements in this area suggests flow directed inland approximately perpendicular to the shore (Figs. B5C, B5D).

CLAST SOURCES

The main sand unit was likely derived from sources along and north of the island's north shore. Between Soldier Point and Warner, a paucity of breaches suggests that the main sand unit was sourced from beach ridges that were leveled by catastrophic overwash and were rebuilt after that. The southern limit of the bioclastic sand may have been extended by wind that swept across overwash areas where plants had been removed or thinned. However, neither lidar nor ground surveys provide evidence for dune morphology in inland areas where the sand is thin and patchy.

As noted in "Fringing Reef and Reef Flat," all the main species of scattered coral clasts were reported living on the fringing reef or the reef flat off northern Anegada in the 1970s (Dunne and Brown, 1979) and were found live on the reef flat in 2015 or 2016 (Figs. A5–A8). In addition, brain coral colonies that lived through 2008 were found onshore at Soldier Point in 2013 (Xu et al., 2015).

Many of the scattered coral clasts were probably entrained directly from the fringing reef or the reef flat. Clustered ages and exterior form suggest that a large fraction of the brain coral boulders were deposited alive ("Inferred Time of Emplacement"). Had the clasts been derived mainly from a coral rubble ridge like the one now at Soldier Point (Fig. A1), the clast surfaces would be more abundantly bored and encrusted, like the clasts in Figures B4D and B4E, and would not parallel annual growth bands as cleanly as in Figure B2.

The youngest of the dated lucine valves, along with the dated conch shells and large quantities of sand, were probably derived from the reef flat off the island's north shore. *C. orbicularis* was living there in 2016 (Fig. A9), as was *S. gigas*. In the lucine sketch redrawn in Figure A9, the valves in life position underlie sediment one shell diameter thick, or ~5 cm for the fossil valves pictured. The main sand unit may then contain sand from the uppermost 5–10 cm of the bottom sediments of the reef flat north of the island. This sediment source is particularly extensive north of the *Codakia*-rich sand deposits that border Red Pond and Bumber Well Pond. Those deposits are due south of the reef flat of Windlass Bight, where sandy shallows extend more than 1 km between the island's north shore and the fringing reef (Fig. 2A).

Older lucine valves, as discussed in the following, may owe their age to having been recycled from reef-flat deposits beneath beach ridges of the north shore. In this attempted explanation for discordant ages, some of the specimens remained articulated as they were entrained in breaches and incorporated in the washover fan as much as 100 m to their south (Fig. B2B). In the example in Figure B3F, an articulated lucine dated 916–1174 cal yr CE was collected <50 m inland from a plunge pool.

Exposed pavement of Pleistocene limestone provides widespread sources for the associated clusters of limestone boulders between Soldier Point and Table Bay. Bare limestone knolls were likely swept clean by flows that built boulder fields in their lee (Red Pond example, Fig. A11).

CLAST AGES

Radiocarbon Results

Coral Skeletons

Among the 27 radiocarbon ages measured on coral clasts, 23 are between 890 ± 25 and 1280 ± 20 ^{14}C yr B.P., 18 are between 890 ± 25 and 1050 ± 15 ^{14}C yr B.P., and none are younger (Table 2). A *Manicina areolata* cobble gave the outlier age, 1960 ± 40 ^{14}C yr B.P. (Fig. B5E, sample 32). Age otherwise varies little with coral clast type and appears unrelated to distance inland (Fig. 5B).

The frequency distribution of the ages on coral clasts can be described most simply as unimodal and asymmetrical, with a long tail from ages older than 1050 ^{14}C yr B.P. (Fig. 5C). This tail likely resulted from reworking of preexisting deposits ("Inferred Time of Emplacement").

With the estimated marine-reservoir adjustment (ΔR) of –50 ± 50 ^{14}C yr and the standard calibration methods noted here, 25 of the 27 coral clast ages correspond mainly or entirely to a calibrated age range, at two standard deviations, that is within the round-number interval 1000–1500 cal yr CE (Fig. 5D). A narrower cluster of 18 coral clast ages gives a range of 1200–1480 cal yr CE; the mode corresponds to the last few centuries of pre-Columbian time. The oldest clast, the *Manicina areolata* cobble, gave a radiocarbon age that corresponds, in calibrated years, to a time no earlier than 200 cal yr CE.

Associated Bivalve Shells

The conch *S. gigas*, with one sample from each of three different sites, gave ages more consistent with one another, and with the youngest coral clast ages, than did eight shells of the lucine *C. orbicularis* (Fig. 5B). Six of the eight lucine ages were measured on articulated valves. The scatter among the ages on articulated valves, between ca. 1000 ^{14}C yr B.P. and 1600 ^{14}C yr B.P. (Table 2), was unexpected because it is thought that an articulated bivalve in an extreme-wave deposit is usually transported while muscles of the living organism still hold the two valves together (Reinhardt et al., 2006; Switzer et al., 2011, p. 424). The discordance among lucine ages is greatest close to breaches in northern beach ridges (Fig. B3B). Perhaps recycled lucines remained articulated by being derived from nearby excavation of plunge pools, if the pools extended downward into reef-flat deposits beneath beach ridges.

Lucines from sand in a pit south of Red Pond, 2 km from the north shore, gave slightly discordant ages of 1040 ± 25 ^{14}C yr B.P. (articulated) and 1150 ± 25 ^{14}C yr B.P. (disarticulated but in a matching pair; Figs. B7E–B7G). These ages figure below in the inference that overwash from the north, after coursing through the sites of Red Pond and Bumber Well Pond, constructed a sandy fan near the south shore and introduced a large *Orbicella* boulder there as well (Table 3; profiles B-B′ and C-C′).

Associated Plant Remains

Radiocarbon ages of plant remains afford partial tests of the ^{14}C ages of two of the coral boulders. The results are consistent with the estimate herein that the coral boulders were emplaced in 1200–1480 cal yr CE.

The ^{14}C age of a twig may be consistent with the radiocarbon age of the solitary coral boulder west of Red Pond. The twig was encountered in one of the pits dug along a north-south cross section to explore the stratigraphic context of the coral boulder (Fig. B2F). The twig was deposited in sand 170 m north of the boulder. This sand projects beneath the nearly horizontal bottom of the boulder, an upright brain coral boulder associated with the problematic lucine discussed herein. The twig, as detritus, should predate deposition of the sand, as well as deposition of the coral boulder and the lucine. The twig age, corresponding to 1169–1269 cal yr CE, is older than the coral age, 1294–1458 cal yr CE, and it overlaps with the lucine age, 967–1213 cal yr CE.

Radiocarbon ages on a piece of wood may be consistent with the age of one of the dated coral boulders east of Warner. The boulder is a brain coral colony found upside down, protruding from a salt flat, and a sample from this boulder gave an age corresponding to the range 1283–1444 cal yr CE (Fig. B6C, sample 2011–3). Digging beside the boulder revealed a horizon of organic sand, interpreted as a buried soil, that contained a piece of wood (Fig. B6D). The organic sand appeared to project beneath the boulder, but the boulder was not excavated to establish whether its lowermost part rests on the organic horizon or is surrounded by it. Two ages were obtained from the wood, which contained close to 20 annual rings; the ages correspond to 1189–1271 cal yr CE and 1192–

1278 cal yr. CE. By stratigraphic superposition, the wood should predate deposition of the coral boulder if the organic horizon extends beneath the coral boulder. The compared ages meet this expectation, notwithstanding the possibility that deposition of the boulder happened some time after the death of the coral colony.

Inferred Time of Emplacement

Inland emplacement during a single pre-Columbian event most simply explains the nearly unimodal radiocarbon ages of the scattered coral clasts, the long tail on the side of earlier ages, the life-like form of many of the brain coral boulders, approximate concordance with all three conch ages, and concordance with two of the eight dated lucine valves (Fig. 5B). It can be supposed that a majority of the coral clasts were alive on arrival in 1200–1480 cal yr CE, the range in which two-thirds of the dated coral clasts cluster (Fig. 5C), and that the other clasts were reworked from preexisting deposits.

Emplacement during multiple events is less likely for two reasons. First, the clustered ages probably limit emplacement to a small slice of late Holocene time. All the coral ages predate 1500 cal yr CE, and 23 of the 27 coral ages at two standard deviations postdate 1000 cal yr CE, as do all three of the conch ages (Table 2). Second, it is difficult to explain this clustering by supposing that Anegada lacked a fringing reef until as recently as 216–550 cal yr CE, the oldest of the ages obtained (Table 2, sample 32). A reef this young would be an anomaly, compared with Caribbean localities where reefs have been present throughout the late Holocene. These localities include Martinique and the U.S. Virgin Islands, as judged from radiocarbon ages on *A. palmata* (Toscano and Macintyre, 2003, p. 263).

SEDIMENTARY ENVIRONMENTS

Proximity to Sea Level and the North Shore

This narrow age range notwithstanding, the sites of the scattered coral clasts were probably close to their present elevation, with respect to sea level, not just at the time of deposition but also for thousands of years before. Regionally, relative sea level has risen approximately one meter per millennium in the past few thousand years (Toscano and Macintyre, 2003). At Anegada, the absence of stranded Holocene shoreline notches ("Holocene Beach Ridges and Ponds" discussion; Fig. 2B) implies negligible net emergence in the centuries since demise of the bygone marine pond. The apparent absence of higher notches tends to rule out net emergence across thousands of years as well.

The net uplift at Anegada has also been small on a longer time scale. As noted in the discussion "Pleistocene Deposits," a Pleistocene coral sample collected a few meters above present sea level gave a uranium-series age close to 120,000 yr B.P. (120 ka). Subsequent net uplift is not required if the coral lived in the last centuries before it came to rest, if it was deposited no more than a few meters below ambient sea level, and if this sea level was close to the last interglacial maximum. Dated corals elsewhere show that global sea level exceeded present levels for much of the time between 125 ka and 115 ka, and that it peaked ca. 124 ka in the range 6–10 m above present levels (Kopp et al., 2009). Examples near Anegada include those reported from Florida (Muhs et al., 2011) and St. Croix (Toscano et al., 2012).

The scattered coral clasts probably came to rest about as far inland as they are today. The greatest late Holocene changes in shoreline position at Anegada are evidenced by the beach ridges farther west, near Flamingo Pond. Northeast Anegada provides little room for late Holocene shoreline change between the Pleistocene limestone and the fringing reef. Much the same holds for the area north of Red Pond, where limestone crops out locally near the north shore. The only coral rubble ridge recognized, whether in the field or on lidar topography, is the one that adjoins the modern shoreline at Soldier Wash.

Vegetation

The scattered coral clasts in northeast Anegada, from Soldier Point southeastward to the vicinity of Warner, were likely transported through trees and shrubs, or through the freshly mowed-down remains of those plants. The plant cover was probably thinner and shorter within a few hundred meters of shore than it was farther inland, as judged from modern vegetation encountered during mapping south of Soldier Point and Table Bay (Figs. A3B and A5B).

The few brain coral clasts encountered to the west, north of Bumber Well Pond and west of Red Pond, likely encountered little vegetation during transport unless they were saltated across the crests and swales of shrubby beach ridges. These coral clasts crossed over or through beach ridges of the north shore before halting in the bygone marine pond. A longer version of this journey likely emplaced the *Orbicella* and *Porites* clasts dated from south of Red Pond and Bumber Well Pond. They faced little impediment from vegetation, and they may have transited a freshly cleaned limestone floor of the trough that now holds Bumber Well Pond (along profile C-C′ of Fig. 6; Table 3).

INFERRED HISTORY OF EXTREME WAVES

Anegada's geological evidence for extreme waves can be grouped most simply into the three categories illustrated in Figures 3B, 3C, and 4B. The groups differ in typical landscape position; in sedimentary architecture; in the size, composition, and likely sources of clasts; and in age. The three groups, named in the following subheadings, connote a hierarchy of hazards. At the lowest rank are hurricanes like those of recent decades. An intermediate hazard is represented by what was perhaps the Lisbon tsunami of 1755. Both these hazards are dwarfed by the catastrophe in 1200–1480 cal yr CE.

Recent Hurricanes

Extreme-wave deposits of the lowest rank were formed or at least refreshed by modern storms. The coarsest are organized into a single coral rubble ridge a few tens of meters wide that hugs the island's north shore. Its limited inland

extent is consistent with a physiographic setting that limits routine storm effects: storm waves break on a fringing reef, and storm surge sinks into deep water beyond the reef. Extensive deposits of modern storms at Anegada have been limited to microbial debris. This debris contrasts with the sand and shell sheet of 1650–1800 cal yr CE, and even more with effects of the overwash in 1200–1480 cal yr CE.

Lisbon Tsunami or Other Extreme Waves in 1650–1800 cal yr CE

The south-directed overwash responsible for the sand and shell sheet poured over and through beach ridges north of the western salt ponds. A pink bioclastic facies was probably derived from the northern beach ridges, whether by reaming out of breaches that had been cut in 1200–1450, or by cutting of new breaches. The flows probably reworked parts of the lowest of the limestone boulder fields north of Bumber Well Pond.

The sand and shell sheet of 1650–1800 might represent the 1755 Lisbon tsunami. In a simulation for Anegada, far-traveled waves of the Lisbon tsunami rise and fall no more than 2 m and have periods of ~20 min (Buckley et al., 2012). Such waves may have risen gradually against beach ridges of the north shore without transporting coarse clasts from the reef or the reef flat. The simulated wave period could be compared further with observations of the 1755 tsunami elsewhere in the Caribbean (Roger et al., 2010).

In any case, the mainly interior source of the sand and shell sheet of 1650–1800 provides local calibration of how a large tsunami of Lisbon source would register geologically at Anegada. Although the sheet represents Anegada flooding more extreme than any other since 1650, this flooding failed to introduce coarse clasts freshly derived from the fringing reef or the reef flat. The 1755 Lisbon tsunami thus failed to replicate the pre-Columbian emplacement of coral boulders and cobbles at Anegada. Those coral clasts were not emplaced by a prior tsunami of remote origin unless its far-traveled waves somehow managed to dwarf those of the 1755 Lisbon tsunami at Anegada.

This reasoning leaves either a tsunami of nearby origin or an unusual storm that produced tsunami-like bores as the cause of the 1200–1480 catastrophe.

Puerto Rico Trench Tsunami or Haiyan-Like Storm in 1200–1480 cal yr CE

Anegada's greatest overwash in recent millennia occurred in the thirteenth, fourteenth, or fifteenth century, probably in a single event. Examples of the inundation heights and distances attained are plotted in blue in Figure 6 and elaborated in Table 3. These examples set minima that might be used to evaluate simulations of tsunamis generated along the Puerto Rico Trench and of tsunami-like bores from an unusual storm.

The pre-Columbian event is evidenced by a great variety of deposits: the main sand sheet, its associated coral clasts and large mollusks, and inland fields of limestone boulders and cobbles. Some of these deposits were built into a marine pond that would later, after 1650, become hypersaline; others extended hundreds of meters inland across limestone uplands. The scattered coral clasts and associated molluscan shells demonstrate entrainment from the fringing reef, the reef flat, or both. Bioclastic sand was also deposited inland from the northeast shore, where it may have been derived through removal of ancestors to the beach ridges shaded yellow along the eastern profiles in Figure 6. In the west, beach ridges were abundantly breached, and a sandy fan with coral clasts and lucine valves was built near the south shore, probably by flows that crossed the island from north to south that attained heights of 4 m or more midway along this transit. A time window of 1200–1480 is indicated by the nearly unimodal, consistently pre-Columbian ages of the brain coral clasts and conch shells, and by the youngest of the lucine ages. This time window likely applies to initial emplacement of the inland fields of scattered limestone boulders and cobbles. Had those fields been inherited from prior overwash thousands of years ago, coral clasts should have given such earlier ages as well.

This geological catastrophe was either a tsunami of nearby origin or a tsunami-like effect of an unusual storm. Its effects at Anegada exceeded those (if any) of the far-traveled waves of the 1755 Lisbon tsunami, or of any other hurricane or tsunami in the past 500 yr or more. A tsunami of nearby origin, generated during normal faulting or thrust faulting along the eastern Puerto Rico Trench, was previously invoked to explain the fields of limestone boulders north of Bumber Well Pond. If instead produced by an unusual storm, the overwash in 1200–1480 probably required bores like those generated in the Philippines by 2013 Typhoon Haiyan at a fringing reef that adjoins deep water ("Tsunami-Like Bores Analogous to Those from Typhoon Haiyan").

In modeling these two alternatives, the burden of proof will rest more on an unusual storm than on a tsunami of nearby origin. A large enough tsunami of nearby origin, particularly from normal faulting along the Puerto Rico Trench, has been shown to be capable of catastrophic inundation at Anegada (Buckley et al., 2012). It remains to be determined, from modeling calibrated to Typhoon Haiyan, whether tsunami-like bores from an unusual storm can produce this much inundation as well, not just where a reef flat is conspicuous (Fig. 6, profiles A-A′, C-C′, I-I′), but also where it is narrow or interrupted (profiles D-D′, F-F′).

CONCLUSIONS

Inland deposits ranging from sand to boulders rank highest in a hierarchy of extreme-wave effects on a low-lying Caribbean island near the Puerto Rico Trench. These deposits were scattered hundreds of meters beyond the island's storm-built rubble ridge. The deposits also exceed the local geological effects, if any, of a tsunami of remote origin. They include coral clasts that were probably emplaced during the last centuries before the arrival of Columbus. The catastrophe far surpassed any other at the island in recent millennia. If not an extraordinary storm, the catastrophe was likely a tsunami generated by thrust or normal faulting along the Puerto Rico Trench. In either case the inland fields of scattered coral clasts attest to a Caribbean and North Atlantic hazard unknown from either satellite geodesy or written history.

Figure A1. Distribution and examples of deposits of modern storms.

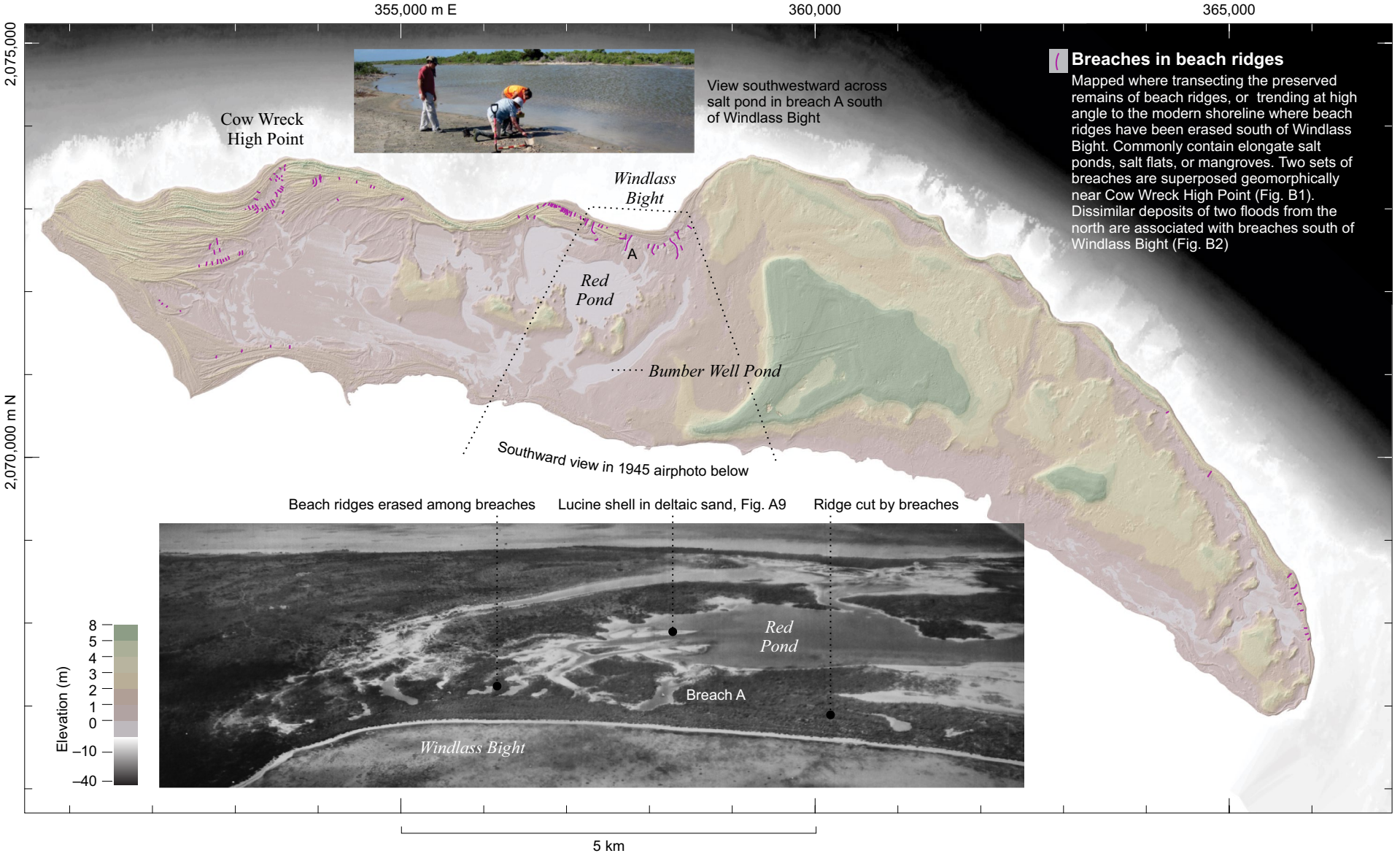

Figure A2. Distribution and examples of breaches in beach ridges.

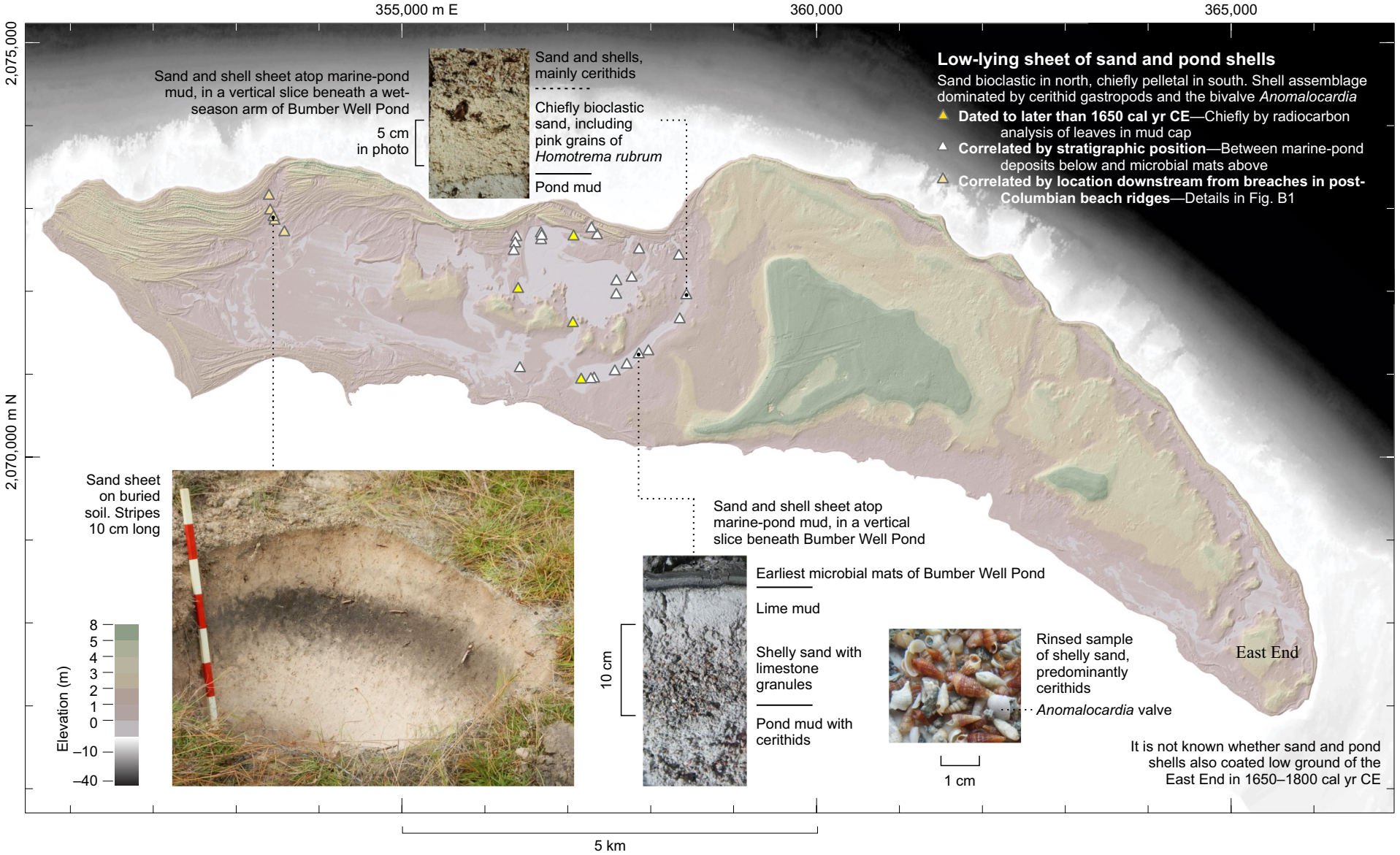

Figure A3. Distribution and examples of low-lying sheet of sand and pond shells.

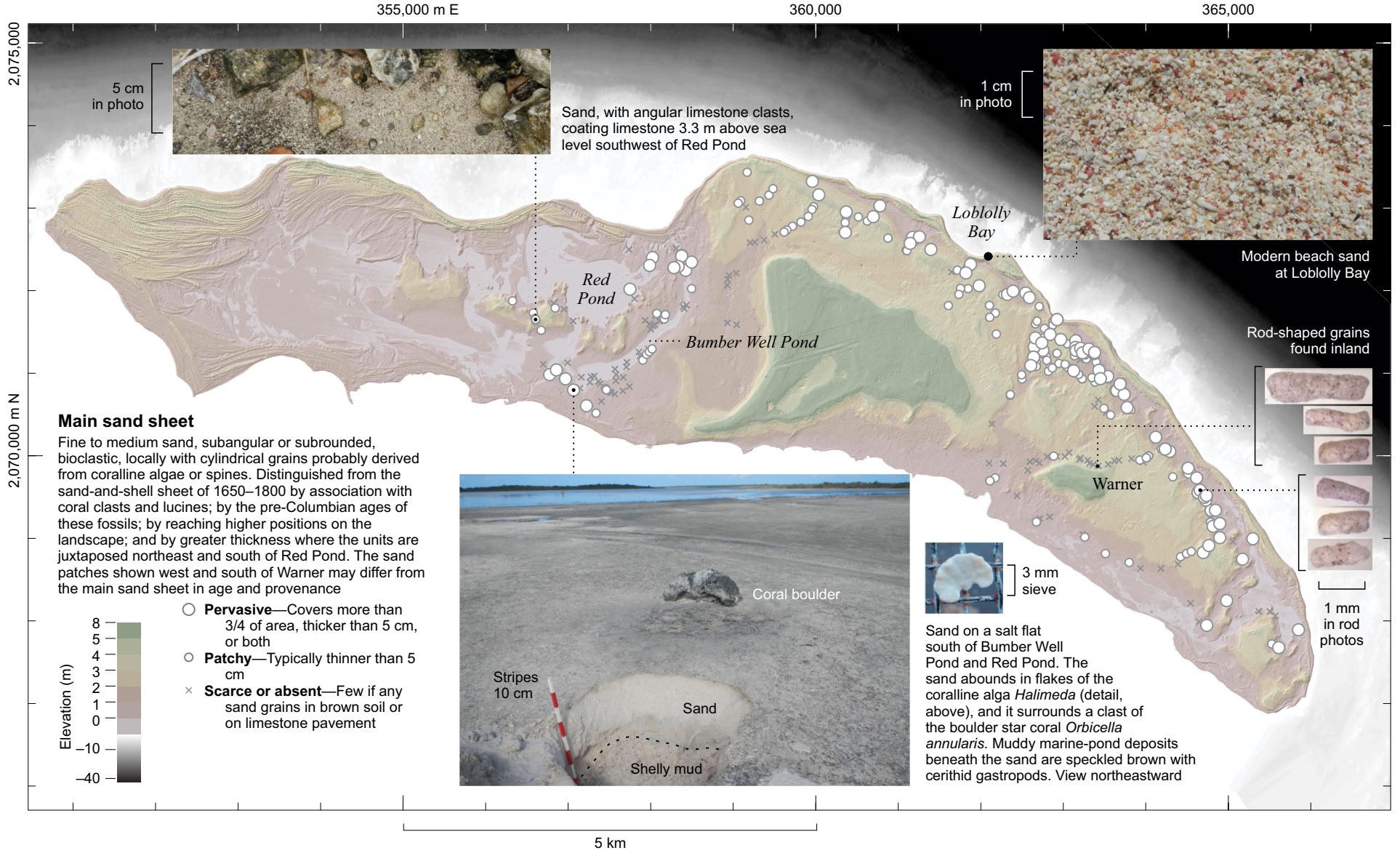

Figure A4. Distribution and examples of main sand sheet.

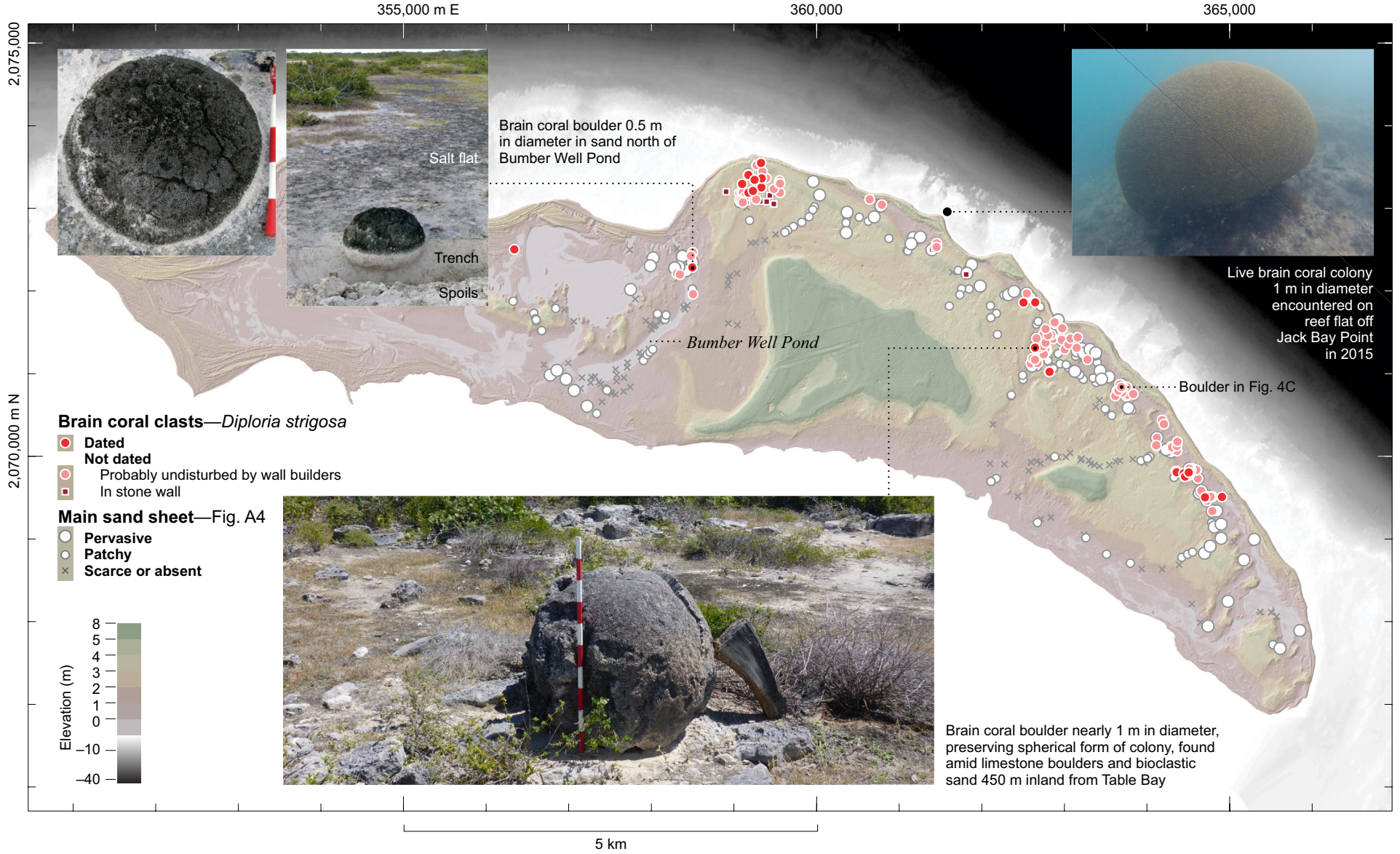

Figure A5. Distribution and examples of boulders and cobbles of brain coral.

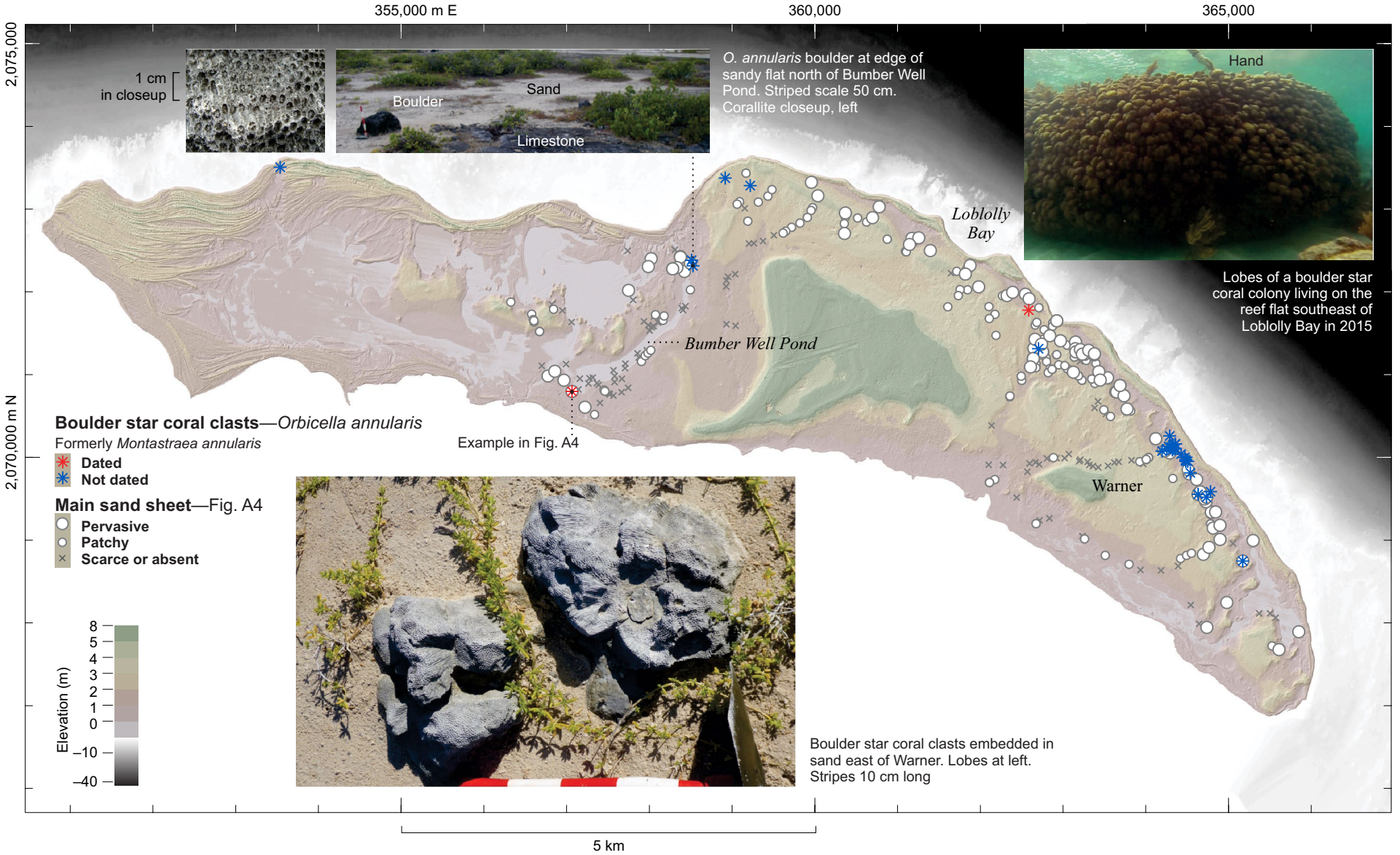

Figure A6. Distribution and examples of large clasts of boulder star coral.

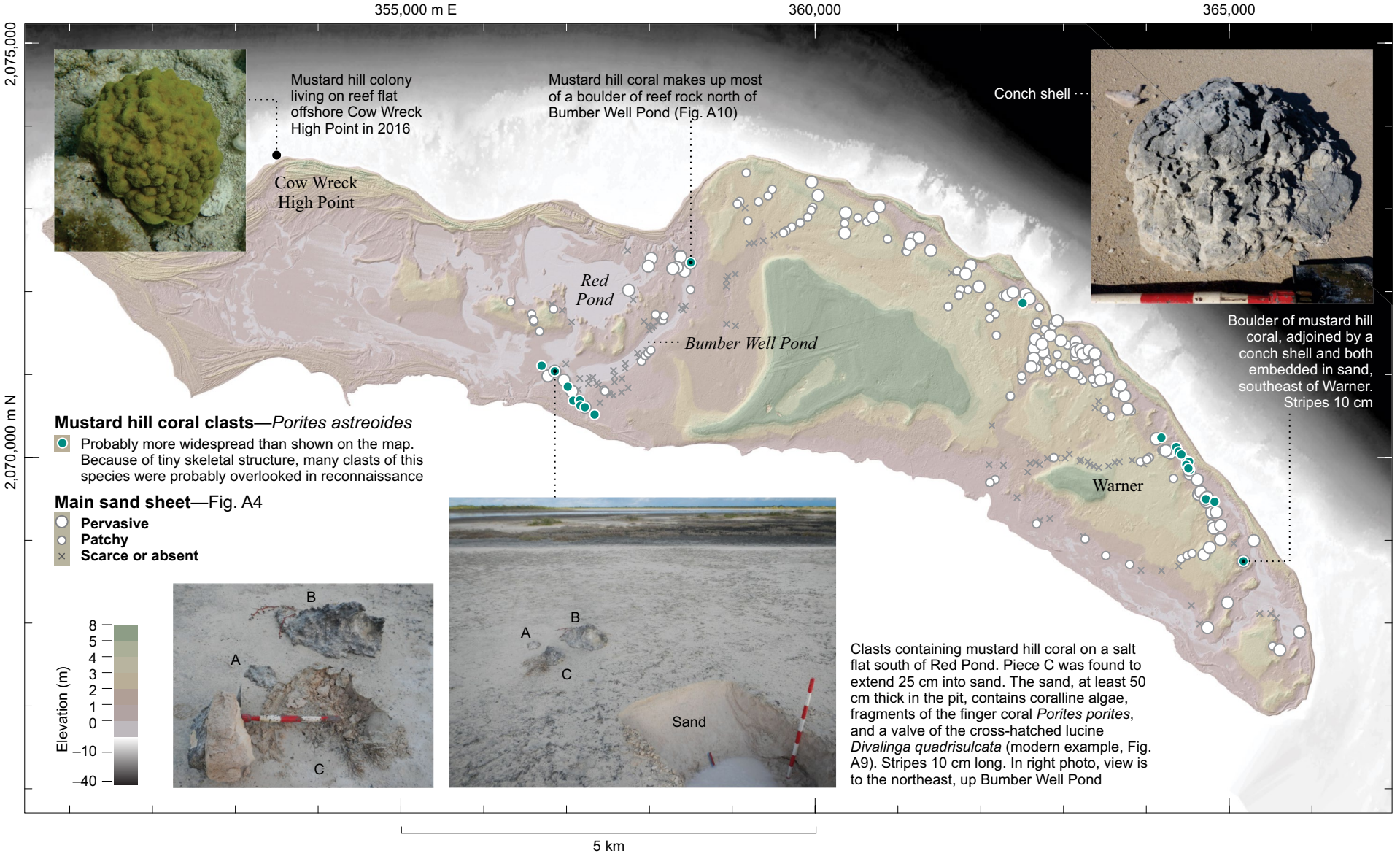

Figure A7. Distribution and examples of large clasts of mustard hill coral.

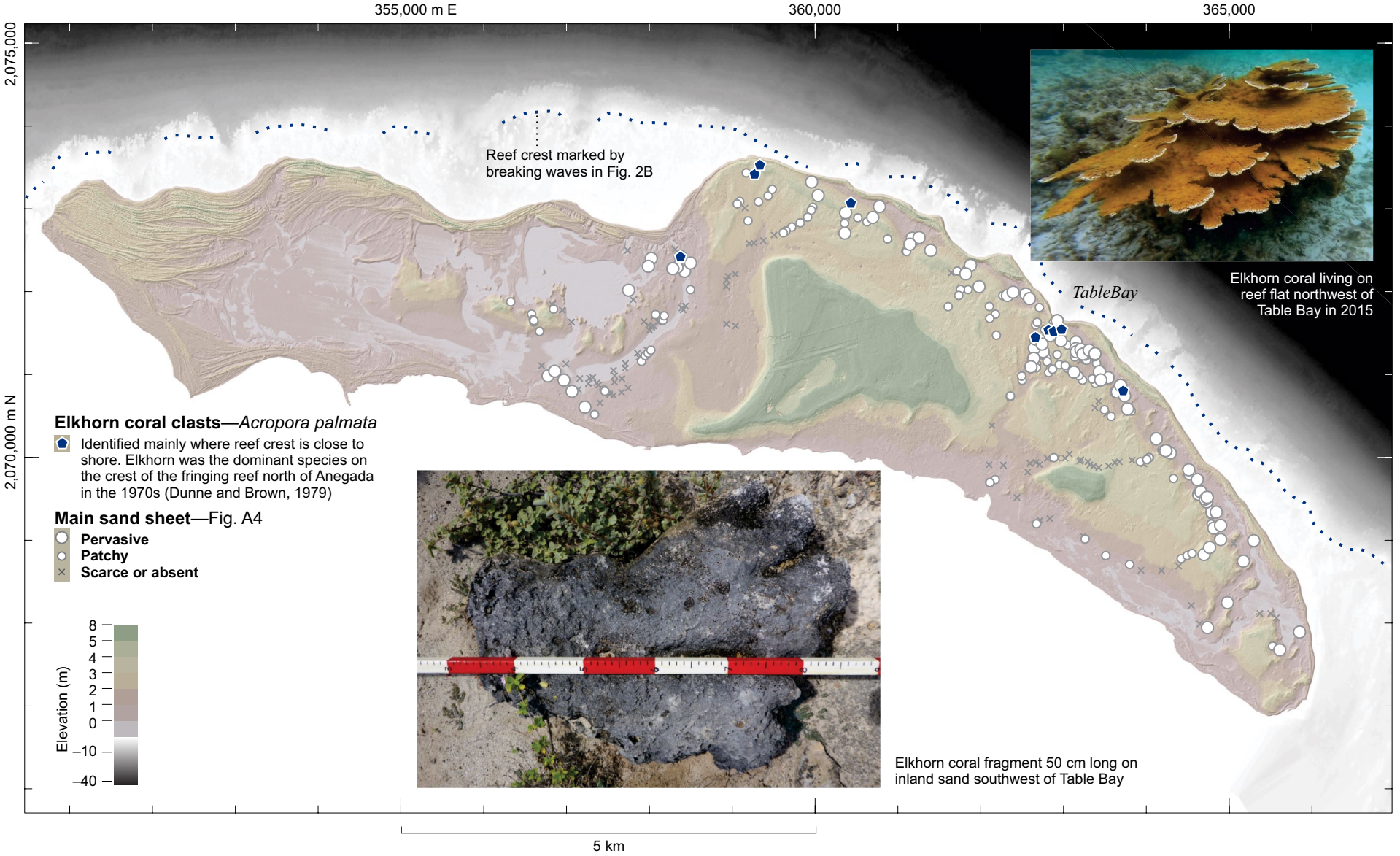

Figure A8. Distribution and examples of large clasts of elkhorn coral.

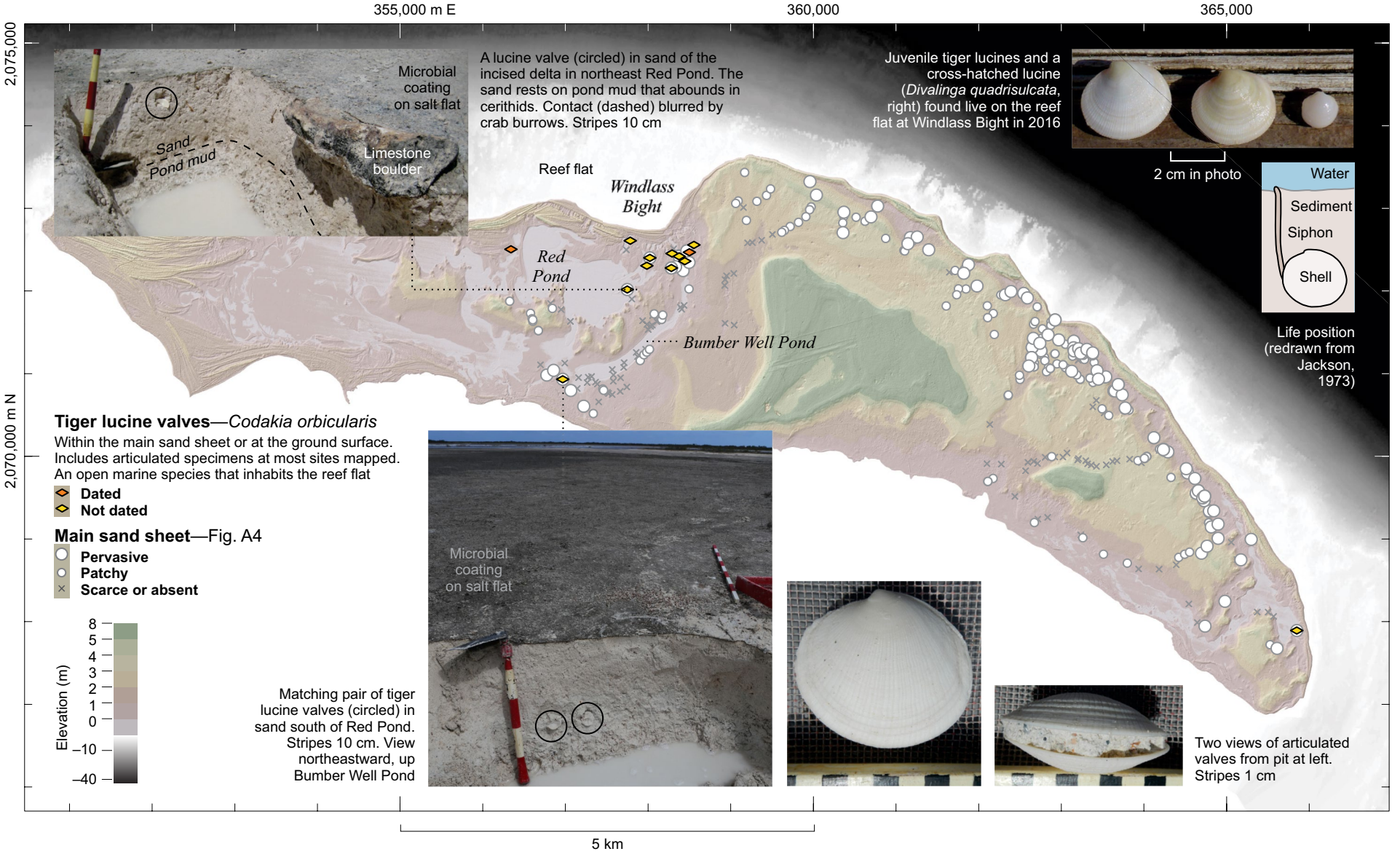

Figure A9. Distribution and examples of valves of tiger lucine.

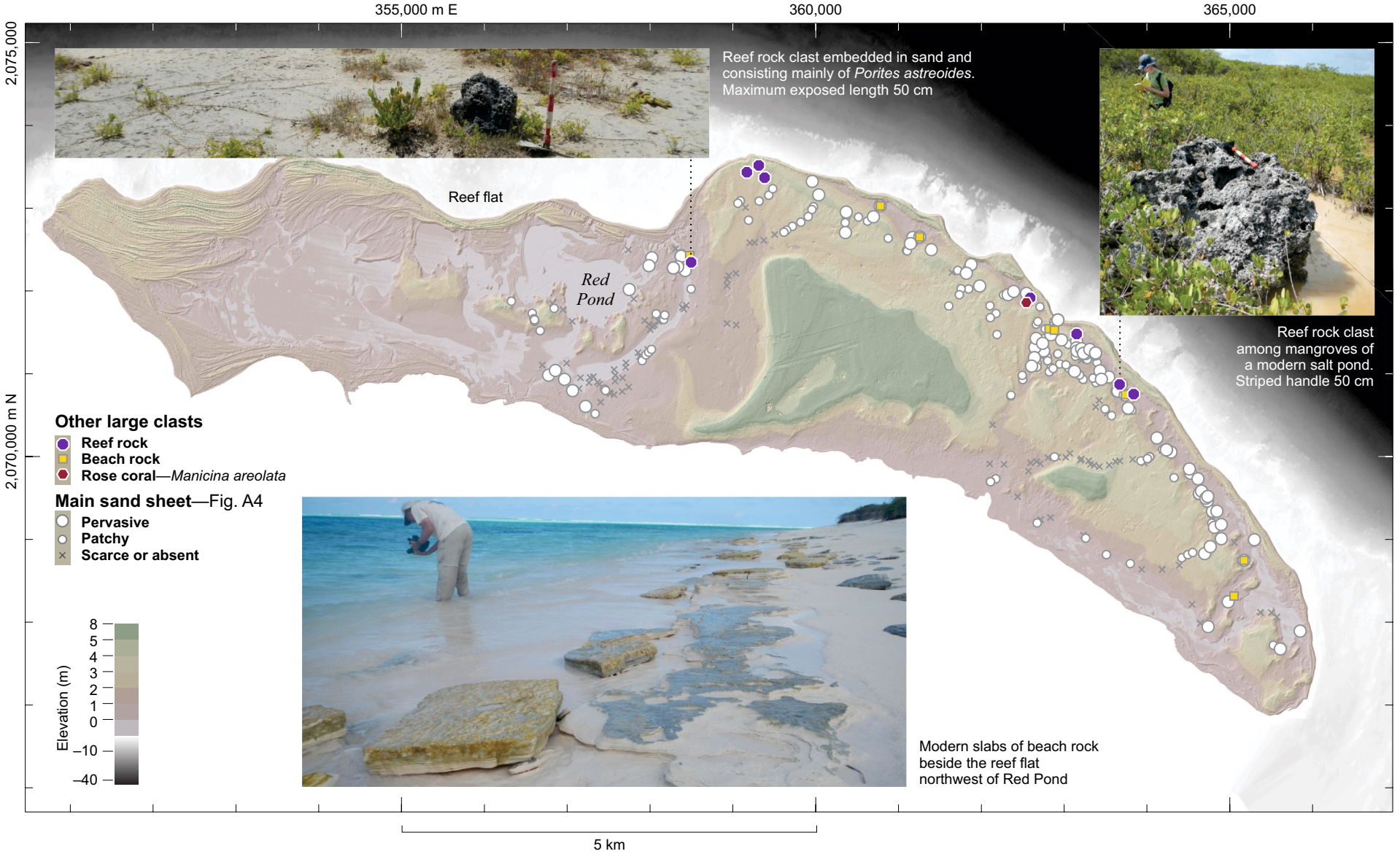

Figure A10. Distribution and examples of boulders of reef rock and beach rock.

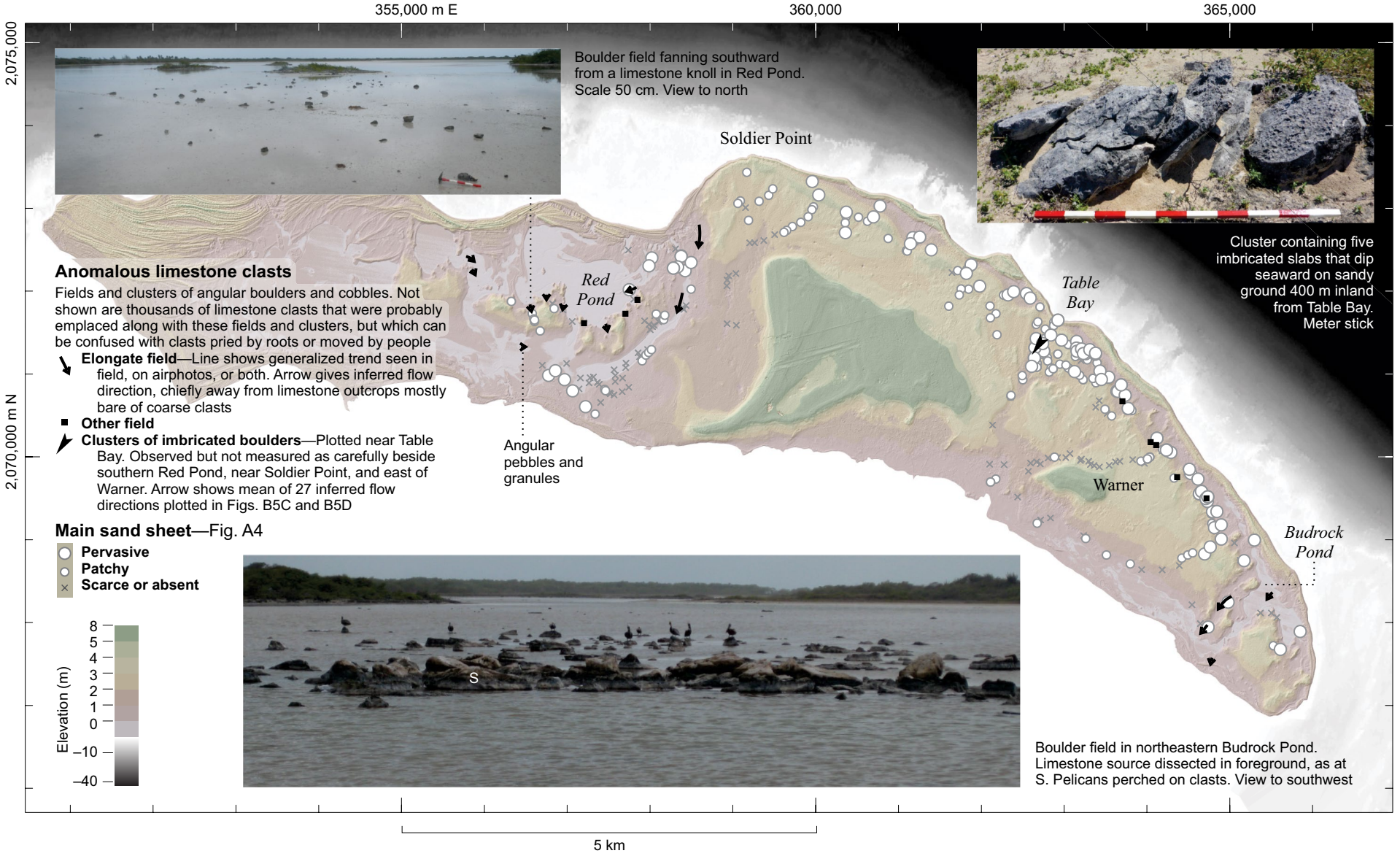

Figure A11. Distribution and examples of anomalous limestone clasts.

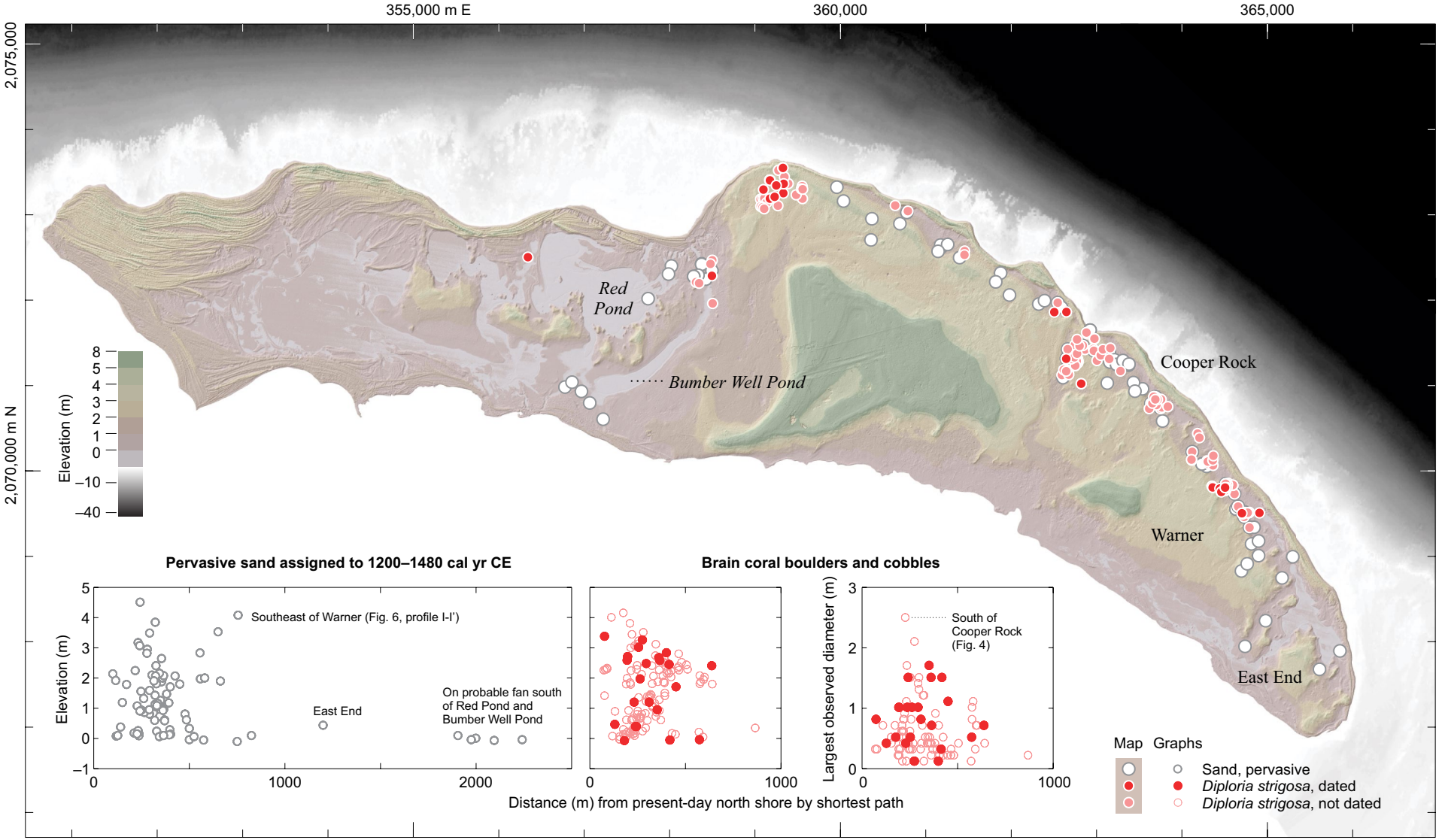

Figure A12. Clast elevation and size in relation to distance inland.

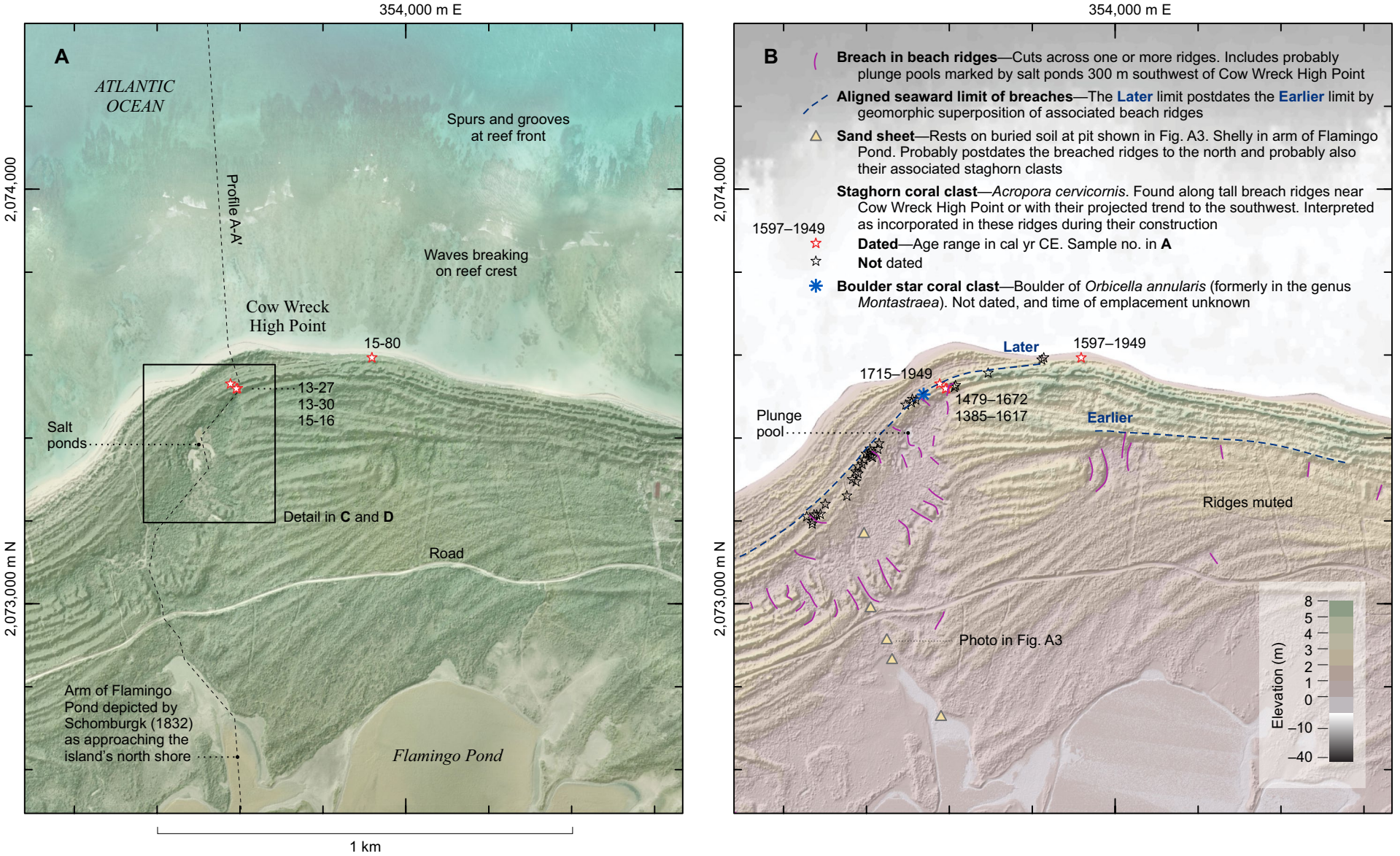

Figure B1 (*on this and following two pages*). Dated samples and their setting near Cow Wreck High Point.

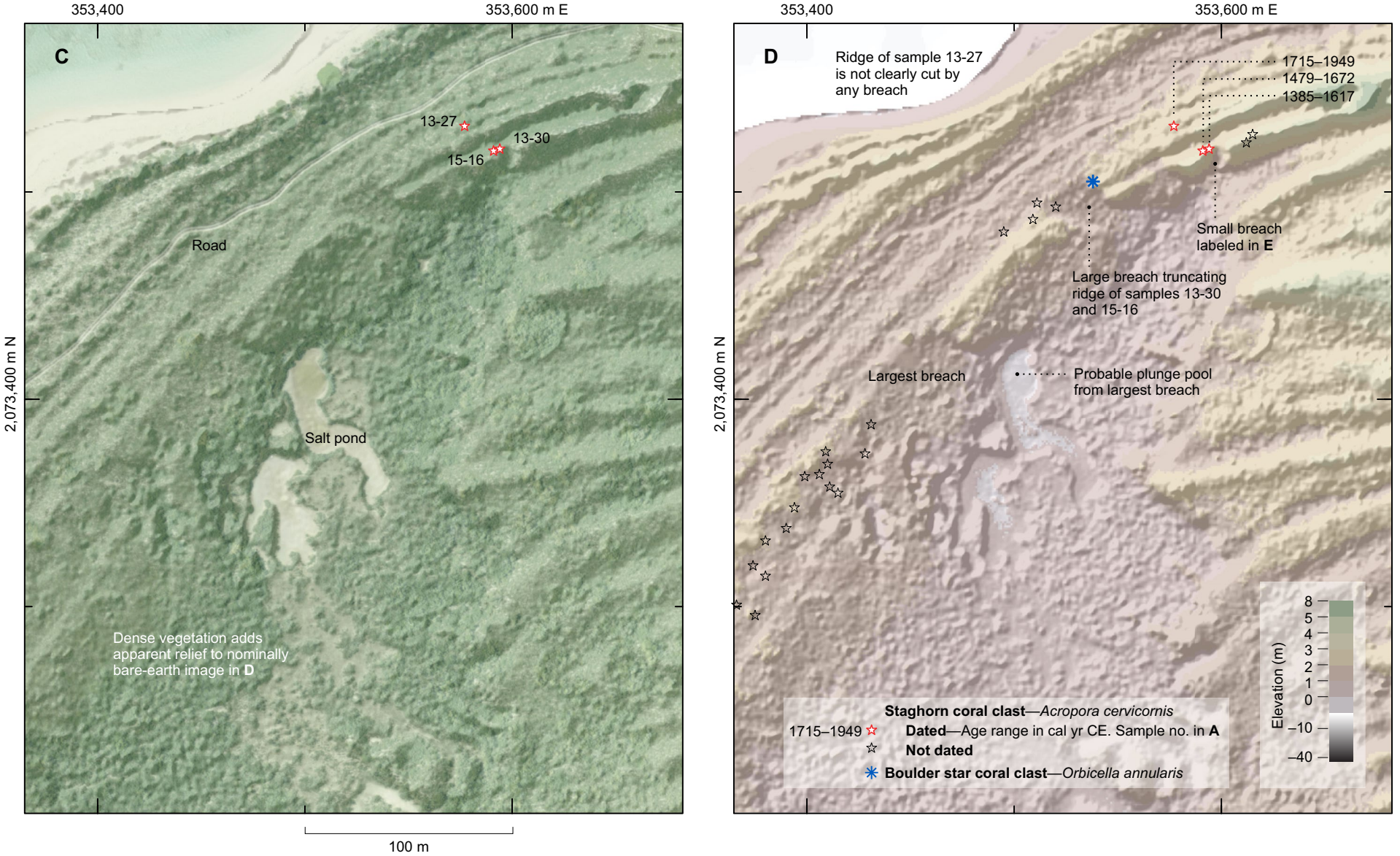

Figure B1 (*continued*).

E **Dated clasts, all *Acropora cervicornis*, listed from youngest age to oldest**

13-27
435 ± 15 ^{14}C yr B.P.
1715–1949 cal yr CE

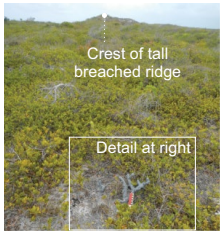

Cross section through staghorn stick that had a weathered exterior

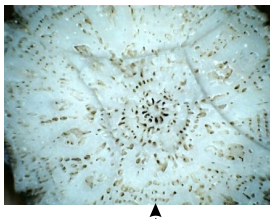

15-80
535 ± 15 ^{14}C yr B.P.
1597–1949 cal yr CE

Unweathered exterior of staghorn sample from eroding bluff beside beach, as at 15-80

Weathered exterior of staghorn sample from setting like those of 13-27 and 13-30

Person in orange vest on crest of tallest beach ridge

13-30
680 ± 15 ^{14}C yr B.P.
1479–1672 cal yr CE

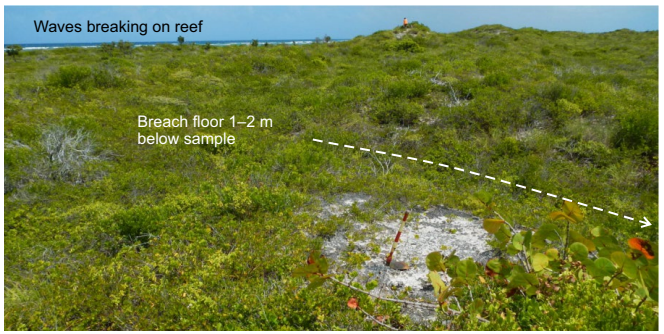

Striped handle 50 cm, beside sample 13-30. March 2012

Exhumed by deflation. 2016

15-16
805 ± 25 ^{14}C yr B.P.
1385–1617 cal yr CE

Photo unavailable

Figure B1 (*continued*).

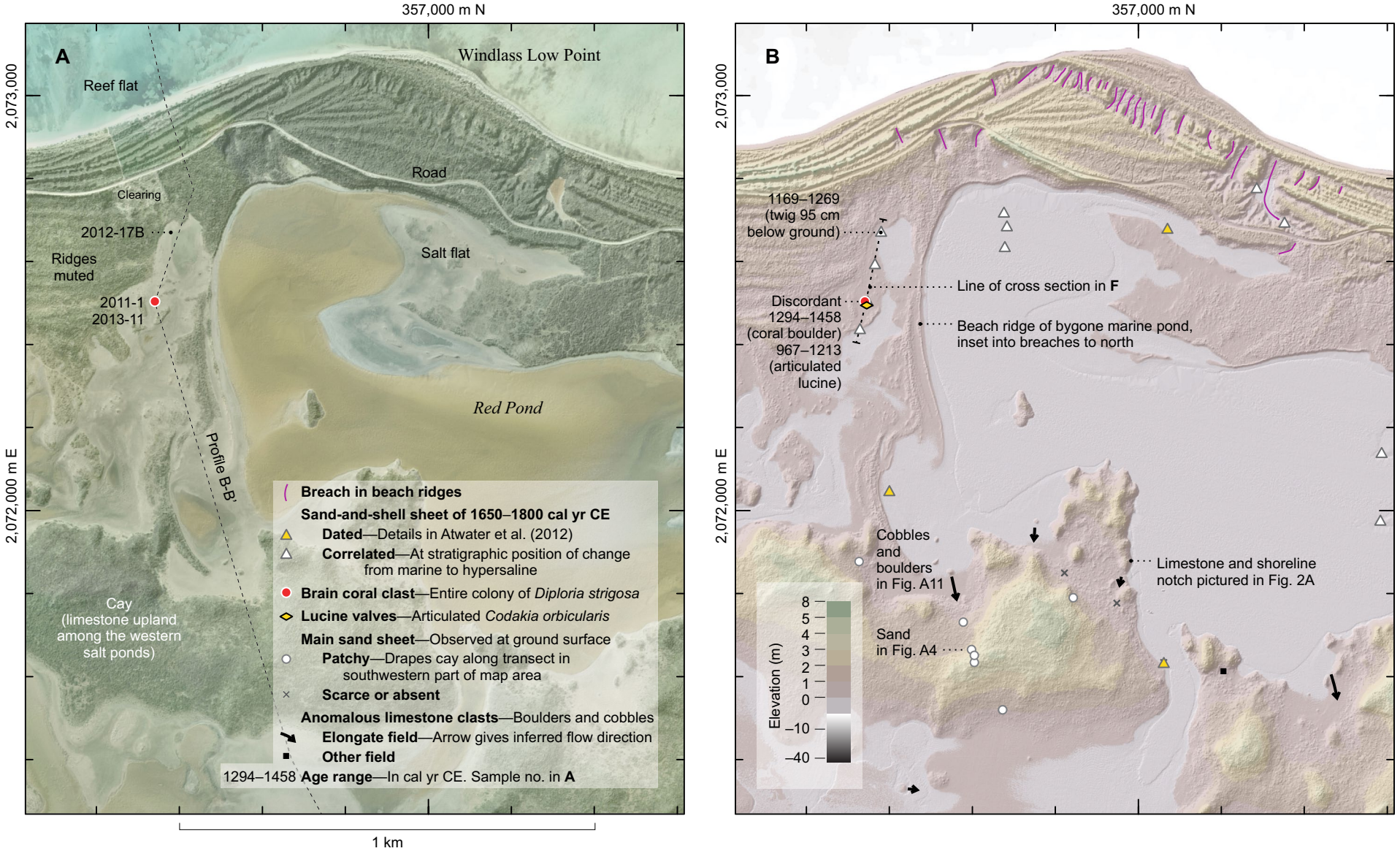

Figure B2 (*on this and following two pages*). Dated samples and their setting at northwest Red Pond.

C Overviews of coral boulder

As encountered in 2009

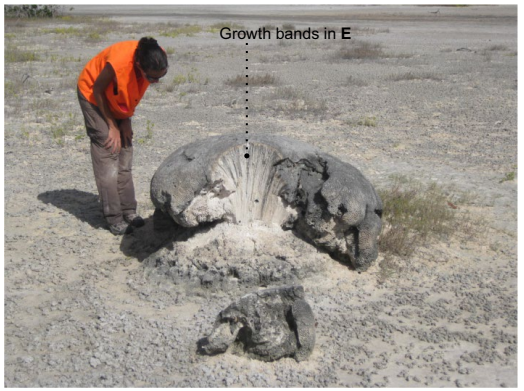

Surrounded in 2011 by dried microbial debris from 2010 Hurricane Earl

D Exterior shape of coral boulder

Exterior surface dimpled where coral probably grew around a worm tube (process described by Patton, 1976, p. 6)

E Interior growth bands

Smooth curve of upper exterior surface parallels annual growth bands. This surface has been exposed to subaerial weathering for six or seven centuries if the head was deposited here, live, in the 14th or 15th century CE (Fig. 5). The head probably protruded slightly above high tide in the bygone interior pond, as judged from modern tide levels in **F**. Figure A10 shows a modern example of a reef-derived boulder surrounded by water and mangroves.

Figure B2 (*continued*).

F **Generalized stratigraphic cross section through coral boulder**—Location in **B**

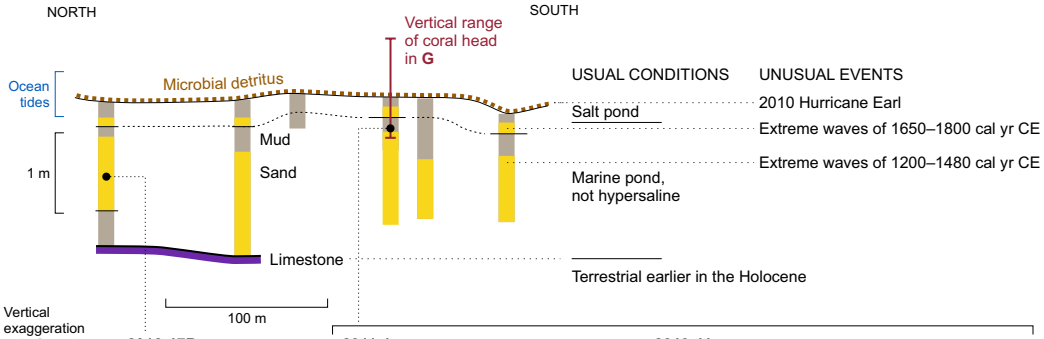

Vertical exaggeration x50. Ground heights surveyed by leveling with 1-cm closure error

2012-17B
Twig
810 ± 30 ^{14}C yr B.P.
1169–1269 cal yr CE

2011-1
Diploria strigosa—Sampled above ground
930 ± 30 ^{14}C yr B.P.
1294–1458 cal yr CE

2013-11
Codakia orbicularis, articulated—From pit in **G** and **H**
1280 ± 20 ^{14}C yr B.P.
967–1213 cal yr CE
Too old to have been deposited live with the *Diploria* unless later contaminated by old carbon

Age ranges in cal yr CE at two standard deviations (Table 2)

G **Excavations beneath and near coral boulder**

Probing the boulder's base, which was found almost flat for 90 cm southward from the north edge

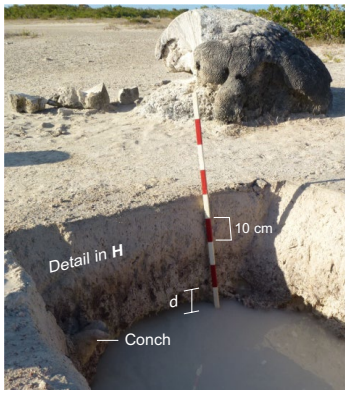

Pit south of boulder. *d*, depth to bottom of boulder 40–50 cm, projected from area probed in photo at left

Same pit

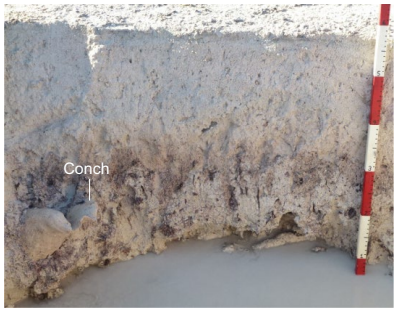

Salt flat—Coated in 2010 hurricane (**C**)
Ground surface

Muddy sand—Mostly correlated with sand-and-shell sheet of 1650–1800 cal yr CE. Built up further by wet-season flooding of modern salt flat, and mixed by burrowing crabs

Burrowed contact

Mud with mangrove roots—Encases the mollusc shells and probably surrounds the lowest part of the coral boulder. The mud probably accumulated in the bygone marine pond

H **Mollusks from pit a few meters south of boulder**

An entire conch *Strombus gigus* (above left) and an articulated bivalve *Codakia orbicularis* (above right) and were found in the depth range of the projected level of the coral-head base. Neither species is part of the molluscan assemblage of the marine pond that persisted until the extreme waves of 1650–1800 cal yr CE (Reinhardt et al., 2012; Atwater et al., 2012).

Figure B2 (*continued*).

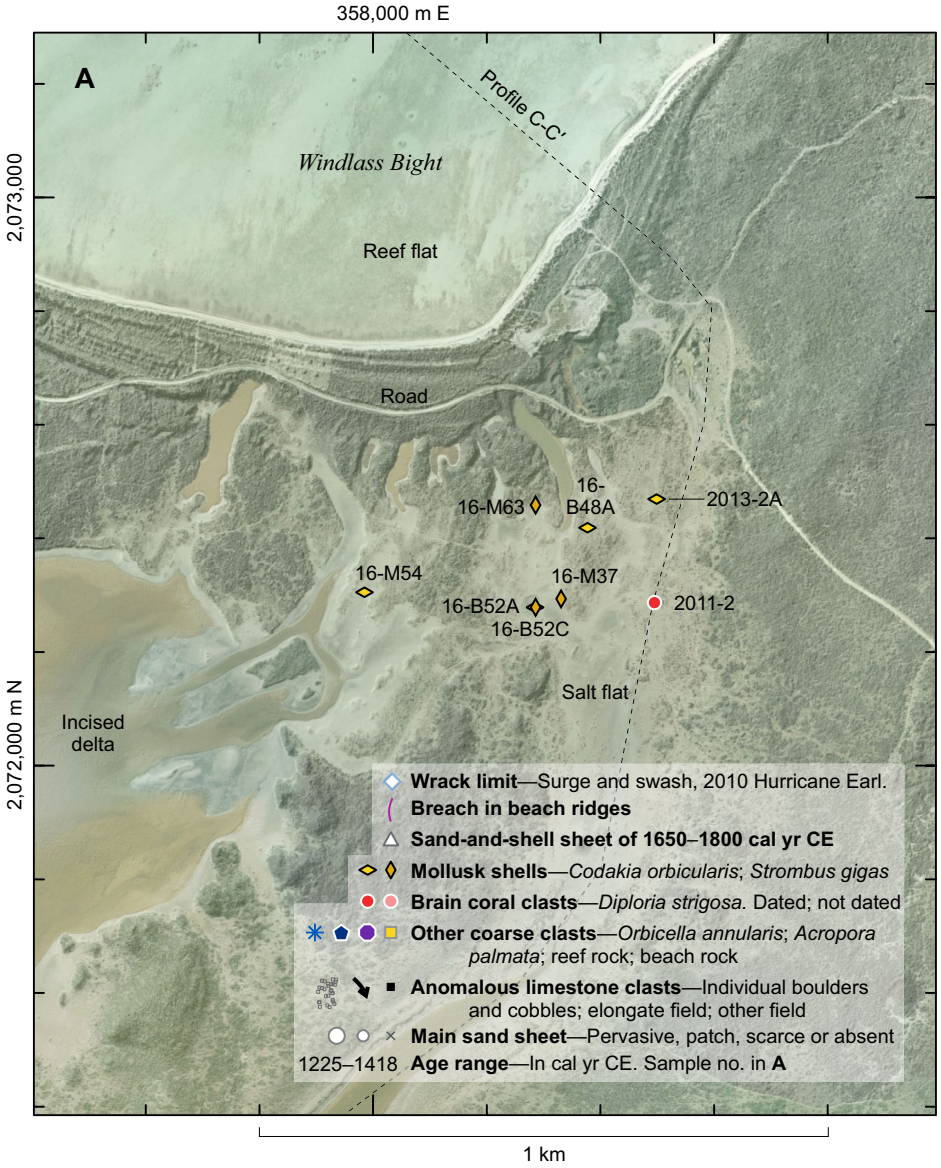

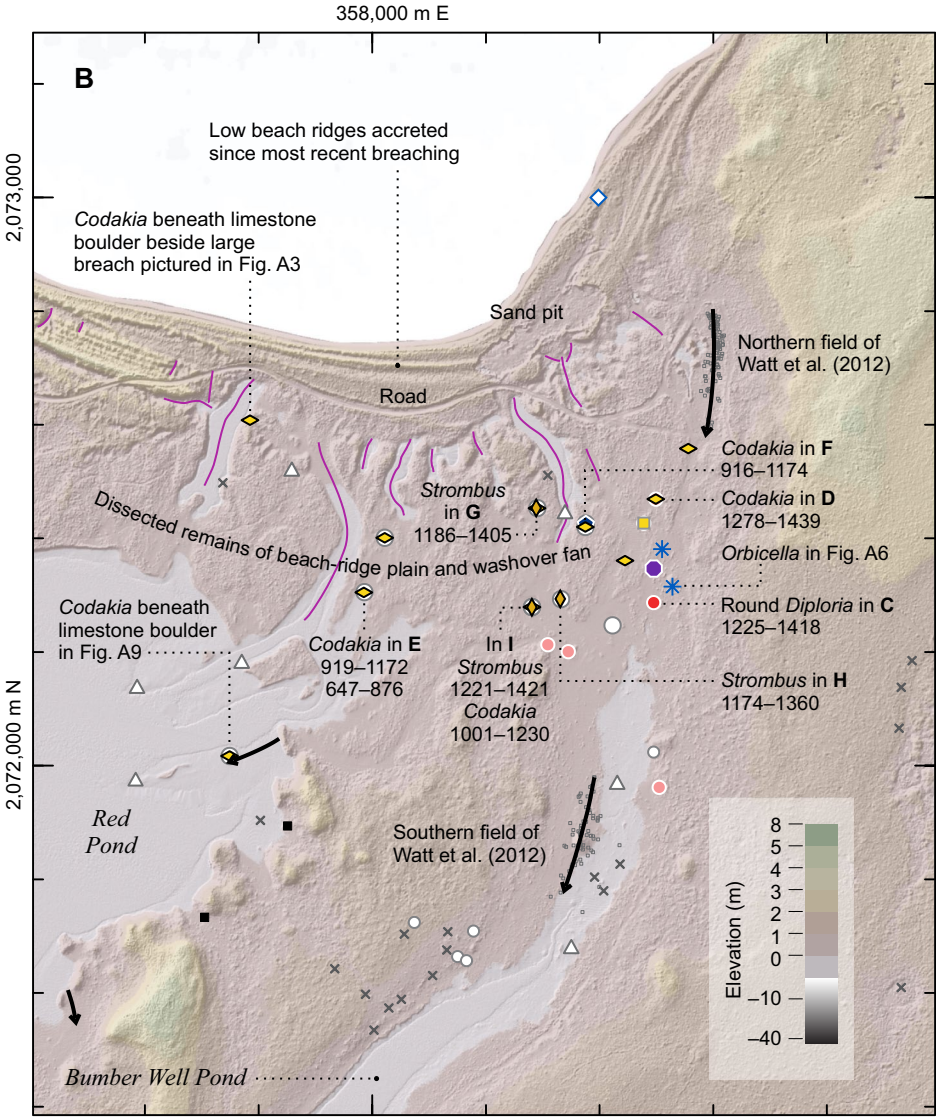

Figure B3 (*on this and following four pages*). Dated samples and their setting near Windlass Bight.

C **Round brain-coral head**

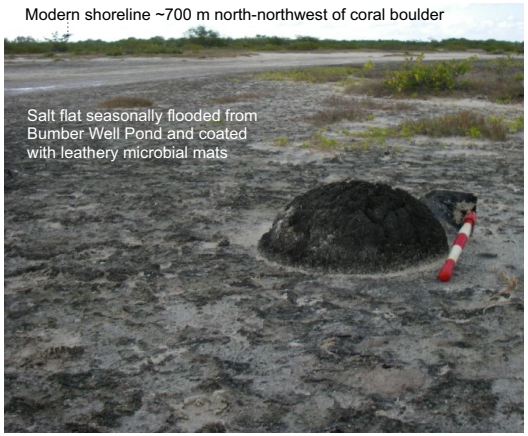

2008

Boots rest on limestone basement. Between limestone and bottom of coral boulder is fine to medium sand that contains cerithid gastropods and disarticulated *Anomalocardia* valves. Trench pictured also in Fig. A5

2011

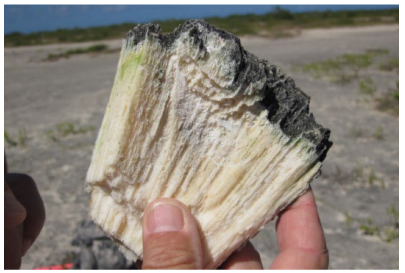

2011-2
1020 ± 25 ^{14}C yr B.P.
1225–1418 cal yr CE

D **Articulated lucine in sand that projects beneath a different brain-coral clast**

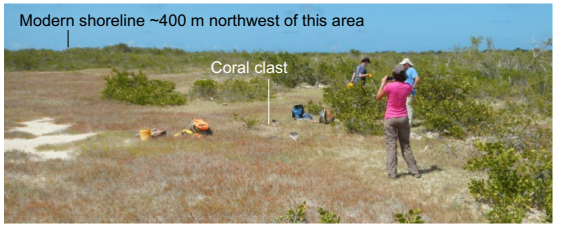

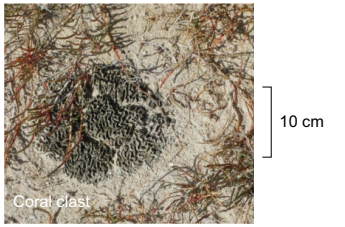

2013

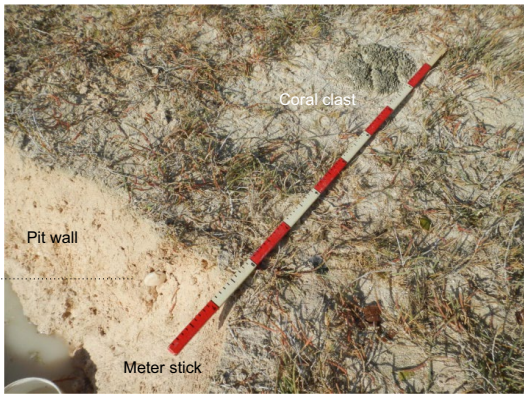

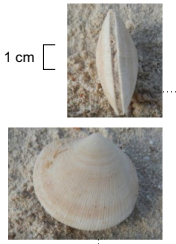

2013-2A
970 ± 20 ^{14}C yr B.P.
1278–1439 cal yr CE

Generalized stratigraphy in pit

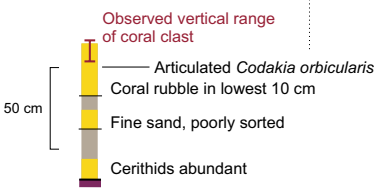

EXPLANATION
Sandy mud or mud
Sand or sandy bioclastic gravel
Limestone, probably in place

Figure B3 (*continued*).

E **Articulated lucine valves dated to 919–1172 cal yr CE and 647–876 cal yr CE**

View to southwest. Inferred flow direction is away from camera

Blue labels give depth below ground surface

16-M54
1310 ± 15 ^{14}C yr B.P.
919–1172 cal yr CE

16-M54
1600 ± 20 ^{14}C yr B.P.
647–876 cal yr CE

Approximately 5 cm

F **Site of articulated lucine valves dated to 916–1174 cal yr CE**

View to northwest. Inferred flow direction is toward the camera

16-B48A
1310 ± 20 ^{14}C yr B.P.
916–1174 cal yr CE

Fine sand, perhaps from overwash in 1650–1800 that re-used the plunge pool

Sand with discontinuous cement, interpreted as a formerly subaerial

Medium sand extending to limestone at 70 cm depth

Approximate stratigraphic position of articulated *Codakia orbicularis* 5.5 cm long encountered 30 cm below ground in a shovel slice. Sample **16-B48A**

Figure B3 (*continued*).

G **Entire conch shell dated to 1186–1405 cal yr CE**

Stripes 10 cm

Conch of 16-M63 exposed in pit wall ~15 cm below

16-M63
1050 ± 30 ^{14}C yr B.P.
1186–1405 cal yr CE

Additional clasts found in pit include this lucine valve and, at far left, cobbles encrusted with pink *Homotrema*

10 cm

H **Site of entire conch shell dated to 1174–1360 cal yr CE**

16-M37
1070 ± 15 ^{14}C yr B.P.
1174–1360 cal yr CE

Conch of 16-M37 (no photo taken) was collected ~20 cm below ground surface in a southern extension of this pit. View to the north. Stripes on shovel handle 10 cm

Pit wall consists of muddy fine to medium sand containing cerithid gastropods and land snails, and riddled with crab burrows. Depth to Pleistocene limestone 30–40 cm

Figure B3 (*continued*).

I Probably discordant ages on a conch shell fragment and a disarticulated lucine valve, both from site 16-B52

View to north, toward inferred offshore source of conch shell

16-B52C
1020 ± 30 ^{14}C yr B.P.
1221–1421 cal yr CE

Conch shell fragment **16-B52C**, extending 22–32 cm below ground surface

View to south, with shadow on pit wall shown in detail below

16-B52A
1250 ± 20 ^{14}C yr B.P.
1001–1230 cal yr CE

Figure B3 (*continued*).

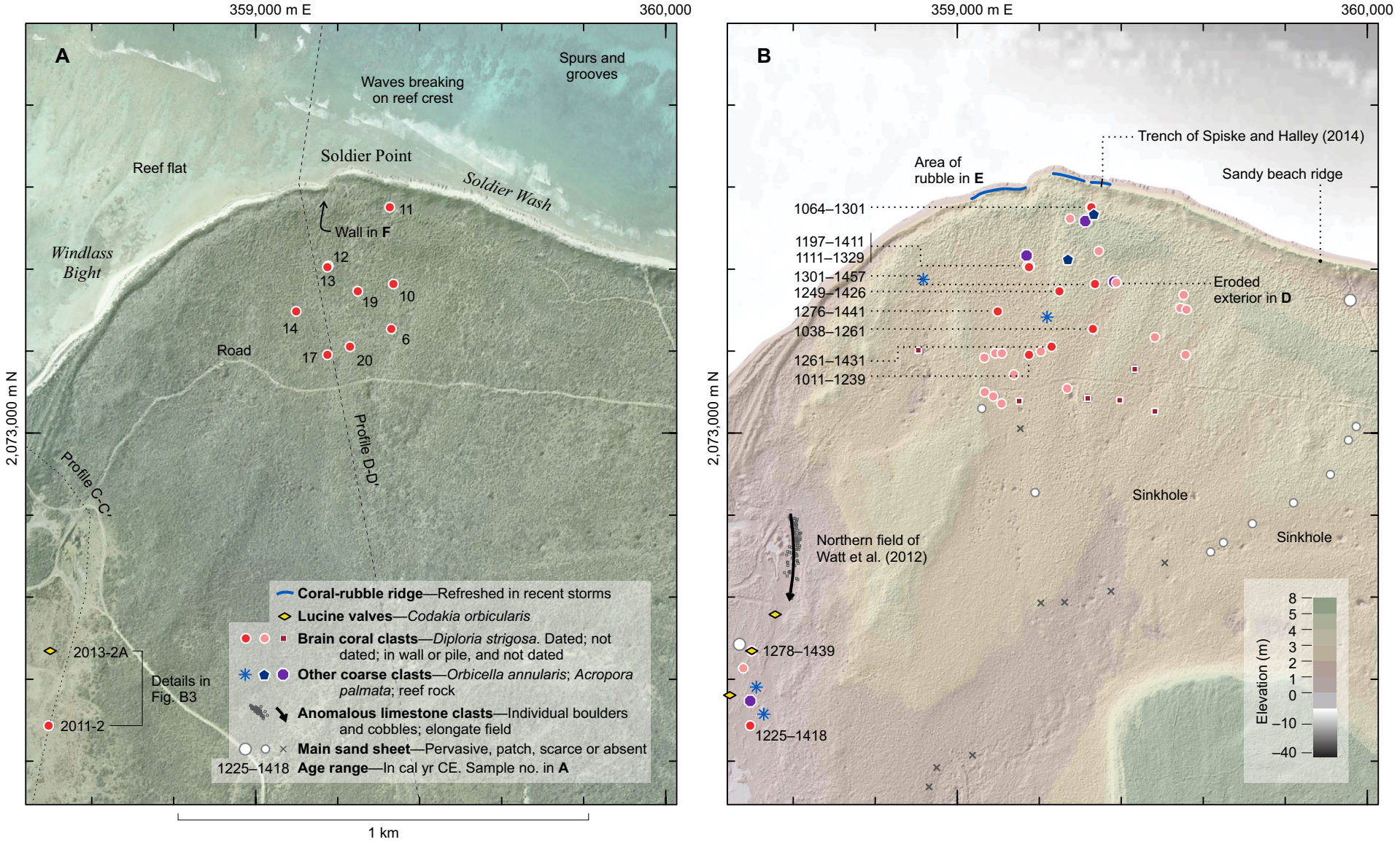

Figure B4 (*on this and following two pages*). Dated samples and their setting near Soldier Point.

C **Dated boulders and cobbles near Soldier Point, listed from youngest age to oldest**

10
925 ± 20 ^{14}C yr B.P.
1301–1457 cal yr CE

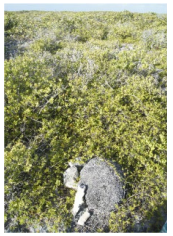
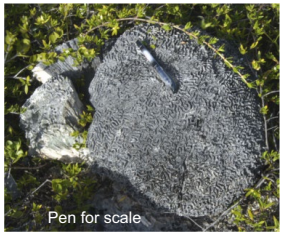

14
970 ± 25 ^{14}C yr B.P.
1276–1441 cal yr CE
Upside down

20
990 ± 20 ^{14}C yr B.P.
1261–1431 cal yr CE

19
1000 ± 20 ^{14}C yr B.P.
1249–1426 cal yr CE

12
1040 ± 30 ^{14}C yr B.P.
1197–1411 cal yr CE


13
1110 ± 20 ^{14}C yr B.P.
1111–1329 cal yr CE
Upside down


11
1150 ± 35 ^{14}C yr B.P.
1064–1301 cal yr CE
Pitted microatoll


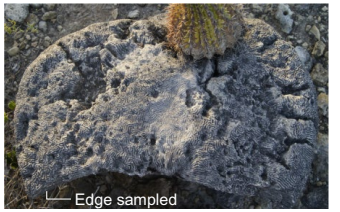

6
1210 ± 20 ^{14}C yr B.P.
1038–1261 cal yr CE


Dimpled but apparently more weathered than smoothly curved surface in Figure B2D

Figure B4 (*continued*).

C **Dated boulders and cobbles near Soldier Point, listed from youngest age to oldest**

17
1240 ± 20 ^{14}C yr B.P.
1011–1239 cal yr CE

Fragment in right photo is partly shaded at center of left photo. Left photo also shows other fragments freshly broken from the coral clast.

D **Coral head not dated**—Eroded exterior encrusted by marine worm and foraminifera. May have arrived long-dead

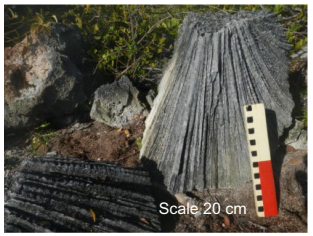

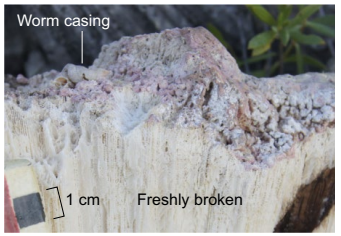

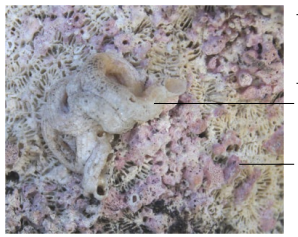

E **Rubble ridge**—Modern analog for a likely source of dated clasts 17, 19, and 20 (in **C**) and 32 and 33 (Fig. B5)

Brain-coral cobbles removed from rubble and photographed

F **Stone walls**—Farmed fields were mapped nearby in 1831 (Schomburgk, 1832)

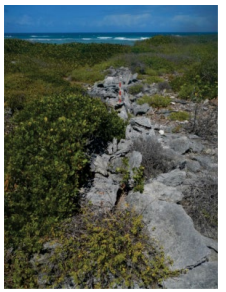

Near north shore (view mapped in **A**)

Probably southwest of site 17 in **A**. Stripes 10 cm long

Some brain-coral clasts were found in stone walls (Fig. A5). None of these clasts were dated.

Made mainly of limestone boulders, the walls can complicate the identification of limestone clasts that were moved by water. Wall builders had little apparent effect, however, on the consistent orientations of imbricated slabs near Table Bay (Figs. A11, B5C, and B5D)

Figure B4 (*continued*).

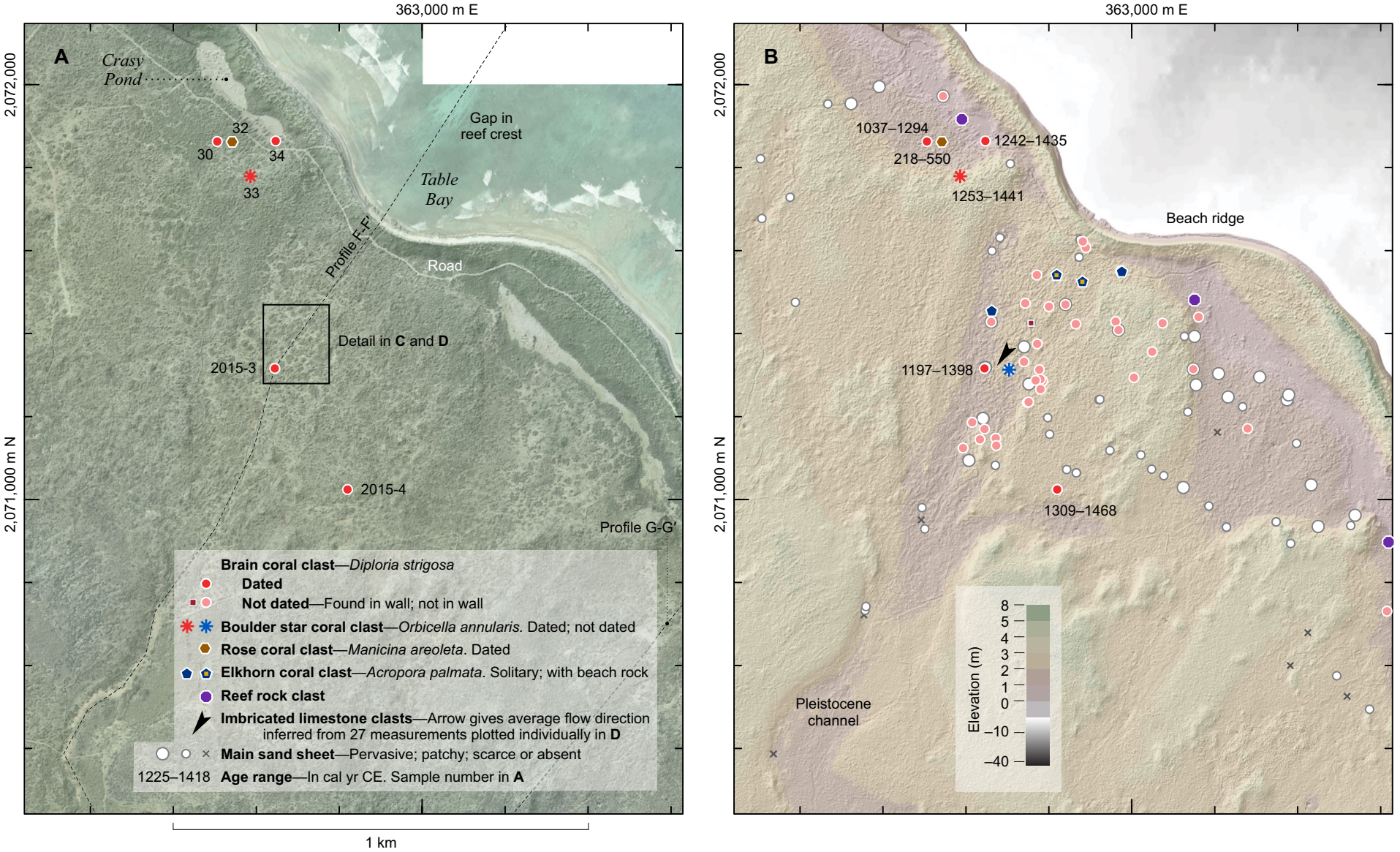

Figure B5 (*on this and following two pages*). Dated samples and their setting near Table Bay.

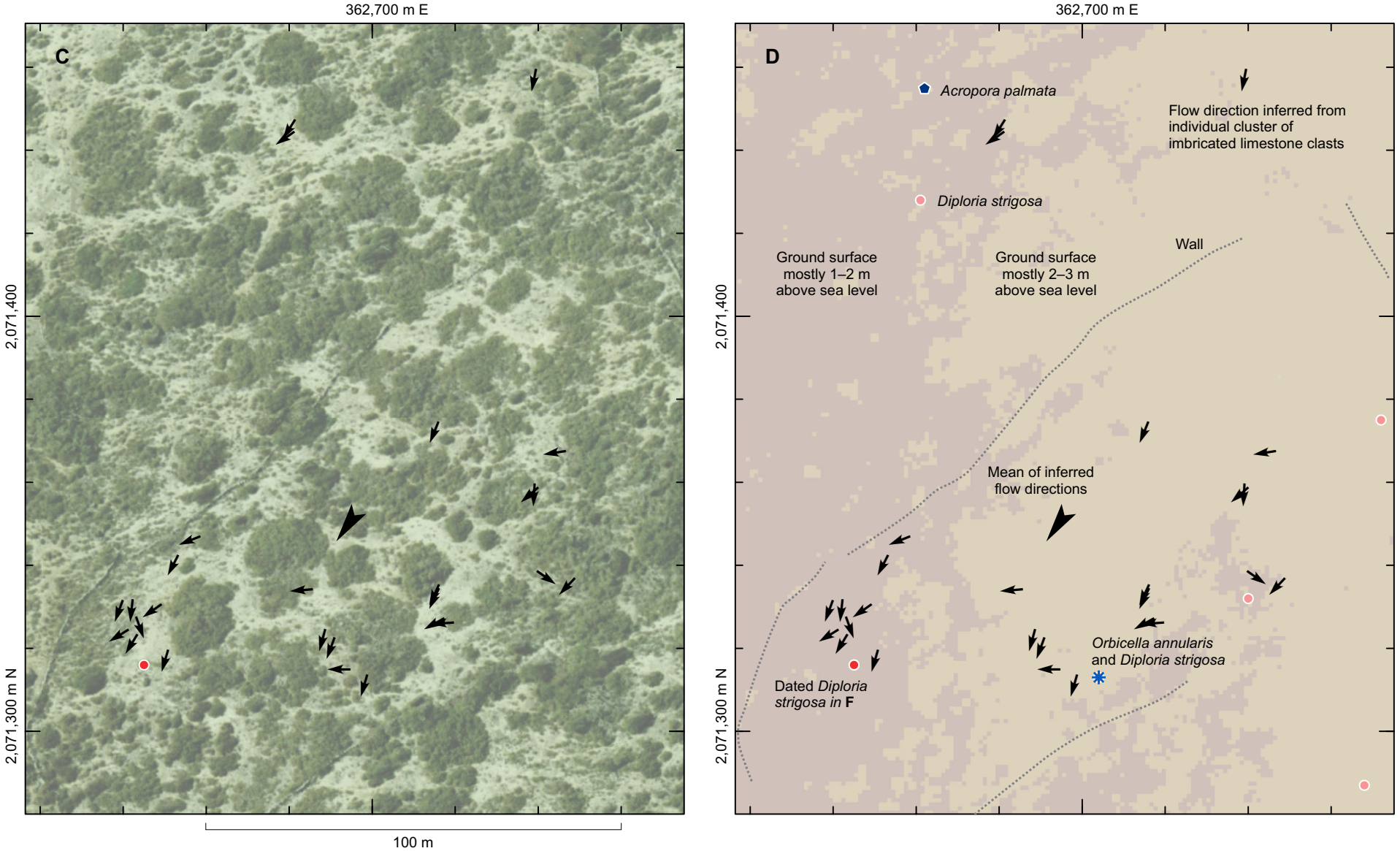

Figure B5 (*continued*).

E **Dated clasts near Crasy Pond, listed from youngest age to oldest**

33
985 ± 35 ^{14}C yr B.P.
1253–1441 cal yr CE
Orbicella annularis
(formerly in the genus *Montastraea*)

34
995 ± 35 ^{14}C yr B.P.
1242–1435 cal yr CE
Diploria strigosa

Clast split for sampling

30
1180 ± 50 ^{14}C yr B.P.
1037–1294 cal yr CE
Diploria strigosa

10 cm lengths marked by color divisions on tape measure

32
1960 ± 40 ^{14}C yr B.P.
216–550 cal yr CE
Manicina areolata

5 cm

F **Dated brain coral boulder near imbricated boulders in D**

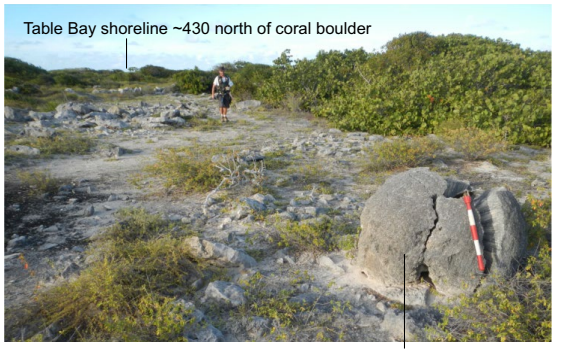

View seaward. Imbricated slabs at left beside man. Shovel handle 0.5 m. Additional views below and in Fig. A4

2015-3
1050 ± 15 ^{14}C yr B.P.
1197–1398 cal yr CE

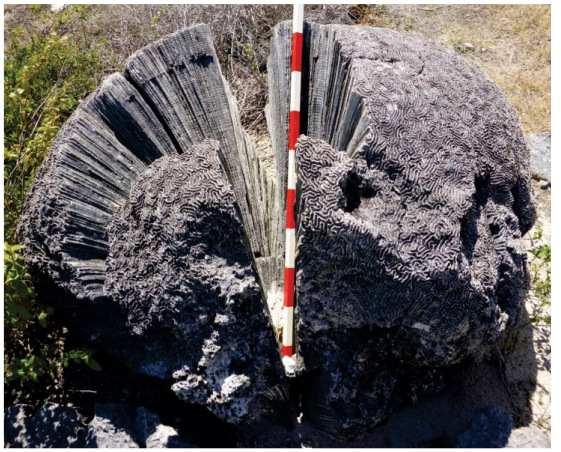

G **Dated brain coral boulder 635 m inland**

Shadow at left obscures additional pieces imaged below

2015-4
905 ± 20 ^{14}C yr B.P.
1309–1468 cal yr CE

Dimple where coral probably grew around a worm tube (Fig. B2**D**)

Figure B5 (*continued*).

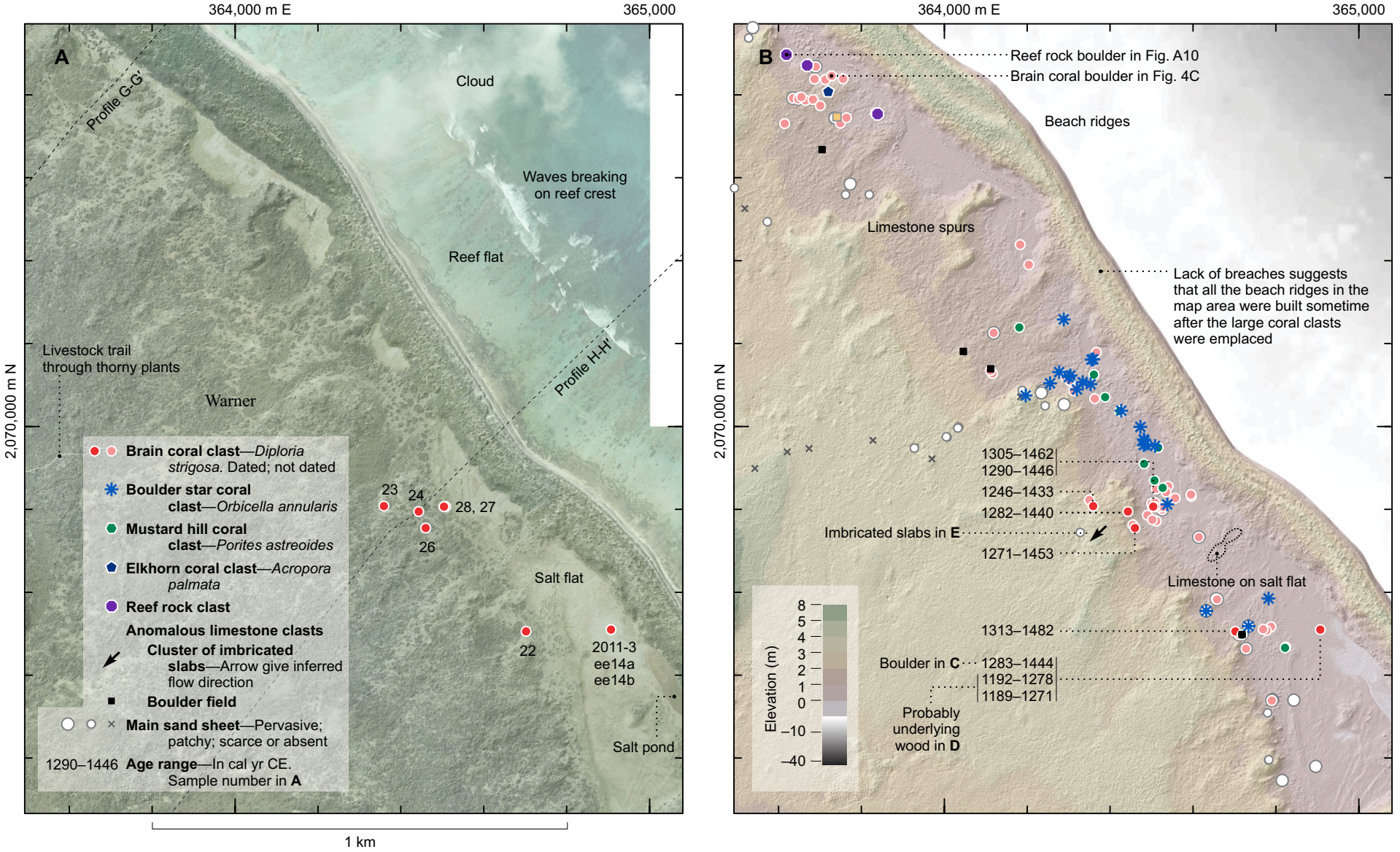

Figure B6 (*on this and following two pages*). Dated samples and their setting at Warner.

C **Dated boulders and cobbles, listed from youngest age to oldest**

22
890 ± 25 ^{14}C yr B.P.
1313–1482 cal yr CE
Microatoll

28
915 ± 20 ^{14}C yr B.P.
1305–1462 cal yr CE

27
950 ± 20 ^{14}C yr B.P.
1290–1446 cal yr CE

2011-3
960 ± 25 ^{14}C yr B.P.
1283–1444 cal yr CE
Upside down

26
960 ± 40 ^{14}C yr B.P.
1271–1453 cal yr CE

24
965 ± 20 ^{14}C yr B.P.
1282–1440 cal yr CE
Upside down

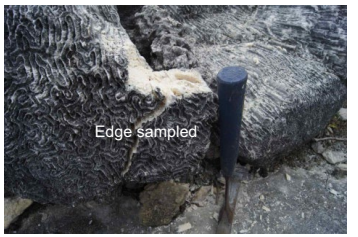

23
995 ± 30 ^{14}C yr B.P.
1246–1433 cal yr CE
Upside down

Figure B6 (*continued*).

D **Dated wood from organic horizon that may extend beneath coral boulder 2011-3**

Floor of salt pond coated with chips of partly desiccated microbial debris from 2010 Hurricane Earl

Coral boulder of sample 2011-3, which gave an age corresponding to the range 1283–1444 cal yr CE (**C**). The boulder was not excavated to establish whether its lowermost part rests on the organic horizon or extends to the underlying limestone

All photos in **C** were taken in 2011

Stratigraphy shown more clearly in shovel slice

Muddy sand with cerithids (brown)

Organic fine sand

Fine sand with *Homotrema* grains

Burrow

The fine sand with *Homotrema* grains rests on Pleistocene limestone

The dated wood (right) was collected from this soil horizon

5 cm

A cross section through the wood revealed close to 20 rings. Outer rings and inner rings gave similar ages

1 cm

ee14b (outer rings)
805 ± 25 ^{14}C yr B.P.
1189–1271 cal yr CE

ee14a (inner rings)
790 ± 30 ^{14}C yr B.P.
1192–1278 cal yr CE

E **Imbricated limestone slabs**

Limestone clasts near white labels **L** dip northeastward, seaward. Slabs imbricated in foreground (beside meter stick) and at middle right

Figure B6 (*continued*).

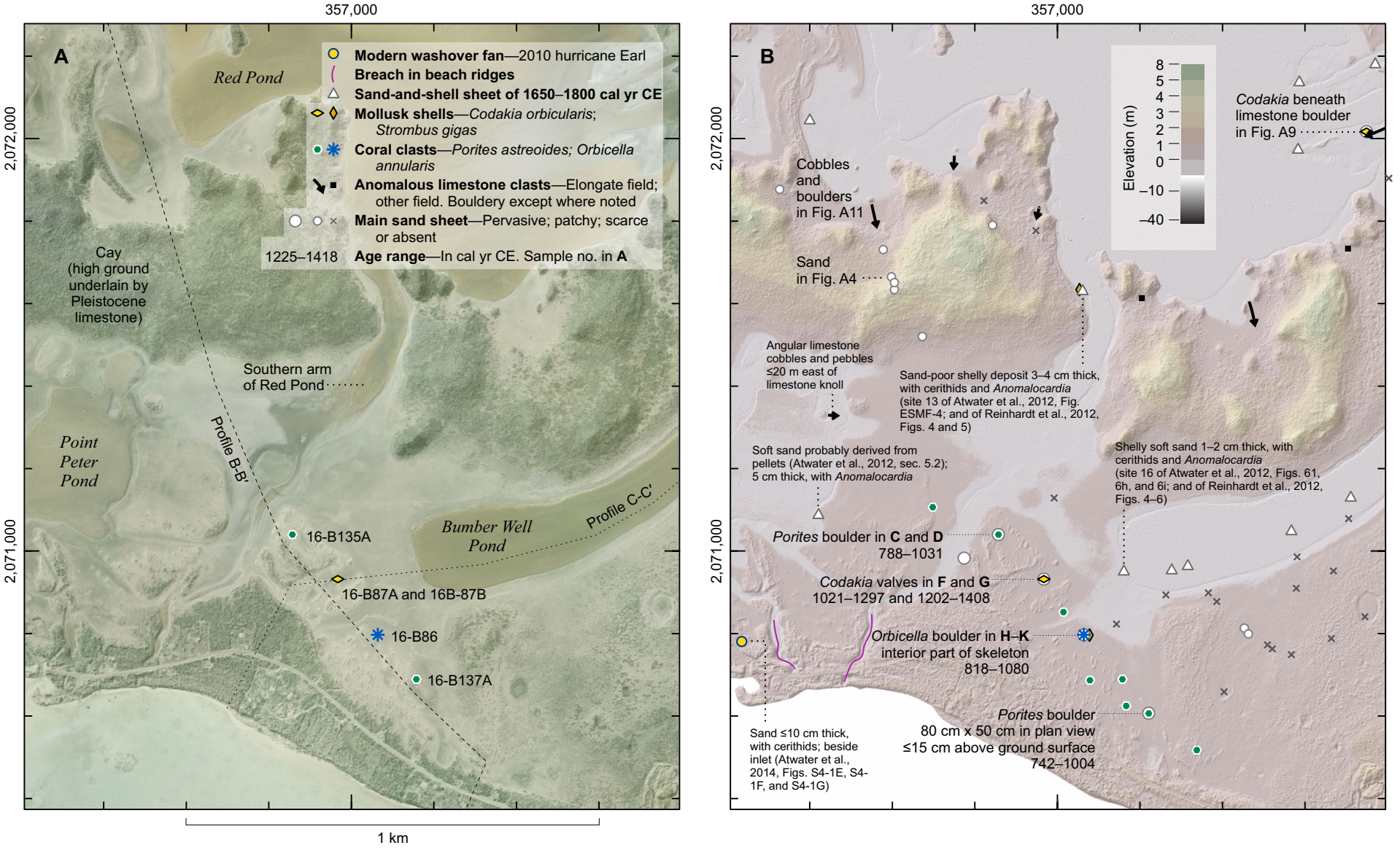

Figure B7 (*on this and following five pages*). Dated samples and their setting northwest of Nutmeg Point.

C **Setting of fragmented *Porites astreoides* boulder of sample 16-B135A**

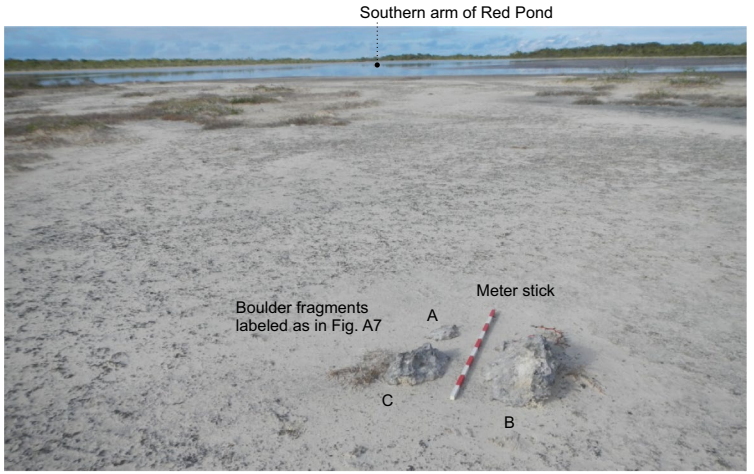

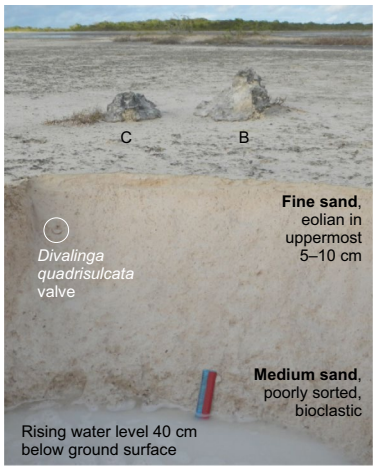

Pit shown also in Fig. A7. Depth to limestone 60 cm. Bioclastic sand extends to depth of 50 cm or more. A rinsed sample of the medium sand, in a sieve with openings of 4 mm, contained coralline algae branches, *Halimeda* flakes, cerithid gastropods, and pink grains intepreted as *Homotrema rubrum*

D **Dated *Porites astreoides* sample from fragment C**

Sample removed from highest part of fragment C, about 10 cm above ground surface. This fragment, shown unearthed at left and in Fig. A7, was found surrounded by bioclastic sand to a depth of 25 cm below ground surface. The fragment does not appear to retain external surfaces comparable to those of the live coral colony in Fig. A7

Trace of ground surface on unearthed clast

INTERPRETATIONS

This boulder, before breaking into pieces, was introduced with the bioclastic sand.

The boulder may have arrived after the sand had built up a thickness of 30 cm or more, as judged from the depth of fragment C. However, the depth ranges of fragments A and B were not determined.

The boulder broke into multiple pieces after deposition, much as did the large brain coral boulder in Fig. 4C.

The dated part of the coral skeleton gives a limiting maximum age for the time of boulder emplacement. The dated material was not necessarily close to the exterior of the coral colony at the time of death, and the colony was not necessarily alive at the time of emplacement.

Figure B7 (*continued*).

E **Setting of *Codakia orbicularis* valves of 16-B87A and 16-B87B**

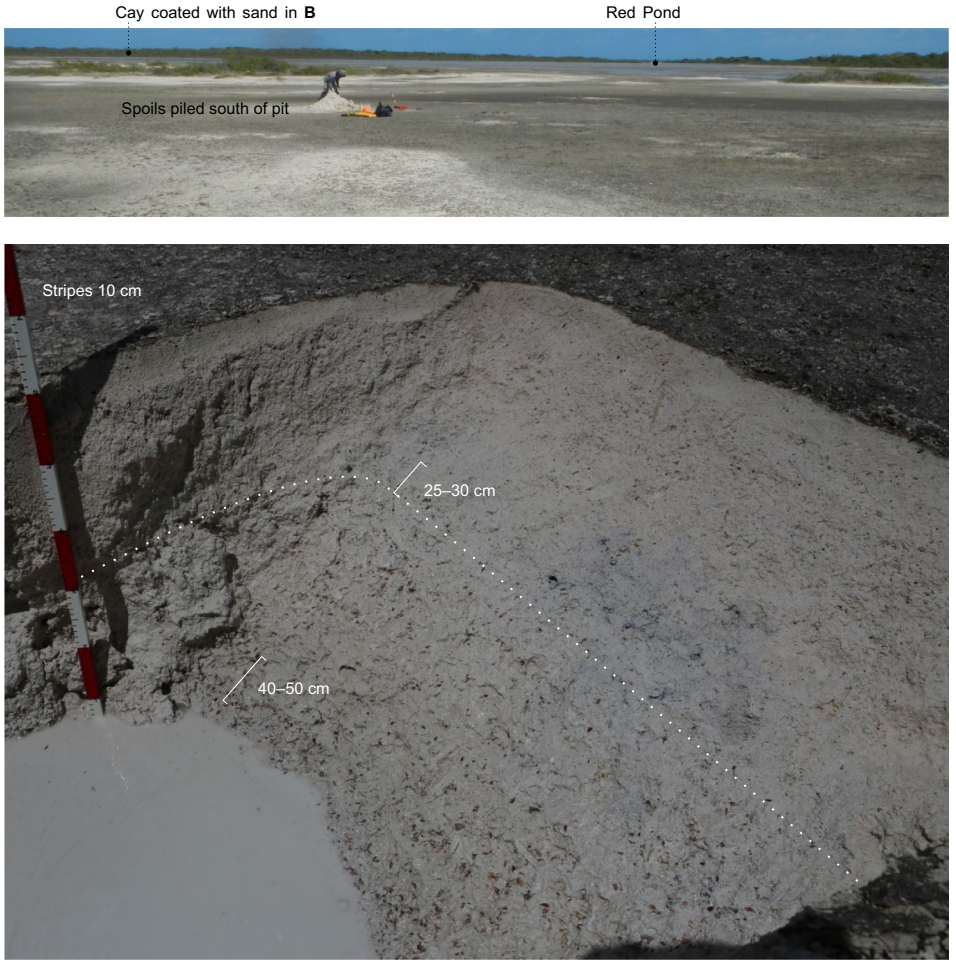

Dotted line shows approximate level, about 30 cm below ground surface, of burrowed contact between muddy, cerithid-rich deposits below and bioclastic, cerithid-poor sand above. Pit wall is nearly vertical behind meter stick but slopes gently in the planar face at right. Depth to Pleistocene limestone 55–60 cm

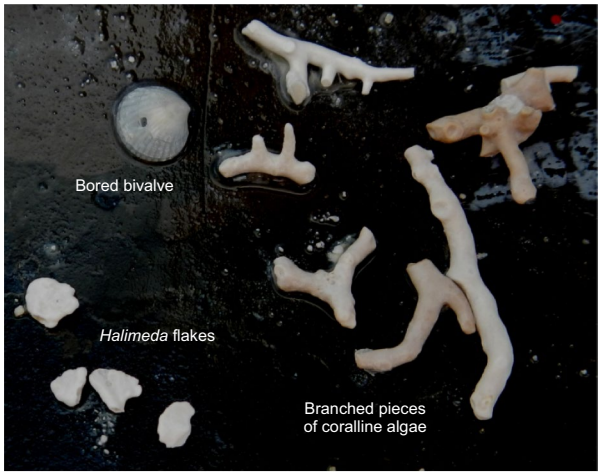

Clasts rinsed from cerithid-poor sand collected 25–30 cm below ground surface. The dated *Codakia* valves (in **F** and **G**) were found in this depth range. Cerithids are present but algal fragments are more common

1 cm in both close-up views above

Clasts rinsed from muddy, cerithid-rich deposits collected 40–50 cm below ground surface. Coralline algae (C) and a *Halimeda* flake (*H*) are present but the cerithid gastropods predominate

Figure B7 (*continued*).

F **Matching pair of disarticulated *Codakia* valves of 16-B87A**

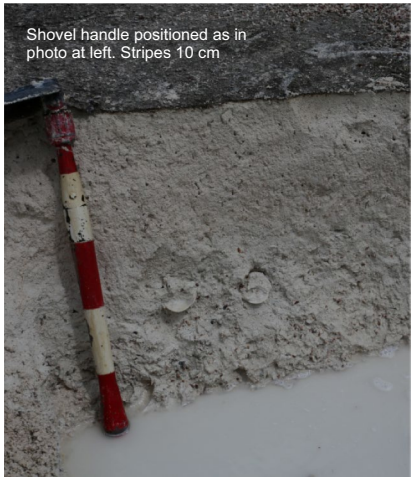

Matching valves circled above and in Fig. A9, which contains a more extensive overview of the pit at this stage of excavation

16-B87A
1150 ± 25 ^{14}C yr B.P.
1071–1279 cal yr CE

G **Articulated *Codakia* valves of 16-B87B**

Six *Codakia* valves were noticed in the walls of this pit while it was being enlarged, and another two valves were found articulated in the spoil pile at left. The spoils also yielded a specimen of the finger coral *Porites porites*

This *Codakia* may have been rotated by digging, but otherwise it is shown here in the position where it was found. Fig. A9 gives two additional views of the articulated valves of this sample, which was dated as 16-B87B

16-B87B
1040 ± 25 ^{14}C yr B.P.
1202–1408 cal yr CE

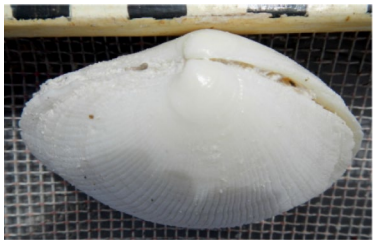

Figure B7 (*continued*).

H **Setting of *Orbicella annularis* boulder, observed 2008**

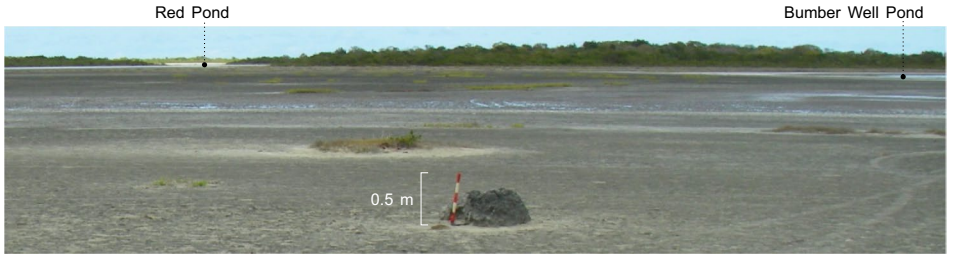

2008

View to north-northeast. Boulder 80 cm high (30 cm exposed) and 100 cm along long axis at ground surface

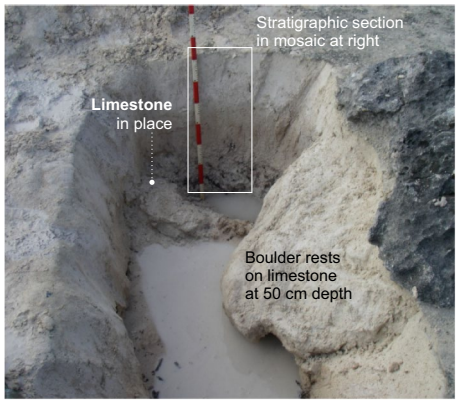

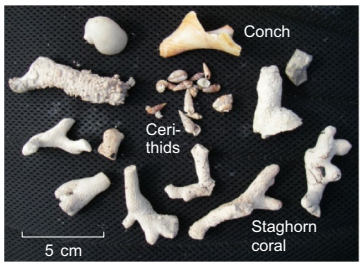

Clasts found near contact with limestone

2008

Surface

Fine sand with interstitial lime mud, bioturbated

Color change from different lighting in mosaic

Fine to medium sand

Muddy sand with cerithids and mangrove roots

Limestone
50–75 cm below ground surface

I **Further context of *Orbicella* boulder, observed 2016**

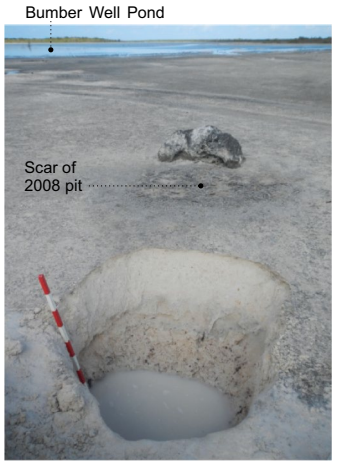

2016

View to east-northeast. Limestone 70 cm below surface

INTERPRETATIONS

The muddy, cerithid-rich sand in both pits probably represents a marine pond more connected with the sea than are Anegada's modern salt ponds.

The overlying sand represents flows that built up the floor of this pond. The flows brought in *Halimeda* flakes from offshore while also entraining onshore snails and limestone fragments.

These same flows introduced the *Orbicella* boulder if erosion or settlement enabled its lowest part to rest directly on the Pleistocene limestone, along with the conch and staghorn fragments.

If derived from Windlass Bight (location, Fig. 2A), this *Orbicella* boulder was transported no less than 2 km from its source (Fig. 5B).

Figure B7 (*continued*).

J **Exposed exterior of *Orbicella* boulder**

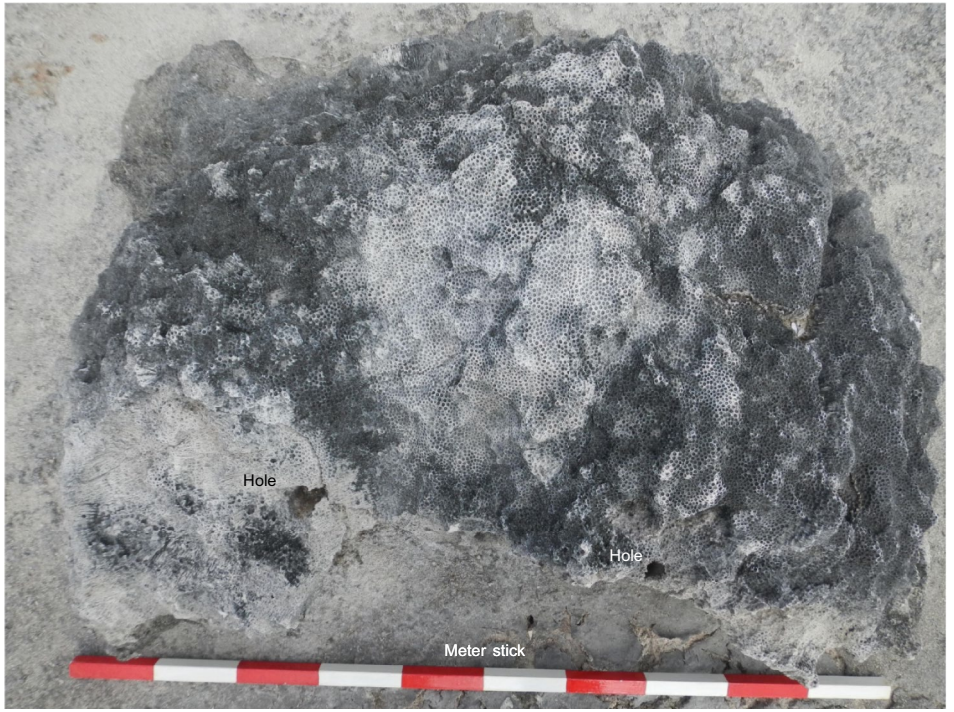

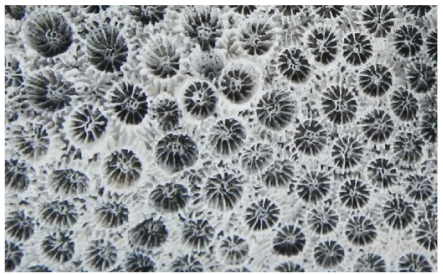

Deep cylindrical holes, labeled above and in **K**, were likely bored while the boulder was on the reef or reef flat.

The exposed part of the coral boulder has the apparent shape of a dome that landed on its side. In the plan view above, the former upper surface of the boulder would then be toward the top of the page, and the dated sample (**K**) would be close to the base. However, more of the apparent height of the boulder is below the present ground surface than above, and in plan view the underground part of the boulder protrudes 30 cm toward the bottom of this page (pit in **H**).

K **Radiocarbon sample from interior of *Orbicella* boulder**

16-B86
1380 ± 20 ^{14}C yr B.P.
818–1080 cal yr CE

INTERPRETATIONS

The dated material of 16-B86 could have formed centuries before the time when the boulder was emplaced, if this part of the coral skeleton formed early in the time of the coral colony, and if the labeled holes in the boulder represent submarine weathering after colony death.

The likely time of boulder emplacement inferred from additional ages is 1200–1480 cal yr CE (Fig. 5). One of those additional ages, 1202–1418 cal yr CE, was obtained from an articulated bivalve 160 m northwest of the boulder (**B** and **G**).

Figure B7 (*continued*).

TABLE 4. AUTHOR ROLES

Author*	Field work	Other input
BA	2008, 2009, 2011, 2012, 2013, 2015, 2016	Manuscript drafts
UtB	2007, 2009, 2011, 2013	Regional tectonics and geophysics. Lidar (light detection and ranging) acquisition
ALC	2015	Historical changes in sandy beach ridges
ZF	2011, 2013	Storm effects on microbial mats
NF	2012	Regional tectonics and geophysics
RH	2009, 2011, 2012, 2013, 2015, 2016	Coral-reef ecology and geology. Radiocarbon samples
CN	2016	Sand composition
ER	2009	Molluscan ecology and taphonomy of bygone interior pond
JR	2015, 2016	Living coral colonies. Hydrodynamic effects of gaps in fringing reef
MS	2013, 2015, 2016	Comparisons with coral rubble ridge. Radiocarbon samples
MT	2008, 2011, 2012	Extreme-wave geology. Air-photo interpretation. Radiocarbon samples
YS	2016	Paleoecology
YW	2009, 2012, 2013, 2016	Unpublished computer simulations of tsunamis and storms
JWA	2012	Radiocarbon samples

*BA—Brian Atwater; UtB—Uri ten Brink, ALC—Anna Cescon, NF—Nathalie Feuillet, ZF—Zamara Fuentes, RH—Robert Halley, CN—Carlos Nuñez, ER—Eduard Reinhardt, JR—Jean Roger, YS—Yuki Sawai, MS—Michaela Spiske, MT—Martitia Tuttle, YW—Yong Wei, JWA—Jennifer Weil-Accardo.

Note: Yong Wei's participation was partly funded by the Joint Institute for the Study of the Atmosphere and Ocean (JISAO) under National Oceanic and Atmospheric Administration (NOAA) Cooperative Agreement NA10OAR430148. This report is JISAO contribution 2467 and NOAA Pacific Marine Environmental Laboratory contribution 4322.

ACKNOWLEDGMENTS

Permissions were arranged by the Department of Disaster Management of the Government of the British Virgin Islands. Residents of Anegada extended many courtesies to the field parties. Quantum Spatial and Wayne Wright made the terrestrial and shallow-water lidar surveys, respectively, with geodetic help from Alberto López-Venegas. Craig Weaver arranged for much of the financial support for the terrestrial survey. Brian Andrews and Harvey Greenberg merged the lidar results.

The paper was improved through a series of insightful reviews. A short version of this manuscript, prepared in 2015, was reviewed by Rónadh Cox, Bruce Jaffe, Jim O'Connor, Raphaël Paris, Patrick Wassmer, and an anonymous referee for *Geology* (Geological Society of America). A longer version was reviewed first by Andrew Kennedy and later, for *Geosphere,* by an anonymous referee and Adam Switzer. Two reviews were provided by Steve Hickman.

REFERENCES CITED

Andrews, B.D., ten Brink, U.S., Danforth, W.W., Chaytor, J.D., Granja Bruña, J., Estrada, P.L., and Carbó-Gorosabel, A., 2013, Bathymetric Terrain Model of the Puerto Rico Trench and the Northeastern Caribbean Region for Marine Geological Investigations: U.S. Geological Survey Open-File Report 2013-1125, 10 p., doi:10.3133/ofr20131125.

Araoka, D., Inoue, M., Suzuki, A., Yokoyama, Y., Edwards, R.L., Cheng, H., Matsuzaki, H., Kan, H., Shikazono, N., and Kawahata, H., 2010, Historic 1771 Meiwa tsunami confirmed by high-resolution U/Th dating of massive Porites coral boulders at Ishigaki Island in the Ryukyus, Japan: Geochemistry, Geophysics, Geosystems, v. 11, Q06014, doi:10.1029/2009GC002893.

Atwater, B.F., ten Brink, U.S., Buckley, M.L., Halley, R.B., Jaffe, B.E., López-Venegas, A.M., Reinhardt, E.G., Tuttle, M.P., Watt, S.G., and Wei, Y., 2012, Geomorphic and stratigraphic evidence for an unusual tsunami or storm a few centuries ago at Anegada, British Virgin Islands: Natural Hazards, v. 63, p. 51–84, doi:10.1007/s11069-010-9622-6.

Atwater, B.F., Cisternas, M., Yulianto, E., Prendergast, A.L., Jankaew, K., Eipert, A.A., Fernando, W.I.S., Tejakusuma, I., Schiappacasse, L., and Sawai, Y., 2013, The 1960 tsunami on beach-ridge plains near Maullín, Chile: Landward descent, renewed breaches, aggraded fans, multiple predecessors: Andean Geology, v. 40, p. 393–418, doi:10.5027/andgeoV40n3-a01.

Atwater, B.F., Fuentes, Z., Halley, R.B., ten Brink, U.S., and Tuttle, M.P., 2014, Geologic effects of 2010 Hurricane Earl amidst evidence for greater overwash at Anegada, British Virgin Islands: Advances in Geosciences, v. 38, p. 21–30, doi:10.5194/adgeo-38-21-2014.

Barkan, R., ten Brink, U.S., and Lin, J., 2009, Far field tsunami simulations of the 1755 Lisbon earthquake: Implications for tsunami hazard to the U.S. East Coast and the Caribbean: Marine Geology, v. 264, p. 109–122, doi:10.1016/j.margeo.2008.10.010.

Bernard, P., and Lambert, J., 1988, Subduction and seismic hazard in the northern Lesser Antilles; revision of the historical seismicity: Seismological Society of America Bulletin, v. 78, p. 1965–1983.

Bernard, P., and Lambert, J., 1992, Subduction and seismic hazard in the Lesser Antilles: Reply: Seismological Society of America Bulletin, v. 82, p. 1544–1551.

Blachford, R., 1813, Chart of the Virgin Isles from Lockwood's Trigonometric Survey Taken in 1811 by Order of the Commander in Cheif Admiral Sir Francis Laforey: London, Bart., scale ~1:95,000.

Buckley, M.L., Wei, Y., Jaffe, B.E., and Watt, S.G., 2012, Inverse modeling of velocities and inferred cause of overwash that emplaced inland fields of boulders at Anegada, British Virgin Islands: Natural Hazards, v. 63, p. 133–149, doi:10.1007/s11069-011-9725-8.

Budd, A.F., Fukami, H., Smith, N.D., and Knowlton, N., 2012, Taxonomic classification of the reef coral family Mussidae (Cnidaria: Anthozoa: Scleractinia): Linnean Society Zoological Journal, v. 166, p. 465–529, doi:10.1111/j.1096-3642.2012.00855.x.

Caribbean Disaster Mitigation Project, 2002, Atlas of Probable Storm Effects in the Caribbean Sea: http://www.oas.org/CDMP/document/reglstrm/Hurratlas7D.ppt, accessed 7 September 2012.

Choowong, M., Murakoshi, N., Hisada, K., Charusiri, P., Daorerk, V., Charoentitirat, T., Chutakositkanon, V., Jankaew, K., and Kanjanapayont, P., 2007, Erosion and deposition by the 2004 Indian Ocean tsunami in Phuket and Phang-nga Provinces, Thailand: Journal of Coastal Research, v. 23, p. 1270–1276, doi:10.2112/05-0561.1.

Cox, R., Zentner, D.B., Kirchner, B.J., and Cook, M.S., 2012, Boulder ridges on the Aran Islands (Ireland): Recent movements caused by storm waves, not tsunamis: Journal of Geology, v. 120, p. 249–272, doi:10.1086/664787.

Craig, T.J., Copley, A., and Jackson, J., 2014, A reassessment of outer-rise seismicity and its implications for the mechanics of oceanic lithosphere: Geophysical Journal International, v. 197, p. 63–89, doi:10.1093/gji/ggu013.

Davis, D., and Oldfield, K., 2003, Archaeological reconnaissance of Anegada, British Virgin Islands: Journal of Caribbean Archaeology, v. 4, p. 1–11.

Defense Mapping Agency, 1996, Saint Thomas to Anegada: National Geospatial-Intelligence Agency nautical chart 25069, scale 1:80,000.

Dolan, J.F., and Wald, D.J., 1998, The 1943–1953 north-central Caribbean earthquakes: Active tectonic setting, seismic hazards, and implications for Caribbean–North America plate motions, *in* Dolan, J.F., and Mann, P., eds., Active Strike-Slip and Collisional Tectonics of the Northern Caribbean Plate Boundary Zone: Geological Society of America Special Paper 326, p. 143–169, doi:10.1130/0-8137-2326-4.125.

Donato, S.V., Reinhardt, E.G., Boyce, J.I., Rothaus, R., and Vosmer, T., 2008, Identifying tsunami deposits using bivalve shell taphonomy: Geology, v. 36, p. 199–202, doi:10.1130/G24554A.1.

Dookhan, I., 1975, A History of the British Virgin Islands, 1672 to 1970: Epping, UK, Caribbean Universities Press, 255 p.

Dunne, R.P., and Brown, B.E., 1979, Some Aspects of the Ecology of Reefs Surrounding Anegada, British Virgin Islands: Atoll Research Bulletin 236, 80 p., http://www.sil.si.edu/digitalcollections/atollresearchbulletin/issues/00236.pdf.

Etienne, S., and Paris, R., 2010, Boulder accumulations related to storms on the south coast of the Reykjanes Peninsula (Iceland): Geomorphology, v. 114, p. 55–70, doi:10.1016/j.geomorph.2009.02.008.

Etienne, S., Buckley, M., Paris, R., Nandasena, A.K., Clark, K., Strotz, L., Chagué-Goff, C., Goff, J., and Richmond, B., 2011, The use of boulders for characterising past tsunamis: Lessons from the 2004 Indian Ocean and 2009 South Pacific tsunamis: Earth-Science Reviews, v. 107, p. 76–90, doi:10.1016/j.earscirev.2010.12.006.

Fagherazzi, S., and Du, X., 2008, Tsunamigenic incisions produced by the December 2004 earthquake along the coasts of Thailand, Indonesia and Sri Lanka: Geomorphology, v. 99, p. 120–129, doi:10.1016/j.geomorph.2007.10.015.

Faulkner, S.W., 2005, Voices in the Wind: The Forgotten Island: Bloomington, Indiana, AuthorHouse, 181 p.

Feuillet, N., Beauducel, F., and Tapponnier, P., 2011, Tectonic context of moderate to large historical earthquakes in the Lesser Antilles and mechanical coupling with volcanoes: Journal of Geophysical Research, v. 116, B10308, doi:10.1029/2011JB008443.

Fichaut, B., and Suanez, S., 2011, Quarrying, transport and deposition of cliff-top storm deposits during extreme events: Banneg Island, Brittany: Marine Geology, v. 283, p. 36–55, doi:10.1016/j.margeo.2010.11.003.

Fredericks, X., ten Brink, U.S., Atwater, B.F., Kranenburg, C.J., and Nagle, D.B., 2016, Coastal Topography—Anegada, British Virgin Islands, 2014: U.S. Geological Survey data release, doi:10.5066/F7GM85F3.

Frohlich, C., Hornbach, M.J., Taylor, F.W., Shen, C., Moala, 'A, Morton, A.E., and Kruger, J., 2009, Huge erratic boulders in Tonga deposited by a prehistoric tsunami: Geology, v. 37, p. 131–134, doi:10.1130/G25277A.1.

Gardner, T.A., Côté, I.M., Gill, J.A., Grant, A., and Watkinson, A.R., 2003, Long-term region-wide declines in Caribbean corals: Science, v. 301, p. 958–960, doi:10.1126/science.1086050.

Gelfenbaum, G., Apotsos, A., Stevens, A.W., and Jaffe, B.E., 2011, Effects of fringing reefs on tsunami inundation; American Samoa: Earth-Science Reviews, v. 107, p. 12–22, doi:10.1016/j.earscirev.2010.12.005.

Giovas, C.M., 2013, Foraging Variability in the Prehistoric Caribbean: Multiple Foraging Optima, Resource Use, and Anthropogenic Impacts on Carriacou, Grenada [Ph.D. thesis]: Seattle, University of Washington, 406 p., https://digital.lib.washington.edu/researchworks/handle/1773/23391.

Goff, J.R., Hicks, D.M., and Hurren, H., 2007, Tsunami Geomorphology in New Zealand: A New Method for Exploring the Evidence of Past Tsunamis: NIWA (National Institute of Water and Atmospheric Research New Zealand) Technical Report 128, 69 p., http://webcat.niwa.co.nz/documents/0478232752.pdf, accessed 16 April 2012.

Goto, K., Miyagi, K., Kawamata, H., and Imamura, F., 2010a, Discrimination of boulders deposited by tsunamis and storm waves at Ishigaki Island, Japan: Marine Geology, v. 269, p. 34–45, doi:10.1016/j.margeo.2009.12.004.

Goto, K., Shinozaki, T., Minoura, K., Okada, K., Sugawara, D., and Imamura, F., 2010b, Distribution of boulders at Miyara Bay of Ishigaki Island, Japan: A flow characteristic indicator of tsunami and storm waves: Island Arc, v. 19, p. 412–426, doi:10.1111/j.1440-1738.2010.00721.x.

Goto, K., Miyagi, K., Kawana, T., Takahashi, J., and Imamura, F., 2011, Emplacement and movement of boulders by known storm waves—Field evidence from the Okinawa Islands, Japan: Marine Geology, v. 283, p. 66–78, doi:10.1016/j.margeo.2010.09.007.

Grindlay, N.R., Mann, P., Dolan, J.F., and van Gestel, J.P., 2005, Neotectonics and subsidence of the northern Puerto Rico–Virgin Islands margin in response to the oblique subduction of high-standing ridges, *in* Mann, P., ed., Active Tectonics and Seismic Hazards of Puerto Rico, the Virgin Islands, and Offshore Areas: Geological Society of America Special Paper 385, p. 31–60, doi:10.1130/0-8137-2385-X.31.

Hall, A.M., Hansom, J.D., Williams, D.M., and Jarvis, J., 2006, Distribution, geomorphology and lithofacies of cliff-top storm deposits: Examples from the high-energy coasts of Scotland and Ireland: Marine Geology, v. 232, p. 131–155, doi:10.1016/j.margeo.2006.06.008.

Hayes, G.P., McNamara, D.E., Seidman, L., and Roger, J., 2014, Quantifying potential earthquake and tsunami hazard in the Lesser Antilles subduction zone of the Caribbean region: Geophysical Journal International, v. 196, p. 510–521, doi:10.1093/gji/ggt385.

Irish, J.L., Lynett, P.J., Weiss, R., Smallegan, S.M., and Cheng, W., 2013, Buried relic seawall mitigates Hurricane Sandy's impacts: Coastal Engineering, v. 80, p. 79–82, doi:10.1016/j.coastaleng.2013.06.001.

Jackson, J.B.C., 1973, The ecology of molluscs of Thalassia communities, Jamaica, West Indies. I. Distribution, environmental physiology, and ecology of common shallow-water species: Bulletin of Marine Science, v. 23, no. 2, p. 313–350.

Jankaew, K., Atwater, B.F., Sawai, Y., Choowong, M., Charoentitirat, T., Martin, M.E., and Prendergast, A., 2008, Medieval forewarning of the 2004 Indian Ocean tsunami in Thailand: Nature, v. 455, p. 1228–1231, doi:10.1038/nature07373.

Jarecki, L., and Walkey, M., 2006, Variable hydrology and salinity of salt ponds in the British Virgin Islands: Saline Systems, v. 2, doi:10.1186/1746-1448-2-2.

Jarecki, L.L., 2003, Salt Ponds of the British Virgin Islands: Investigations in an Unexplored Ecosystem [Ph.D. thesis]: Canterbury, University of Kent at Canterbury, 206 p., plus appendices.

Kain, C., Gomez, C., Wassmer, P., Lavigne, F., and Hart, D., 2014, Truncated dunes as evidence of the 2004 tsunami in North Sumatra and environmental recovery post-tsunami: New Zealand Geographer, v. 70, p. 165–178, doi:10.1111/nzg.12052.

Kanamori, H., 1971, Seismological evidence for a lithospheric normal faulting—The Sanriku earthquake of 1933: Physics of the Earth and Planetary Interiors, v. 4, p. 289–300, doi:10.1016/0031-9201(71)90013-6.

Kennedy, A.B., Mori, N., Zhang, Y., Yasuda, T., Chen, S., Tajima, Y., Pecor, W., and Toride, K., 2016, Observations and modeling of coastal boulder transport and loading during Super Typhoon Haiyan: Coastal Engineering Journal, v. 58, 1640004, doi:120.1142/S0578563416400040.

Kilbourne, K.H., Quinn, T.M., Guilderson, T.P., Webb, R.S., and Taylor, F.W., 2007, Decadal- to interannual-scale source water variations in the Caribbean Sea recorded by Puerto Rican coral radiocarbon: Climate Dynamics, v. 29, p. 51–62, doi:10.1007/s00382-007-0224-2.

Knight, J., and Burningham, H., 2011, Boulder dynamics on an Atlantic-facing rock coastline, northwest Ireland: Marine Geology, v. 283, p. 56–65, doi:10.1016/j.margeo.2010.07.008.

Kon'no, E., Iwai, J., Kitamura, N., Kotaka, T., Mii, H., Nakagawa, H., Onuki, Y., Shibata, T., and Takayanagi, Y., 1961, Geological observations of the Sanriku coastal region damaged by the tsunami due to the Chile earthquake in 1960: Contributions to the Institute of Geology and Paleontology of Tohoku University, v. 52, p. 1–40.

Kopp, R.E., Simons, F.J., Mitrovica, J.X., Maloof, A.C., and Oppenheimer, M., 2009, Probabilistic assessment of sea level during the last interglacial stage: Nature, v. 462, p. 863–867, doi:10.1038/nature08686.

Kunkel, C.M., Hallberg, R.W., and Oppenheimer, M., 2006, Coral reefs reduce tsunami impact in model simulations: Geophysical Research Letters, v. 33, L2361, doi:10.1029/2006GL027892.

Lander, J.F., Whiteside, L.S., and Lockridge, P.A., 2002, A brief history of tsunamis in the Caribbean Sea: Science of Tsunami Hazards, v. 20, p. 57–94.

Liew, S.C., Gupta, A., Wong, P.P., and Kwoh, L.K., 2010, Recovery from a large tsunami mapped over time: The Aceh coast, Sumatra: Geomorphology, v. 114, p. 520–529, doi:10.1016/j.geomorph.2009.08.010.

Lynch, J.J., and Bodle, R.R., 1948, The Dominican earthquakes of August, 1946: Seismological Society of America Bulletin, v. 38, p. 1–17.

May, S.M., Engel, M., Brill, D., Cuadra, C., Lagmay, A.M.F., Santiago, J., Suarez, J.K., Reyes, M., and Brückner, H., 2015, Block and boulder transport in eastern Samar (Philippines) during Super-typhoon Haiyan: Earth Surface Dynamics, v. 3, p. 739–771, doi:10.5194/esurfd-3-739-2015.

Mercado Irizarry, A., and Justiniano Sepulveda, H., 2003, Tsunami coastal flood mapping for Puerto Rico and adjacent islands; Appendix H, Puerto Rico Trench: University of Puerto Rico, Mayagüez, 31 p., http://poseidon.uprm.edu/public/Final-Reports/mercado/Appendix-H-Puerto-Rico-Trench.pdf.

Morison, S.E., 1942, Admiral of the Ocean Sea, A Life of Christopher Columbus: Boston, Little, Brown and Co., 893 p.

Morton, R.A., Richmond, B.M., Jaffe, B.E., and Gelfenbaum, G., 2008, Coarse-clast ridge complexes of the Caribbean: A preliminary basis for distinguishing tsunami and storm-wave origins: Journal of Sedimentary Research, v. 78, p. 624–637, doi:10.2110/jsr.2008.068.

Mueller, C.S., Frankel, A.D., Petersen, M.D., and Leyendecker, E.V., 2003, Documentation for 2003 USGS seismic hazard maps for Puerto Rico and the U.S. Virgin Islands: U.S. Geological Survey Open-File Report 03-379, http://pubs.usgs.gov/of/2003/ofr-03-379/ofr-03-379.html, accessed 12 May 2015.

Muhs, D.R., Simmons, K.R., Schumann, R.R., and Halley, R.B., 2011, Sea-level history of the past two interglacial periods: New evidence from U-series dating of reef corals from south Florida: Quaternary Science Reviews, v. 30, p. 570–590, doi:10.1016/j.quascirev.2010.12.019.

National Marine Fisheries Service, 2014, Endangered and threatened wildlife and plants: Notice of 12-month finding on a petition to list the queen conch as threatened or endangered under the Endangered Species Act (ESA): Federal Register, v. 79, no. 214, p. 65628–65643, https://federalregister.gov/a/2014-26324.

National Marine Fisheries Service, undated, Queen conch, *Strombus gigas* (Linnaeus 1758) status report: 101 p., http://sero.nmfs.noaa.gov/protected_resources/listing_petitions/archive/index.html.

Olsson, I.U., 1974, Some problems in connection with the evaluation of C^{14} dates: Geologiska Föreningens i Stockholm Förhandlingar, v. 96, p. 311–320, doi:10.1080/11035897409454285.

Paris, R., et al., 2009, Tsunamis as geomorphic crises; lessons from the December 26, 2004 tsunami in Lhok Nga, west Banda Aceh (Sumatra, Indonesia): Geomorphology, v. 104, p. 59–72, doi:10.1016/j.geomorph.2008.05.040.

Patton, W.K., 1976, Animal associates of living reef corals, *in* Jones, O.A., and Endean, R., eds., Geology and Biology of Coral Reefs, volume III, Biology 2: New York, Academic Press, p. 1–36, doi:10.1016/B978-0-12-395527-2.50008-1.

Perkins, B.F., and Turney, W.J., 1972, Molluscan Distribution in Florida Bay: University of Miami Rosenstiel School of Marine & Atmospheric Science, 37 p.

Pickering, V.W., 1983, Early History of the British Virgin Islands: From Columbus to Emancipation: New York, Falcon Publications International, 248 p.

Pilarczyk, J., and Reinhardt, E., 2012, *Homotrema rubrum* (Lamarck) taphonomy as an overwash indicator in marine ponds on Anegada, British Virgin Islands: Natural Hazards, v. 63, p. 85–100, doi:10.1007/s11069-010-9706-3.

Ramalho, R.S., Winckler, G., Madeira, J., Helffrich, G.R., Hipólito, A., Quartau, R., Adena, K., and Schaefer, J.M., 2015, Hazard potential of volcanic flank collapses raised by new megatsunami evidence: Science Advances, v. 1, no. 9, e1500456, doi:10.1126/sciadv.1500456.

Reimer, P., et al., 2013, IntCal13 and Marine13 radiocarbon age calibration curves 0–50,000 years cal BP: Radiocarbon, v. 55, p. 1869–1887, doi:10.2458/azu_js_rc.55.16947.

Reinhardt, E.G., Goodman, B.N., Boyce, J.I., Lopez, G., Hengstum, P.V., Rink, W.J., Mart, Y., and Raban, A., 2006, The tsunami of 13 December A.D. 115 and the destruction of Herod the Great's harbor at Caesarea Maritima, Israel: Geology, v. 34, p. 1061–1064, doi:10.1130/G22780A.1.

Reinhardt, E., Pilarczyk, J., and Brown, A., 2012, Probable tsunami origin for a shell and sand sheet from marine ponds on Anegada, British Virgin Islands: Natural Hazards, v. 63, p. 101–117, doi:10.1007/s11069-011-9730-y.

Richmond, B.M., Watt, S., Buckley, M., Jaffe, B.E., Gelfenbaum, G., and Morton, R.A., 2011, Recent storm and tsunami coarse-clast deposit characteristics, southeast Hawai'i: Marine Geology, v. 283, p. 79–89, doi:10.1016/j.margeo.2010.08.001.

Roeber, V., and Bricker, J.D., 2015, Destructive tsunami-like wave generated by surf beat over a coral reef during Typhoon Haiyan: Nature Communications, v. 6, 7854, doi:10.1038/ncomms8854.

Roger, J., Allgeyer, S., Hebert, H., Baptista, M.A., Loevenbruck, A., and Schindele, F., 2010, The 1755 Lisbon tsunami in Guadeloupe Archipelago: Source sensitivity and investigation of resonance effects: Open Oceanography Journal, v. 4, p. 58–70, doi:10.2174/1874252101004010058.

Roger, J., Baptista, M.A., Sahal, A., Accary, F., Allgeyer, S., and Hebert, H., 2011, The transoceanic 1755 Lisbon tsunami in Martinique: Pure and Applied Geophysics, v. 168, p. 1015–1031, doi:10.1007/s00024-010-0216-8.

Roger, J., Dudon, B., and Zahibo, N., 2013, Tsunami hazard assessment of Guadeloupe Island (F.W.I.) related to a megathrust rupture on the Lesser Antilles subduction interface: Natural Hazards and Earth System Sciences, v. 13, p. 1169–1183, doi:10.5194/nhess-13-1169-2013.

Roger, J., Dudon, B., Krien, Y., and Zahibo, N., 2014, Discussion about tsunami interaction with fringing coral reef, *in* Kontar, Y., et al., eds., Tsunami Events and Lessons Learned; Environmental and Societal Significance: Dordrecht, Springer, p. 161–176, doi:10.1007/978-94-007-7269-4_8.

Sawai, Y., Namegaya, Y., Tamura, T., Nakashima, R., and Tanigawa, K., 2015, Shorter intervals between great earthquakes near Sendai: Scour ponds and a sand layer attributable to A.D. 1454 overwash: Geophysical Research Letters, v. 42, p. 4795–4800, doi:10.1002/2015GL064167.

Schomburgk, R.H., 1832, Remarks on Anegada: Royal Geographical Society of London Journal, v. 2, p. 152–170, doi:10.2307/1797761.

Shepherd, J.B., 1992, Comment on Subduction and seismic hazard in the Lesser Antilles by Pascal Bernard and Jerome Lambert: Seismological Society of America Bulletin, v. 82, p. 1534–1543.

Shimozono, T., Tajima, Y., Kennedy, A.B., Nobuoka, H., Sasaki, J., and Sato, S., 2015, Combined infragravity wave and sea-swell runup over fringing reefs by super typhoon Haiyan: Journal of Geophysical Research, v. 120, p. 4463–4486, doi:10.1002/2015JC010760.

Soria, J.L.A., Switzer, A.D., Villanoy, C.L., Fritz, H.M., Bilgera, P.H.T., Cabrera, O.C., Siringan, F.P., Maria, Y.Y., Ramos, R.D., and Fernandez, I.Q., 2016, Repeat storm surge disasters of Typhoon Haiyan and its 1897 predecessor in the Philippines: American Meteorological Society Bulletin, v. 97, p. 31–48, doi:10.1175/BAMS-D-14-00245.1.

Spiske, M., 2016, Coral-rubble ridges as dynamic coastal features—Short-term reworking and weathering processes: Advances in Geosciences, v. 38, p. 55–61, doi:10.5194/adgeo-38-55-2016.

Spiske, M., and Halley, R.B., 2014, A coral-rubble ridge as evidence for hurricane overwash, Anegada (British Virgin Islands): Advances in Geosciences, v. 38, p. 9–20, doi:10.5194/adgeo-38-9-2014.

Stuiver, M., and Brazunias, T.F., 1993, Modeling atmospheric ^{14}C influences and ^{14}C ages of marine samples to 10,000 BC: Radiocarbon, v. 35, p. 137–189, doi:10.1017/S0033822200013874.

Stuiver, M., Reimer, P.J., and Reimer, R., 2015, CALIB radiocarbon calibration, version 7.1: http://calib.qub.ac.uk/calib/, accessed 24 May 2015.

Stuiver, M., Reimer, P.J., and Reimer, R.W., 2016, 14CHRONO marine reservoir correction database: Queens University, Belfast, http://calib.qub.ac.uk/marine/ (last accessed 2 May 2016).

Suter, J.R., Nummedal, D., Maynard, A.K., and Kemp, P., 1982, A process-response model for hurricane washovers, *in* Edge, B.L., ed., Coastal Engineering: 1982 Proceedings: New York, American Society of Civil Engineers, p. 1459–1478, doi:10.1061/9780872623736.089.

Switzer, A.D., and Burston, J.M., 2010, Competing mechanisms for boulder deposition on the southeast Australian coast: Geomorphology, v. 114, p. 42–54, doi:10.1016/j.geomorph.2009.02.009.

Switzer, A.D., Mamo, B.L., Dominey-Howes, D., Strotz, L.C., Courtney, C., Jones, B.G., Haslett, S.K., and Everett, D.M., 2011, On the possible origins of an unusual (mid to late Holocene) coastal deposit, Old Punt Bay, south-east Australia: Geographical Research, v. 49, p. 408–430, doi:10.1111/j.1745-5871.2011.00700.x.

Symithe, S., Calais, E., de Chabalier, J.B., Robertson, R., and Higgins, M., 2015, Current block motions and strain accumulation on active faults in the Caribbean: Journal of Geophysical Research, v. 120, p. 3748–3774, doi:10.1002/2014JB011779.

Tanaka, H., Xuan Tinh, N., Umeda, M., Hirao, R., Pradjoko, E., Mano, A., and Udo, K., 2012, Coastal and estuarine morphology changes induced by the 2011 great east Japan earthquake tsunami: Coastal Engineering Journal, v. 54, 1250010, doi:10.1142/S0578563412500106.

ten Brink, U., 2005, Vertical motions of the Puerto Rico Trench and Puerto Rico and their cause: Journal of Geophysical Research, v. 110, B06404, doi:10.1029/2004JB003459.

ten Brink, U.S., and López-Venegas, A.M., 2012, Plate interaction in the NE Caribbean subduction zone from continuous GPS observations: Geophysical Research Letters, v. 39, L10304, doi:10.1029/2012GL051485.

ten Brink, U.S., Geist, E.L., Lynett, P., and Andrews, B., 2006, Submarine slides north of Puerto Rico and their tsunami potential, *in* Mercado, A., and Liu, P., eds., Caribbean Tsunami Hazards: Singapore, World Scientific Publishers, p. 67–90, doi:10.1142/9789812774613_0004.

ten Brink, U.S., Bakun, W.H., and Flores, C.H., 2011, Historical perspective on seismic hazard to Hispaniola and the northeast Caribbean region: Journal of Geophysical Research, v. 116, B12318, doi:10.1029/2011JB008497.

ten Brink, U.S., Chaytor, J.D., Geist, E.L., Brothers, D.S., and Andrews, B.D., 2014, Assessment of tsunami hazard to the U.S. Atlantic margin: Marine Geology, v. 353, p. 31–54, doi:10.1016/j.margeo.2014.02.011.

Terry, J.P., Lau, A.Y.A., and Etienne, S., 2013, Reef-Platform Coral Boulders; Evidence for High-Energy Marine Inundation Events on Tropical Coastlines: Singapore, Springer, 105 p., doi: 10.1007/978-981-4451-33-8.

Toscano, M., Macintyre, I., and Lundberg, J., 2012, Last interglacial reef limestones, northeastern St. Croix, US Virgin Islands—Evidence of tectonic tilting and subsidence since MIS 5.5: Coral Reefs, v. 31, p. 27–38, doi:10.1007/s00338-011-0822-7.

Toscano, M.A., and Macintyre, I.G., 2003, Corrected western Atlantic sea-level curve for the last 11,000 years based on calibrated ^{14}C dates from *Acropora palmata* framework and intertidal mangrove peat: Coral Reefs, v. 22, p. 257–270, doi:10.1007/s00338-003-0315-4.

Usami, T., 2003, Saishinban nihon higai jishin soran: 416–2001 [Materials for Comprehensive List of Destructive Earthquakes in Japan]: Tokyo, University of Tokyo Press, 605 p.

Watt, S., Buckley, M., and Jaffe, B., 2012, Inland fields of dispersed cobbles and boulders as evidence for a tsunami on Anegada, British Virgin Islands: Natural Hazards, v. 63, p. 119–131, doi:10.1007/s11069-011-9848-y.

Weil-Accardo, J., Feuillet, N., Jacques, E., Deschamps, P., Beauducel, F., Cabioch, G., Tapponnier, P., Saurel, J., and Galetzka, J., 2016, Two hundred thirty years of relative sea level changes due to climate and megathrust tectonics recorded in coral microatolls of Martinique (French West Indies): Journal of Geophysical Research, v. 121, p. 2873–2903, doi:10.1002/2015JB012406.

Weiss, R., 2012, The mystery of boulders moved by tsunamis and storms: Marine Geology, v. 295–298, p. 28–33, doi:10.1016/j.margeo.2011.12.001.

Xu, Y., Pearson, S., and Halimeda Kilbourne, K., 2015, Assessing coral Sr/Ca–SST calibration techniques using the species Diploria strigosa: Palaeogeography, Palaeoclimatology, Palaeoecology, v. 440, p. 353–362, doi:10.1016/j.palaeo.2015.09.016.

Yamada, M., Fujino, S., and Goto, K., 2014, Deposition of sediments of diverse sizes by the 2011 Tohoku-oki tsunami at Miyako City, Japan: Marine Geology, v. 358, p. 67–78, doi:10.1016/j.margeo.2014.05.019.